
PERSONALIZED MULTI-TIER FEDERATED LEARNING

Sourasekhar Banerjee, Ali Dadras, Alp Yurtsever, Monowar Bhuyan

Umeå University

Umeå

Sweden

{firstname.lastname}@umu.se

ABSTRACT

The key challenge of personalized federated learning (PerFL) is to capture the statistical heterogeneity properties of data with inexpensive communications and gain customized performance for participating devices. To address these, we introduced personalized federated learning in multi-tier architecture (PerMFL¹) to obtain optimized and personalized local models when there are known team structures across devices. We provide theoretical guarantees of PerMFL, which offers linear convergence rates for smooth strongly convex problems and sub-linear convergence rates for smooth non-convex problems. We conduct numerical experiments demonstrating the robust empirical performance of PerMFL, outperforming the state-of-the-art in multiple personalized federated learning tasks.

Keywords Personalized federated learning · Multi-tier federated learning · Hierarchical federated learning.

1 Introduction

Federated learning (FL) is a distributed on-device learning framework that employs the heterogeneous data privately available at the edge for learning. In classical machine learning, edge devices are supposed to send data to the centralized server for training. However, FL relaxes this restriction by enabling the training of each model on the end devices and aggregating them on the global server. Classical FL learns a single global model by utilizing the private data of the devices locally and exchanging only the model information in a communication-efficient and privacy-preserving manner [1].

The early FL literature focuses mainly on a simplistic network architecture where all devices communicate directly with a single server [1]. An example of such a network architecture is typical on a local area network (LAN) with all devices connected to a single server. However, real-world Internet applications often occur on more complex, multi-tiered network architecture, e.g., wide area networks (WAN) that span multiple geographic locations and connect heterogeneous LANs. Hence, the conventional FL architecture is not suitable for such a setting. To address this, we study a multi-tier FL model Figure 1b where an intermediate layer of mediators, called *team servers* (TS_i), acts as a bridge between the end devices (N_i) and the global server (GS) and facilitates intermediate aggregations. From a systems standpoint, this multi-tier FL model resembles the cloud-edge continuum architecture [2]. In this model, the distant cloud serves as a central server responsible for generating a global model, and the edge servers located in various geographical regions act as team servers that establish connections with both the distant cloud and end devices. In contrast, the end devices perform local model computations. Multi-tier FL models, which are also referred to as hierarchical FL, have been studied by researchers in various applications and have shown significant advantages such as cost efficiency and scalability [3], reduced communication overheads [4, 5], enhanced privacy [6], improved system adaptability and performance [7], and faster convergence speeds (both theoretically and empirically) and reduced training time [8].

Data heterogeneity poses a significant challenge in FL, as data across different devices may exhibit varying characteristics and originate from diverse data distributions. The conventional FL systems assume that a single global model fits all devices, hindering the convergence speed and more crucially, the model accuracy when data is disseminated in a

¹https://github.com/sourasb05/PerMFL_1.git

non-independent and identically distributed (non-IID) manner. In this scenario, using a ‘global model for all’ disallows adaptation to unique needs and preferences embedded in each user’s data characteristics, possibly leading to subpar performance and user dissatisfaction [9]. To tackle this challenge, personalized FL (PerFL) methods learn local models suitable for each user’s unique needs for downstream tasks while still benefiting from collaborative training to achieve customized performance. Popular PerFL approaches include regularization techniques that penalize the distance between local and global models [10], smoothing techniques such as Moreau envelopes [11], and other heuristics such as taking extra local steps after the global model has converged [12, 13].

Multi-tier FL also suffers from data heterogeneity, but the existing literature on personalized multi-tier FL is limited. To address this challenge, we introduce a personalized multi-tier federated learning method (PerMFL). Our method is based on a new problem formulation that explicitly incorporates individual models for each team and device, in addition to the global server’s model. We enforce the proximity between team models and the global model and between device models and their associated team models using squared Euclidean distance regularization. As a result, our method leverages the multi-tiered architecture and simultaneously learns three models: (1) a global model, (2) a personalized model for each team, and (3) a personalized model for each device. Geometrically, the global model serves as a central estimate that is agreed upon by all teams and end devices. On the contrary, personalized models are designed to deviate from the global model in specific directions that align with their local data distributions. To facilitate efficient communication, our algorithm restricts direct communication between devices and the global server, allowing devices to communicate only with the team servers, which in turn communicate with the global server. Our primary goal with PerMFL is to achieve personalized on-device model performance while still maintaining comparably high accuracy for the global model, which can compete with conventional FL methods, all while ensuring efficient communication and collaboration among the devices and team servers.

Our key **contributions** are as follows:

1. We formulate an optimization problem for multi-tier personalized FL by introducing personal decision variables for teams and devices through squared Euclidean distance regularization, and we propose an algorithm (PerMFL) to solve this problem. Our algorithm flexibly accommodates local objectives during joint training of global and personalized models.
2. To provide a theoretical basis for our approach, we analyze the convergence guarantees of the proposed algorithm under the assumptions of smooth strongly convex and smooth non-convex loss functions. We show that the method converges with linear and sublinear rates, respectively, and we derive explicit theoretical bounds on hyperparameter settings to provide guidance for implementation.
3. We conduct extensive numerical experiments to evaluate the empirical performance of PerMFL. We compare our method to state-of-the-art (SOTA) approaches for both conventional and multi-tier FL settings using benchmark datasets (MNIST, FMNIST, EMNIST-10, FEMNIST, CIFAR100) and non-image tabular synthetic datasets with non-IID data dissemination. Moreover, we have examined the effect of hyperparameters on the convergence of PerMFL, ablation studies on different team formations, and ablation studies on team and client participation on the convergence of PerMFL.

2 Related Work

This section reviews existing studies and summarizes the differences between existing works and proposed efforts. We emphasize three different categories of FL models - multi-tier and personalized FL.

Multi-tier FL. A multi-tier (*aka* hierarchical) FL model leverages the combined capabilities of cloud and edge devices within the FL framework. In [8], the authors demonstrated that a multi-tier FL strategy, both theoretically and empirically, exhibits a faster convergence rate compared to traditional FL algorithms. In [14], the concept of “upward” and “downward” divergences were introduced, exploring their implications in the context of multi-tier FL. Additionally, [15] presented Cross-Silo FL, which encompasses multi-tier networks and utilizes vertical and horizontal data partitioning strategies. In [3], they introduced FEDn, a multi-tier FL framework designed explicitly for horizontally scalable distributed deployments. [6] identified several potential advantages of multi-tier FL in addressing privacy concerns. Firstly, multi-tier FL helps reduce the concentration of power and control in a central server, promoting a more distributed and decentralized approach. Secondly, multi-tier FL allows for the flexible placement of defense and verification mechanisms within the hierarchical structure, enabling the practical application of these methods. Lastly, multi-tier FL leverages the trust between users to mitigate the number of potential threats.

Personalized FL. FedAvg [1] is a classical baseline method in FL, renowned for its simplicity and low communication cost. However, it faces challenges when dealing with heterogeneous (non-iid) data, leading to unstable performance due to the concept drift problem. Concept drift arises when a single global model does not perform well for all clients. To address these issues, FL has increasingly leaned toward personalized models [16, 17, 9]. In [12], the authors proposed a personalized version of model-agnostic meta-learning (MAML) for FL. They identified the problem of how fast the initial shared model adapts to their local dataset with fewer gradient descent steps using individual client data. In [17], a systematic learning-theoretic study of personalization led to the proposal of three model-agnostic approaches: user clustering, data interpolation, and model interpolation. Another approach, presented in [11], formulated a personalized FL problem that utilized Moreau envelopes to regularize devices’ loss functions. In [18], the authors introduced an Asynchronous Loopless Local Gradient Descent (Async-L2GD) method for users from multiple known clusters, simultaneously training three models: a global model, a model-specific cluster, and a personalized model for each device. The architecture is similar to PerMFL, except that L2GD is an asynchronous approach. [19] introduced DemLearn, an FL algorithm that employs hierarchical agglomeration clustering. Unlike our model, where teams remain static throughout the FL process, DemLearn dynamically assembles teams after each global round. Recent research on personalized FL also includes works such as [20, 21, 22, 23, 9, 24, 10].

Motivation. A hierarchical structure in FL addresses the scalability and failure tolerance limitations observed in the centralized architecture [6]. In addition, it is also beneficial in addressing the management difficulties, system adaptivity, and performance [7] that arise due to fully decentralized architecture [6]. The key challenge of personalization is the heterogeneity of data, locally customized models, and identifying and collaborating among clients those having similar information [18]. By adding personalization at team and device levels, we aim to capture customized and refined personalized properties of the model that align well with real-world applications [2, 25]. Communication with the global server is often the most expensive step in FL [26], and communications within a team are typically cheaper [8]. By employing the multi-tier architecture and accommodating a large portion of the communication within the teams, PerMFL economizes significantly on the communication iterations with the global server, preventing biases to local clients, and achieving faster convergence [6]. These advantages motivated us to propose multi-tier FL.

3 PerMFL

A multi-tier FL framework (see Figure 1b) is different from the conventional FL framework (see Figure 1a) as it follows a hierarchy. All devices are divided into M teams. Each team has a team server (TS_i), which is connected with N_i devices of the respective team. Global server (GS) only communicates with TS_i ’s team.

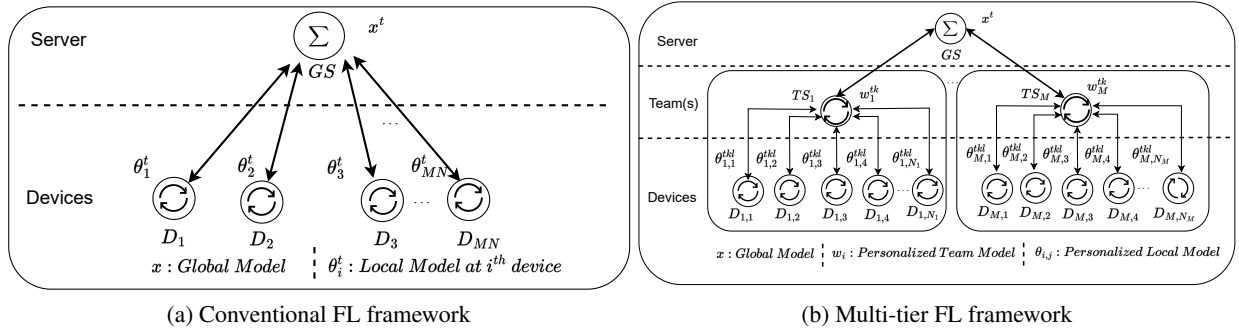


Figure 1: Federated learning work-flow

3.1 Team formation

By definition, FL can be seen as a cross-silo or cross-device setting [27]. In cross-silo settings, a limited number of devices, typically between 2 and 100, participate in each round, and their participation remains fixed. On the other hand, in cross-device setups, the client pool is extensive, potentially in the millions, but only a small fraction of devices take part in each iteration [27]. In a multi-tier structure, teams can be constituted in four ways: (1) Both teams and devices within teams have full participation, (2) Teams have full participation, whereas devices within teams are participating partially, (3) Teams have partial participation, but all devices within teams are participating, and (4) Teams and devices both have partial participation.

Various FL methods with different team formation strategies have been proposed in the literature [28, 29]. PerMFL does not explicitly address the creation of teams. Instead, it exhibits adaptability to accommodate any team formation mechanism. It is important to note that PerMFL is most efficient when communication with the team servers is cheaper compared to communication with the global server. This situation often occurs when devices are geographically

distributed and connected to their nearest teams, similar to the Cloud-Edge model [30]. We can also argue that team-level personalization is more effective when the data within each team exhibits distinctive characteristics that differentiate it from the data in other teams. Nonetheless, we provide a comprehensive ablation study that thoroughly examines different types of team selection, including poorly constructed and randomly constructed team formations. In cases where teams do not exhibit such distinctive characteristics, our model can still benefit from device-level personalization and reduced communication costs with the global server.

3.2 PerMFL formulation

We consider a multi-tier FL setup, consisting of M teams, each with N_i devices ($i = 1, \dots, M$). In this setup, empirical risk minimization can be expressed as:

$$\min_{x \in \mathbb{R}^d} \frac{1}{M} \sum_{i=1}^M \frac{1}{N_i} \sum_{j=1}^{N_i} f_{i,j}(x). \quad (1)$$

Here, $f_{i,j}(\cdot)$ represents the loss function of the j^{th} device from the i^{th} team. This formulation relies on a single decision variable x that all clients are expected to converge upon. However, this model is unsuitable for scenarios involving non-homogeneous data distributions, as the existence of a global model capable of accommodating all devices becomes unreasonable.

To address this challenge, we introduce decision variables for every team and device, denoted as w_i and $\theta_{i,j}$, respectively. Our goal is to find a global model representing a rough average, capturing common characteristics across all teams and devices; personalized team models that are close to the global model but can deviate from aligning with shared features within each team; and personalized device models that resemble the team model but can deviate to accommodate the unique characteristics of each device. We adopt a quadratic penalty approach to enforce that the device models are close to the team models and the team models to the global model. The parameters $\gamma \geq 0$ and $\lambda \geq 0$ control the degree of personalization impact at the team and device levels respectively.

$$\min_{x \in \mathbb{R}^d} \min_{w_i \in \mathbb{R}^d} \min_{\theta_{i,j} \in \mathbb{R}^d} \frac{1}{M} \sum_{i=1}^M \frac{1}{N_i} \sum_{j=1}^{N_i} \left(f_{i,j}(\theta_{i,j}) + \frac{\lambda}{2} \|\theta_{i,j} - w_i\|^2 + \frac{\gamma}{2} \|w_i - x\|^2 \right). \quad (2)$$

We are now prepared to outline the algorithm design. Our approach involves the use of three iteration counters: t for the global rounds, k for team-level rounds, and ℓ for device-level rounds.

Device-level updates. Given a team model $w_i^{t,k}$, the objective of the device (i, j) is to solve the following subproblem:

$$\tilde{f}_{i,j}^\lambda(w_i^{t,k}) := \min_{\theta_{i,j} \in \mathbb{R}^d} f_{i,j}(\theta_{i,j}) + \frac{\lambda}{2} \|\theta_{i,j} - w_i^{t,k}\|^2 \quad (3)$$

The exact solution to this problem is $\text{prox}_{f_{i,j}/\lambda}(w_i^{t,k})$; however, in general, there is no closed-form solution available for this proximal operator. Consequently, each device employs the gradient method to approximate the solution to (3). Starting with an initial value of $\theta_{i,j}^{t,k,0} = w_i^{t,k}$, and utilizing a positive step-size α , we perform the following update rule for $\ell = 0, 1, \dots, L-1$:

$$\theta_{i,j}^{t,k,\ell+1} = \theta_{i,j}^{t,k,\ell} - \alpha_{i,j} \nabla f_{i,j}(\theta_{i,j}^{t,k,\ell}) - \alpha_{i,j} \lambda (\theta_{i,j}^{t,k,\ell} - w_i^{t,k}). \quad (4)$$

Team-level updates. Similarly, the goal in team-level updates is to solve a regularized subproblem. We define the team-level loss function as

$$F_i(w_i) := \frac{1}{N_i} \sum_{j=1}^{N_i} \tilde{f}_{i,j}^\lambda(w_i). \quad (5)$$

With the addition of regularization towards the global server's model x^t , Team (i) aims to solve the following subproblem:

$$\text{clust} \tilde{F}_i^\gamma(x^t) := \min_{w_i \in \mathbb{R}^d} F_i(w_i) + \frac{\gamma}{2} \|w_i - x^t\|^2. \quad (6)$$

Once again, the solution is given by the proximal operator, $\text{prox}_{F_i/\gamma}(x^t)$, which can be difficult to compute. Instead, we can find an approximate solution by using the gradient method. Starting from $w_i^{t,0} = x^t$, and using a positive step-size $\eta > 0$, the gradient method update becomes

$$\begin{aligned} w_i^{t,k+1} &= w_i^{t,k} - \eta_i \nabla F_i(w_i^{t,k}) - \eta_i \gamma (w_i^{t,k} - x^t) \\ &= w_i^{t,k} - \frac{\eta_i}{N_i} \sum_{j=1}^{N_i} \nabla \tilde{f}_{i,j}^\lambda(w_i^{t,k}) - \eta_i \gamma (w_i^{t,k} - x^t). \end{aligned} \quad (7)$$

Here, the second line follows from the definition of F_i . Since we do not have the exact gradient $\nabla \tilde{f}_{i,j}(w_i^{t,k})$, we approximate it by:

$$\nabla \tilde{f}_{i,j}^\lambda(w_i^{t,k}) = \lambda(w_i^{t,k} - \text{prox}_{f_{i,j}/\lambda}(w_i^{t,k})) \approx \lambda(w_i^{t,k} - \theta_{i,j}^{t,k,L}). \quad (8)$$

By combining (7) and (8), we construct the following update rule for $k = 0, 1, \dots, K-1$:

$$w_i^{t,k+1} = (1 - \eta_i(\lambda + \gamma))w_i^{t,k} + \eta_i\gamma x^t + \frac{\lambda\eta_i}{N_i} \sum_{j=1}^{N_i} \theta_{i,j}^{t,k,L}. \quad (9)$$

Server-level updates. Finally, the server applies the gradient method for

$$\min_{x \in \mathbb{R}^d} \phi(x) := \frac{1}{M} \sum_{i=1}^M \tilde{F}_i^\gamma(x). \quad (10)$$

Starting from an initial state $x^0 \in \mathbb{R}^d$ and using a positive step-size β , the gradient update becomes:

$$x^{t+1} = x^t - \frac{\beta}{M} \sum_{i=1}^M \nabla \tilde{F}_i^\gamma(x^t). \quad (11)$$

Again, we use an approximation for $\nabla \tilde{F}_i(x^t)$ based on the team-level models:

$$\nabla \tilde{F}_i^\gamma(x^t) = \gamma(x^t - \text{prox}_{F_i/\gamma}(x^t)) \approx \gamma(x^t - w_i^{t,K}). \quad (12)$$

Finally, we construct the server-level update rule by combining (11) and (12). For $t = 0, 1, \dots, T-1$, the server performs the following update rule:

$$x^{t+1} = (1 - \beta\gamma)x^t + \frac{\beta\gamma}{M} \sum_{i=1}^M w_i^{t,K}. \quad (13)$$

Synthesis. By combining device, team, and server-level updates, we propose PerMFL (Algorithm 1) for personalized multi-tier FL.

Algorithm 1 PerMFL : Personalized Multi-tier FL

Input : x^0
Output : $\forall_{i=1}^M \forall_{j=1}^{N_i} \theta_{i,j}^{T,K,L}, x^T$
Initialize : $\forall_{i=1}^M w_i^{0,0} = x^0, \forall_{i=1}^M \forall_{j=1}^{N_i} \theta_{i,j} = w_i^{0,0}, T, K, L, \alpha_{i,j}, \beta, \gamma, \lambda, \eta_i$

```

1: for  $t = 0, 1, \dots, T-1$  do // Global iterations
2:   global server sends  $x^t$  to the teams. // Global model
3:   for  $k = 0, 1, \dots, K-1$  do // Team iterations
4:     Teams send  $w_i^{t,k}$  to the devices. // Team-level personalized model
5:     for  $l = 0, 1, \dots, L-1$  do // Local iterations
6:        $\theta_{i,j}^{t,k,l+1} = \theta_{i,j}^{t,k,l} - \alpha_{i,j} \nabla f_{i,j}(\theta_{i,j}^{t,k,l}) - \alpha_{i,j} \lambda(\theta_{i,j}^{t,k,l} - w_i^{t,k})$  // Personalized local models
7:     end for
8:      $\bar{\theta}_i^{t,k} = \frac{1}{N_i} \sum_{j=1}^{N_i} \theta_{i,j}^{t,k,L}$  // Aggregation within a team
9:      $w_i^{t,k+1} = (1 - \eta_i\lambda - \eta_i\gamma)w_i^{t,k} + \eta_i\gamma x^t + \lambda\eta_i\bar{\theta}_i^{t,k}$  // Personalized team update
10:   end for
11:    $\bar{w}^t = \frac{1}{M} \sum_{i=1}^M w_i^{t,K}$  // Global aggregation
12:    $x^{t+1} = (1 - \beta\gamma)x^t + \beta\gamma\bar{w}^t$  // Global update
13: end for
    
```

Initialization: Global server initializes the global model (x^0). Every team connected to the global server, copies the global model to their respective team model ($\forall_{i=1}^M w_i^{0,0} = x^0$). Each device within a team copies the initial team model ($w_i^{0,0}$) as their local model ($\theta_{i,j}$). Global server initializes the total number of global iterations, team iterations, and local iterations as T , K , and L , respectively.

Iterations: At each global iteration t , the global server broadcasts the global model x^t to every team. Similarly, at each team iteration k , each team broadcasts $w_i^{t,k}$ to all the devices within the team. For each local iteration (l), each device solves (3) separately, but in parallel to obtain the personalized model $\theta_{i,j}^{t,k,l}$. The team server of each team collects the device updates from the respective devices after L local iterations and performs aggregation ($\bar{\theta}_i^{t,k}$) on the device updates. Each team broadcasts the updated team-level model to the devices registered with that team and continues steps 3 to 10 for the next $K-1$ team iterations. After all teams finished K team iterations, the global server collects team updates ($w_i^{t,K}$) from each team and performs averaging (\bar{w}^t) on team updates over M teams. The global server produces a global update (x^t) by solving (13). The global server broadcasts the updated global model to teams and continues steps 1 to 13 for the upcoming $T-1$ global iterations.

Remark 1. The quadratic penalty approach leads to the concept of Moreau envelopes, a mathematical tool frequently employed in optimization theory for smoothing functions. For a function $g : \mathbb{R}^d \rightarrow \mathbb{R}$, we define the Moreau envelope $\tilde{g}^\sigma : \mathbb{R}^d \rightarrow \mathbb{R}$ with parameter $\sigma \geq 0$ as

$$\tilde{g}^\sigma(x) := \min_{u \in \mathbb{R}^d} \left\{ g(u) + \frac{\sigma}{2} \|u - x\|^2 \right\}. \quad (14)$$

Clearly, we can interpret (3) and (6) as the Moreau envelopes of $f_{i,j}$ and F_i , respectively. It is important to note that Moreau envelopes have been used before in [11] for personalization in the conventional FL setting.

3.3 Convergence guarantees

This section presents the convergence guarantees of PerMFL. We consider two different settings, with strongly convex and non-convex loss functions. In both cases, we assume that the loss functions are smooth in the sense that they have Lipschitz continuous gradients. The next Theorem formalizes the guarantees of when $f_{i,j}$ is strongly convex.

Theorem 1 (Strongly convex). *Consider the minimization problem $\min_x \phi(x)$ when $\phi(x)$ is defined in (10) with L_f -smooth and μ_f -strongly convex loss functions $f_{i,j}(x)$. For large enough numbers of inner iterations of orders $L = \Omega(K)$ and $K = \Omega(T)$, see the supplementary copy for the bounds, estimation $\{x^t\}_{t=0}^T$ generated by PerMFL with step-size β satisfies:*

$$\|x^T - x^*\|^2 \leq 2(1 - \beta)^T \|x^0 - x^*\|^2. \quad (15)$$

where learning rates should satisfy $\beta \leq \frac{\mu_{\tilde{F}}}{4\gamma}$, $\eta_i \leq \frac{1}{2(\lambda + \gamma)}$, $\alpha_{i,j} \leq \frac{1}{L_f + \lambda}$, $\mu_{\tilde{F}} := \frac{\lambda\gamma\mu_f}{\lambda\mu_f + \gamma\mu_f + \lambda\gamma}$, and $\gamma > 2\lambda > 4L_f$.

Proof sketch. We analyze the algorithm in three levels: (i) The devices find approximate solutions to problem (3) by using the gradient method. We can control the accuracy of this stage by choosing L (the number of iterations for the gradient method) large enough. (ii) The teams solve problem (6) approximately, again by using a gradient method. We use an inexact gradient at this stage since the exact gradient requires exact solutions from the devices to which we do not have access. At this stage, K is the number of iterations, and L modulates the accuracy of our gradients. By choosing both K and L large enough, we can control the solution accuracy achieved at the teams' level. (iii) Finally, the Server solves the problem (10), the original FL problem, by using the information provided by the Teams. It is worth noting that for a fixed T , we can decrease the error (down to a threshold) by increasing K and L . More precisely, we achieve linear convergence rates when we choose K and L in the order of $\Omega(T)$. The complete proof is left to the supplementary material.

The next Theorem shows that PerMFL finds a first-order stationary point with sublinear rates when $f_{i,j}$ are smooth but non-convex.

Theorem 2 (Non-convex). *Consider the minimization problem $\min_x \phi(x)$ when $\phi(x)$ is defined in (10) with non-convex L_f -smooth loss functions $f_{i,j}(x)$. For large enough numbers of inner iterations of orders $L = \Omega(K)$ and $K = \Omega(T)$, see the appendix for the bounds, then, estimation $\{x^t\}_{t=0}^T$ generated by PerMFL with step-size β satisfies:*

$$\mathbb{E}[\|\nabla\phi(x^{\tilde{t}})\|^2] \leq \frac{\phi(x^0) - \phi(x^*)}{\beta T} \quad (16)$$

where $\beta \leq \frac{1}{4\gamma}$, $\eta_i \leq \frac{1}{\lambda + \gamma}$, $\alpha_{i,j} \leq \frac{1}{\lambda}$, $\gamma > 2\lambda > 4L_f$, and \tilde{t} is uniformly sampled from $\{0, \dots, T - 1\}$

Proof sketch. The analysis follows a similar structure to the previous setting. The main difference is that the errors in subproblems are guaranteed as a bound on the gradient norms, which we translate to error bounds on objective residual by tuning λ and γ . The proof can be found in the supplementary material.

Remark 2. At first glance, it may come as a surprise that our guarantees do not necessitate a bounded drift condition, which is common in FL methods involving multiple local steps. It is important to note a fundamental distinction between the conventional FL template (1) and our personalized multi-tier FL template (2). The former lacks consideration for data heterogeneity as it relies solely on a single global variable. This can result in 'drift-away' issues when multiple local steps are taken, especially in the presence of data heterogeneity. In contrast, our formulation explicitly incorporates team and device-level variables, and our local steps are tailored to solve device and team-level subproblems (3) and (6). The regularization employed in these subproblems prevents 'over-drifting' by explicitly penalizing the divergence between device, team, and global models in a suitable manner.

4 Experiments

We studied classification problems to validate PerMFL using both benchmarks (MNIST [31], FMNIST [32] EMNIST [33] with 10 classes (EMNIST-10), EMNIST with 62 classes (FEMNIST), CIFAR100 [34]) and non-image synthetic datasets. For the MNIST, FMNIST, EMNIST-10, and synthetic datasets, the data was distributed among multiple devices in a non-iid manner, ensuring each device had data from at most two classes. Subsequently, the devices were randomly grouped into four teams, each consisting of 10 devices, before performing PerMFL. We considered the full participation of teams and devices in each global round for the performance and convergence evaluation. For the FEMNIST and CIFAR100 datasets, the data was distributed to 3,500 and 350 devices, respectively, with each device holding data from the 3 classes. The devices are arranged into 5 teams. All datasets are split into training and validation sets with a 3:1 ratio.

We considered a multi-class logistic regression (MCLR) model with a softmax activation function for strongly convex scenarios. For synthetic datasets, we constructed deep neural networks with two hidden layers, while for image datasets, we built two-layered convolutional neural networks for non-convex scenarios. More details of the experimental setup, datasets, and learning models are in the supplementary copy.

In this paper, we conducted (1) the performance comparison between PerMFL with FedAvg [1], pFedMe[11], PerFedAvg [13], pFedBayes [20], Ditto [10], and performance and convergence comparison with two hierarchical FL algorithms, such as hierarchical-SGD (h-SGD)[5], Asynchronous L2GD (AL2GD)[18], and a hierarchical-clustered FL algorithm DemLearn [19]. (2) We investigated the impact of β , γ , and λ on the convergence of PerMFL. (3) An ablation study to explore team formation. (4) An ablation study to analyze the influence of team and device participation. Moreover, in the supplementary copy, we gave an ablation study that explores the effects of team iterations on the convergence of PerMFL. Throughout the experiments, we denoted the personalized model and global model as (PM) and (GM), respectively. We have made the implementation of PerMFL available at https://github.com/sourasb05/PerMFL_1.git

4.1 Results and Analysis

4.1.1 Performance:

From table 1, we observed that PerMFL(PM) outperformed the state-of-the-art for non-convex cases in all datasets. PerMFL(GM) outperformed other global models, including FedAvg(GM), pFedMe(GM), and Ditto(GM), and nearly equivalent with h-SGD(GM) and DemLearn(GM) for the MNIST dataset. For the synthetic dataset, PerMFL(GM) outperformed the state-of-the-art. For FMNIST and EMNIST-10 datasets, the performance of PerMFL(GM) is better than the conventional FL models and DemLearn(GM). For strongly convex cases, PerMFL(PM) outperformed the state of the art in MNIST and Synthetic datasets. For the FMNIST dataset, PerMFL(PM)'s performance is better than the conventional FL state-of-the-art. Moreover, the performance of PerMFL(PM) is nearly equivalent to the DemLearn(PM) for FMNIST and EMNIST-10. PerMFL(PM) also achieved better performance than h-SGD and AL2GD on FEMNIST and CIFAR100 given in the supplementary copy. PerMFL(GM) outperformed the state-of-the-art in Synthetic and FMNIST datasets. PerMFL(GM) performs better than conventional methods in all datasets and is nearly equivalent to h-SGD(GM) on MNIST and EMNIST-10. From these observations, we can infer that PerMFL(PM) performs better than the 7 state-of-the-art methods on 6 out of 8 experiments. The reason could be, the personalization in both team and devices helps to get better performance.

4.1.2 Convergence:

From fig. 2, we observed that the convergence of PerMFL(PM) is equivalent to DemLearn and is faster than h-SGD and AL2GD. Similar findings were also observed in EMNIST-10, Synthetic, and MNIST datasets given in the supplementary copy. It is because, inside each team multiple iterations are happening, that helps the personalized model to converge quickly.

4.1.3 Effect of hyperparameters β , γ , and λ :

From fig. 3, we observed if we increase the value of β , γ , and λ separately then PerMFL(PM) converge faster. A similar observation is found for FMNIST, and the synthetic dataset is given in the supplementary copy. In all experiments, the hyperparameters followed the bounds given in theorem 1 for strongly convex and theorem 2 for non-convex and smooth problems.

Table 1: Performance (Validation accuracy(mean/std)(%)) comparison of PerMFL with state-of-the-art.

Architecture	MCLR (Strongly convex)				
	Algorithm	MNIST	Synthetic	FMNIST	EMNIST-10
Conventional	FedAvg(GM)[11]	84.87 (\pm 0.054)	84.87(\pm 0.054)	79.80 (\pm 0.002)	91.60(\pm 0.001)
	Per-FedAvg (PM)[13]	94.81 (\pm 0.00)	83.91(\pm 0.15)	94.75 (\pm 0.00)	97.57(\pm 0.0)
	pFedMe(GM)[11]	75.50(\pm 0.00)	81.93(\pm 0.21)	83.45(\pm 0.21)	88.78(\pm 0.01)
	pFedMe(PM)[11]	88.89(\pm 0.001)	87.61(\pm 0.32)	91.32 (\pm 0.08)	91.23(\pm 0.01)
	pFedBayes(PM)[20]	94.13(\pm 0.27)	87.05(\pm 0.5)	92.14(\pm 0.001)	94.13(\pm 0.001)
	Ditto (GM) [10]	84.81(\pm 0.001)	82.35(\pm 0.001)	74.02(\pm 0.001)	91.03 (\pm 0.0003)
Multi-tier	h-SGD (GM) [14]	87.41 (\pm 6.35)	84.29(\pm 5.18)	81.653(\pm 1.8)	92.33 (\pm 0.001)
	AL2GD(PM) [18]	93.70 (\pm 0.13)	84.75(\pm 0.03)	98.52 (\pm 0.004)	98.72 (\pm 0.001)
	DemLearn (GM)[19]	87.32(\pm 0.002)	67.93(\pm 0.04)	62.60(\pm 0.002)	69.09(\pm 0.12)
	DemLearn (PM)[19]	91.26 (\pm 0.01)	81.21(\pm 0.01)	97.50(\pm 0.0)	97.24(\pm 0.005)
	PerMFL(GM) [ours]	86.92 (\pm 0.013)	84.92 (\pm 0.06)	83.71 (\pm 0.001)	91.68 (\pm 0.0)
	PerMFL(PM) [ours]	96.87 (\pm 0.0)	87.94 (\pm 0.001)	96.77 (\pm 0.0)	96.49(\pm 0.0)
Architecture	DNN or CNN (Non-convex)				
	Algorithm	MNIST	Synthetic	FMNIST	EMNIST-10
Conventional	FedAvg(GM)	93.17 (\pm 0.02)	84.53(\pm 0.067)	84.14 (\pm 0.00)	92.73(\pm 0.003)
	Per-FedAvg(PM)	91.845(\pm 0.00)	75.93 (\pm 0.18)	88.69(\pm 0.269)	97.37(\pm 0.01)
	pFedMe(GM)	80.12(\pm 0.01)	81.23(\pm 0.19)	68.64 (\pm 0.009)	91.81 (\pm 0.0002)
	pFedMe(PM)	97.40(\pm 0.001)	87.86(\pm 0.06)	96.30 (\pm 0.001)	97.18(\pm 0.0003)
	Ditto(GM)	87.30(\pm 0.03)	81.12(\pm 0.006)	57.80(\pm 0.001)	90.58(\pm 0.004)
Multi-tier	h-SGD(GM)	86.59 (\pm 7.14)	87.42 (\pm 5.67)	79.84 (\pm 0.035)	96.03 (\pm 0.001)
	AL2GD(PM)	91.04 (\pm 0.035)	84.92 (\pm 0.02)	71.32(\pm 0.13)	92.94 (\pm 0.14)
	DemLearn(GM)	90.75 (\pm 0.001)	68.91(\pm 0.05)	64.84 (\pm 0.002)	96.63 (\pm 0.005)
	DemLearn(PM)	97.20(\pm 0.001)	82.74(\pm 0.008)	98.64(\pm 0.0)	98.74(\pm 0.0)
	PerMFL(GM) [ours]	89.39 (\pm 0.001)	87.53 (\pm 0.0)	79.15(\pm 0.0)	93.12(\pm 0.0)
	PerMFL(PM) [ours]	98.15 (\pm 0.0)	87.89 (\pm 0.0)	98.67 (\pm 0.0)	98.79 (\pm 0.0)

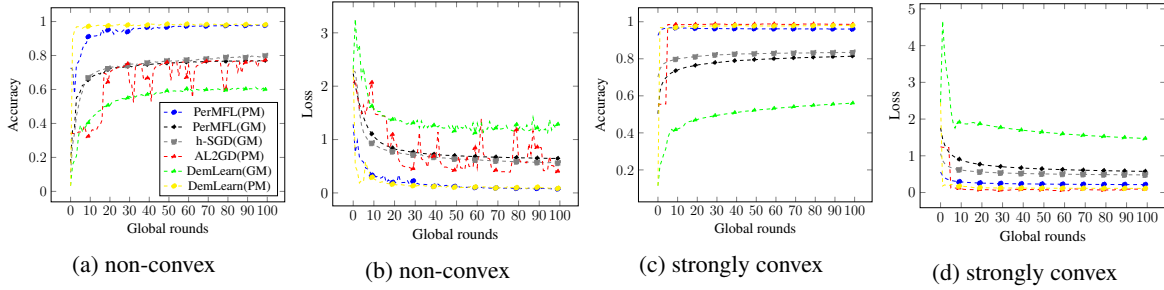
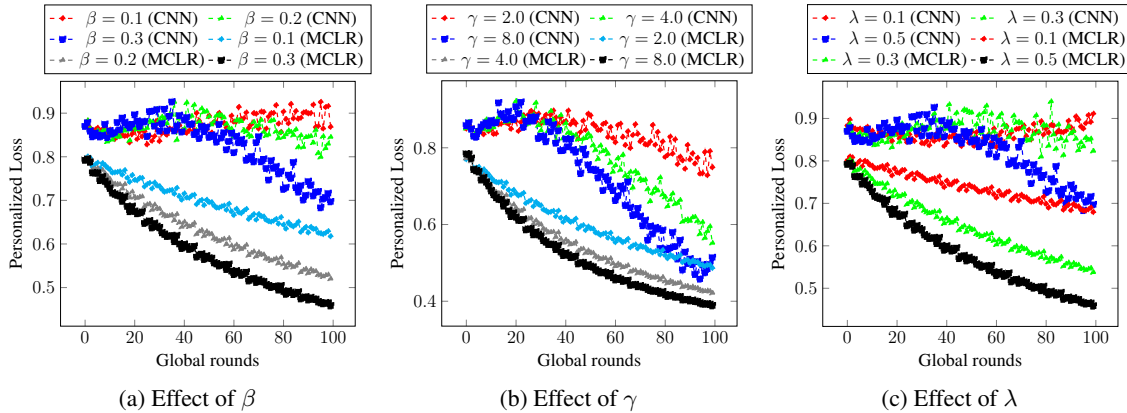


Figure 2: Convergence of PerMFL with multi-tier SOTA in strongly convex and non-convex settings on FMNIST


 Figure 3: Effect of β , γ , and λ on convergence of PerMFL(PM) in non-convex(CNN) and strongly convex(MCLR) settings using MNIST dataset

4.1.4 Ablation studies on team formation:

In table 2, we evaluated PerMFL for both worst-case (team 1 with labels $\{0, 1, 2, 3, 4\}$ and team 2 with $\{5, 6, 7, 8, 9\}$) and average-case (teams with overlapping labels, team 1 with labels $\{0, 1, 2, 3, 4, 5, 6\}$ and team 2 with $\{5, 6, 7, 8, 9, 0, 1\}$)

over 400 global iterations which include 10 and 20, team and local iterations respectively, with the hyperparameter settings $\lambda = 0.5$, $\gamma = 1.5$, $\beta = 0.6$, and, $\alpha = 0.01$. PerMFL(GM) showed a 4% improvement in average-case over the worst-case with FMNIST data. Likewise, PerMFL(PM) had slightly better results in average-case than worst-case for non-convex setups (CNN) with MNIST and FMNIST datasets, indicating PerMFL(PM)’s performance is mostly unaffected by team formation.

Table 2: Performance of PerMFL (Validation accuracy (%)) on worst-case and average-case team formation

Team Formation	Algorithm	MNIST		FMNIST		EMNIST-10	
		MCLR(%)	CNN(%)	MCLR(%)	CNN(%)	MCLR(%)	CNN(%)
Worst case	PerMFL(PM)	96.86	95.80	97.14	95.62	96.57	98.13
	PerMFL(GM)	80.48	82.21	76.18	70.28	88.05	87.05
Average case	PerMFL(PM)	97.01	97.02	96.72	97.38	96.39	98.15
	PerMFL(GM)	80.86	83.59	74.45	74.66	90.36	87.43

4.1.5 Ablation study on teams and clients participation:

PerMFL achieves quick convergence with complete participation from both teams and devices (fig. 4a) or when teams fully participate but devices do so partially (fig. 4b), in contrast to slower convergence under partial participation from both teams and devices (fig. 4d). Moreover, expanding the number of teams does not impact the convergence speed of PerMFL(PM) when there is full participation from all teams and devices throughout all global rounds (fig. 4a). Increased device involvement leads to faster convergence (fig. 4b), whereas lower team engagement (fig. 4c) decelerates it. Nonetheless, when team participation reaches 50% in each global round, the convergence rate is comparable to that observed in scenarios with complete participation (fig. 4a). When all teams are fully participating, increasing the number of team iterations leads to quicker convergence. However, in scenarios where both team and device participation is minimal (2%) as shown in fig. 4d, PerMFL(PM) requires more global and team iterations to achieve convergence. Extended experimental results are reported in the supplementary copy.

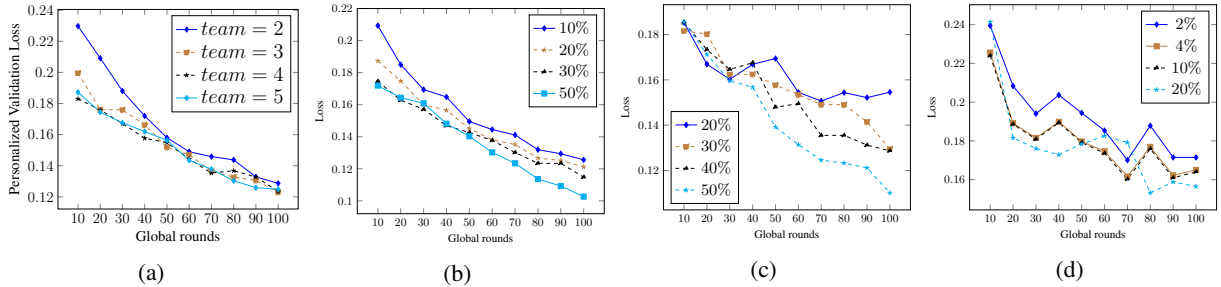


Figure 4: Ablation study on team and client’s participation on MNIST datasets in convex settings (MCLR): fig. 4a Full teams and devices participation, fig. 4b Full participation of 5 teams but partial participation of devices, fig. 4c partial participation of teams but full participation of devices, and fig. 4d Partial participation of teams (2%) with partial participation of clients

5 Conclusions

We introduced, PerMFL, a personalized multi-tier federated learning approach involving global servers, teams, and devices. PerMFL utilized squared euclidean distance regularization on both devices and teams. By employing PerMFL, we are able to generate personalized models for each device and simultaneously obtain a global model. The performance of PerMFL demonstrates linear baseline rates for strongly convex scenarios and sublinear baseline rates for non-convex and smooth scenarios. Empirically we observed that PerMFL(PM) converges quickly and outperformed the state-of-the-art. PerMFL performs best when both teams and devices participate fully. Very low team and device participation degrade the performance of PerMFL(GM). It requires more global and team iterations to converge. Also, in worst-case team formation, the performance of the global model decreases, while the personalized model is able to maintain its performance. Moreover right combination of λ , β , and γ enhances the convergence of PerMFL.

6 Acknowledgement

This work was supported by the Wallenberg AI, Autonomous Systems and Software Program (WASP) funded by the Knut and Alice Wallenberg Foundation. The computations were enabled by the Berzelius resource provided by the Knut and Alice Wallenberg Foundation at the National Supercomputer Centre.

References

- [1] McMahan, B et al. Communication-efficient learning of deep networks from decentralized data. *AISTATS, PMLR*, pages 1273–1282, 2017.
- [2] Wu, J et al. Hierarchical personalized federated learning for user modeling. In *Proceedings of the Web Conference 2021*, pages 957–968, 2021.
- [3] Ekmefjord, Morgan et al. Scalable federated machine learning with fedn. In *22nd CCGrid*, pages 555–564. IEEE, 2022.
- [4] Abad, Mehdi Salehi Heydar et al. Hierarchical federated learning across heterogeneous cellular networks. In *ICASSP*, pages 8866–8870. IEEE, 2020.
- [5] Liu, L et al. Hierarchical federated learning with quantization: Convergence analysis and system design. *IEEE Trans. on Wireless Communications*, 2022.
- [6] Wainakh, A et al. Enhancing privacy via hierarchical federated learning. In *IEEE (EuroS&PW)*, pages 344–347. IEEE, 2020.
- [7] Lin, T et al. Don’t use large mini-batches, use local sgd. *ICLR*, 2020.
- [8] Liu, L et al. Client-edge-cloud hierarchical federated learning. In *ICC*, pages 1–6. IEEE, 2020.
- [9] Tan, A et al. Towards personalized federated learning. *IEEE TNNLS*, 2022.
- [10] Li, T et al. Ditto: Fair and robust federated learning through personalization. In *ICML*, pages 6357–6368. PMLR, 2021.
- [11] T Dinh, C et al. Personalized federated learning with moreau envelopes. *Advances in Neural Information Processing Systems*, 33:21394–21405, 2020.
- [12] Finn, C et al. Model-agnostic meta-learning for fast adaptation of deep networks. *ICML, PMLR*, pages 1126–1135, 2017.
- [13] A et al. Fallah. Personalized federated learning: A meta-learning approach. *arXiv preprint arXiv:2002.07948*, 2020.
- [14] Wang, J et al. Demystifying why local aggregation helps: Convergence analysis of hierarchical SGD. In *Proceedings of the AAAI Conference on Artificial Intelligence*, pages 8548–8556, 2022.
- [15] Das, A et al. Cross-silo federated learning for multi-tier networks with vertical and horizontal data partitioning. *ACM TIST*, 13(6):1–27, 2022.
- [16] Karimireddy, S et al. Scaffold: Stochastic controlled averaging for federated learning. *ICML, PMLR*, pages 5132–5143, 2020.
- [17] Mansour, Y et al. Three approaches for personalization with applications to federated learning. *arXiv preprint arXiv:2002.10619*, 2020.
- [18] Lyu, B et al. Personalized Federated Learning with Multiple Known Clusters. *arXiv preprint arXiv:2204.13619*, 2022.
- [19] Nguyen, M et al. Self-organizing democratized learning: Toward large-scale distributed learning systems. *IEEE TNNLS*, 2022.
- [20] X et al. Zhang. Personalized Federated Learning via Variational Bayesian Inference. *ICML, (PMLR)*, pages 26293–26310, 2022.
- [21] Gasanov, E et al. FLIX: A Simple and Communication-Efficient Alternative to Local Methods in Federated Learning. *AISTATS, PMLR*, pages 11374–11421, 2022.
- [22] Pillutla, K et al. Federated learning with partial model personalization. *ICML, PMLR*, pages 17716–17758, 2022.
- [23] Chen, D et al. pFL-Bench: A Comprehensive Benchmark for Personalized Federated Learning. *arXiv preprint arXiv:2206.03655*, 2022.

- [24] Tziotis, I et al. Straggler-Resilient Personalized Federated Learning. *arXiv preprint arXiv:2206.02078*, 2022.
- [25] Zhou, H et al. Toward robust hierarchical federated learning in internet of vehicles. *IEEE TITS*, 24(5):5600–5614, 2023.
- [26] Abdellatif et al. Communication-efficient hierarchical federated learning for IoT heterogeneous systems with imbalanced data. *FGCS*, 128:406–419, 2022.
- [27] Kairouz, P et al. . Advances and open problems in federated learning. *Foundations and Trends® in Machine Learning*, 14(1–2):1–210, 2021.
- [28] Long, G et al. Multi-center federated learning: clients clustering for better personalization. *World Wide Web*, 26(1):481–500, 2023.
- [29] Yan, Y et al. Clustered Federated Learning in Heterogeneous Environment. *IEEE TNNLS*, pages 1–14, 2023.
- [30] Bittencourt, L et al. The internet of things, fog and cloud continuum: Integration and challenges. *IoT*, 3:134–155, 2018.
- [31] LeCun, Y et al. Gradient-based learning applied to document recognition. *Proceedings of the IEEE*, 86(11):2278–2324, 1998.
- [32] Xiao, H et al. Fashion-mnist: a novel image dataset for benchmarking machine learning algorithms. *arXiv preprint arXiv:1708.07747*, 2017.
- [33] Cohen, G et al. EMNIST: Extending MNIST to handwritten letters. In *IJCNN*, pages 2921–2926. IEEE, 2017.
- [34] Krizhevsky, A et al. Learning multiple layers of features from tiny images. 2009.
- [35] Caldas, S et al. Leaf: A benchmark for federated settings. *arXiv preprint arXiv:1812.01097*, 2018.
- [36] Li, T et al. Federated optimization in heterogeneous networks. *Proceedings of Machine learning and systems*, 2:429–450, 2020.

A Preliminaries and Supporting Lemmas

Definition 1 (Strong convexity). *A differentiable function $g : \mathbb{R}^d \rightarrow \mathbb{R}$ is μ_g -strongly convex if there exists a positive constant μ_g such that*

$$g(x) \leq g(y) + \langle \nabla g(x), x - y \rangle - \frac{\mu_g}{2} \|x - y\|^2, \quad \forall x, y \in \mathbb{R}^d. \quad (17)$$

If g is μ_g -strongly convex, then

$$\mu_g \|x - y\| \leq \|\nabla g(x) - \nabla g(y)\|, \quad \forall x, y \in \mathbb{R}^d. \quad (18)$$

Definition 2 (Smoothness). *A differentiable function $g : \mathbb{R}^d \rightarrow \mathbb{R}$ is L_g -smooth if there exists a non-negative constant L_g such that*

$$\|\nabla g(y) - \nabla g(x)\| \leq L_g \|x - y\|, \quad \forall x, y \in \mathbb{R}^d. \quad (19)$$

If g is L_g -smooth, then

$$|g(y) - g(x) - \langle \nabla g(x), y - x \rangle| \leq \frac{L_g}{2} \|y - x\|^2, \quad \forall x, y \in \mathbb{R}^d. \quad (20)$$

Definition 3 (Expected Smoothness). *The second moment of the stochastic gradient $\tilde{\nabla}g(x)$ satisfies*

$$\mathbb{E} \|\tilde{\nabla}g(x)\|^2 \leq 2A(g(x) - g(x^*)) + B \cdot \|\nabla g(x)\|^2 + C, \quad (21)$$

for some $A, B, C \geq 0$ and $\forall x \in \mathbb{R}^d$.

Definition 4 (Moreau Envelope). *For a function g , its Moreau envelope \tilde{g} is defined as*

$$\tilde{g}(x) = \min_{u \in \mathbb{R}^d} \left(g(u) + \frac{\lambda}{2} \|u - x\|^2 \right). \quad (22)$$

Proposition 1. *Let g be a convex function and \tilde{g} be its Moreau Envelope with parameter λ . Then*

1. \tilde{g} is convex.
2. \tilde{g} is continuously differentiable (even if g is not) and

$$\nabla \tilde{g}(x) = \lambda(x - \text{prox}_{g/\lambda}(x)), \quad \text{where} \quad \text{prox}_{g/\lambda}(x) := \arg \min_{u \in \mathbb{R}^d} \{g(u) + \frac{\lambda}{2} \|u - x\|^2\}. \quad (23)$$

Moreover \tilde{g} is λ -smooth.

3. *If g is μ -strongly convex, then \tilde{g} is $\mu_{\tilde{g}}$ -strongly convex with $\mu_{\tilde{g}} = \frac{\mu\lambda}{\mu+\lambda}$.*

Proposition 2. *If g is non-convex and L_g -smooth, then $\nabla \tilde{g}(x)$ is λ -smooth with the condition that $\lambda > 2L_g$.*

Proposition 3. *If $g : \mathbb{R}^d \rightarrow \mathbb{R}$ is convex and L_g -smooth, then*

$$\|\nabla g(x) - \nabla g(y)\|^2 \leq 2L_g \left(g(x) - g(y) - \langle \nabla g(y), x - y \rangle \right), \quad \forall x, y \in \mathbb{R}^d.$$

Proposition 4. *If $g : \mathbb{R}^d \rightarrow \mathbb{R}$ is μ_g -strongly convex, then*

$$\frac{\mu_g}{2} \|x - x^*\|^2 \leq g(x) - g(x^*), \quad \forall x \in \mathbb{R}^d. \quad (24)$$

Remark 3. *For any set of vectors $\{y_i\}_{i=1}^n$, we have*

$$\frac{1}{n} \sum_{i=1}^n \|y_i\|^2 = \frac{1}{n} \sum_{i=1}^n \|y_i - \bar{y}\|^2 + \|\bar{y}\|^2 \quad (25)$$

that leads to

$$\left\| \sum_{i=1}^n y_i \right\|^2 \leq n \cdot \sum_{i=1}^n \|y_i\|^2. \quad (26)$$

where $\bar{y} := \frac{1}{n} \sum_{i=1}^n y_i$.

Remark 4 (Young's inequality). *For any $\epsilon > 0$ and vectors $y, z \in \mathbb{R}^d$, we have*

$$2|\langle y, z \rangle| \leq \frac{2}{\epsilon} \|y\|^2 + \frac{\epsilon}{2} \|z\|^2$$

Remark 5 (Parameters in PerMFL). *Here, we consider two setups.*

- If $f_{i,j}$ is μ_f -strongly convex, then
 - $\tilde{f}_{i,j}$ is $\mu_{\tilde{f}}$ -strongly convex where $\mu_{\tilde{f}} = \frac{\lambda\mu_f}{\lambda+\mu_f}$
 - $\tilde{f}_{i,j}$ is λ -smooth.
 - F_i is μ_F -strongly convex where $\mu_F = \mu_{\tilde{f}} = \frac{\lambda\mu_f}{\lambda+\mu_f}$.
 - \tilde{F}_i is $\mu_{\tilde{F}}$ -strongly convex where

$$\mu_{\tilde{F}} = \frac{\mu_F\gamma}{\mu_F + \gamma} = \frac{\frac{\lambda\mu_f}{\lambda+\mu_f}\gamma}{\frac{\lambda\mu_f}{\lambda+\mu_f} + \gamma} = \frac{\lambda\gamma\mu_f}{\lambda\mu_f + \gamma\mu_f + \lambda\gamma}. \quad (27)$$

- ϕ is μ_ϕ -strongly convex where $\mu_\phi = \mu_{\tilde{F}} = \frac{\lambda\gamma\mu_f}{\lambda\mu_f + \gamma\mu_f + \lambda\gamma}$
- If $f_{i,j}$ is L_f -smooth then
 - $\tilde{f}_{i,j}$ is $L_{\tilde{f}}$ -smooth with the condition that $L_{\tilde{f}} = \lambda > 2L_f$.
 - F_i is L_F -smooth with the condition that $L_F = L_{\tilde{f}} = \lambda > 2L_f$.
 - \tilde{F}_i is $L_{\tilde{F}}$ -smooth with the condition that $L_{\tilde{F}} = \gamma > 2\lambda > 4L_f$.
 - ϕ is L_ϕ -smooth with the condition that $L_\phi = L_{\tilde{F}} = \gamma > 2\lambda > 4L_{\tilde{f}}$.

Definition 5 (Inexact Gradient Update). *Consider an equivalent algorithm to Algorithm 1 as Algorithm 2. Note that, We can re-write the update rule in Algorithm 1 as*

$$x^{t+1} = \frac{1}{M} \sum_{i=1}^M x_i^t = \frac{1}{M} \sum_{i=1}^M (x^t - \beta g_i^t) = x^t - \beta \frac{1}{M} \sum_{i=1}^M g_i^t = x^t - \beta g^t \quad (28)$$

where $g^t := \frac{1}{M} \sum_{i=1}^M g_i^t$.

Algorithm 2

```

set  $x^1, \lambda, \eta, \beta$ 
for round  $t = 1, 2, \dots, T$  do
    — Team-level training —————
    for team  $i = 1, 2, \dots, M$  do
         $w_i^{t,K} = \text{approx} \left\{ \arg \min_{u \in \mathbb{R}^d} \{F_i(u) + \frac{\gamma}{2} \|u - x^t\|^2\} \right\}$ 
         $g_i^t = \gamma(x^t - w_i^{t,K})$ 
         $x_i^t = x^t - \beta g_i^t$ 
        Client communicates  $x_i^t$  to the server.
    end for
    — Server-level aggregation —————
     $x^{t+1} = \frac{1}{M} \sum_{i=1}^M x_i^t$ 
    Server communicates  $x^{t+1}$  to the clients.
end for
    
```

B Convergence of PerMFL (strongly convex case)

Let us consider the team-level update as in Algorithm 2. We start with analyzing the convergence of this algorithm when having access to the approximate solution to $\text{prox}_{F_i/\gamma}(\cdot)$ in Theorem 3. Secondly we upper bound the approximation error in Theorem 4. We analyze the client level convergence in Theorem 5. Finally, we combine these results in Appendix B.3 and complete the proof of Theorem 1.

Theorem 3. Let $f_{i,j}$ be μ_f -strongly convex and assume that $w_i^{t,K}$ is an approximate solution to $\text{prox}_{F_i/\gamma}(x^t)$ such that $\|w_i^{t,K} - \text{prox}_{F_i/\gamma}(x^t)\|^2 \leq \nu_i$. Suppose that the sequence $\{x^t\}$ is generated by PerMFL with $\beta \leq \frac{\mu_{\tilde{F}}}{4L_{\tilde{F}}}$. Then, we have

$$\|x^T - x^*\|^2 \leq (1 - \beta)^T \|x^0 - x^*\|^2 + \frac{12\gamma^2\nu}{\mu_{\tilde{F}}^2}, \quad (29)$$

where $\mu_{\tilde{F}} = \frac{\lambda\gamma\mu_f}{\lambda\mu_f + \gamma\mu_f + \lambda\gamma}$, $L_{\tilde{F}} = \gamma$, and $\nu := \frac{1}{M} \sum_{i=1}^M \nu_i$.

Proof. Using (28), we have

$$\|x^{t+1} - x^*\|^2 = \|x^t - \beta g^t - x^*\|^2 = \|x^t - x^*\|^2 - 2\beta \langle g^t, x^t - x^* \rangle + \beta^2 \|g^t\|^2. \quad (30)$$

Now, we bound $J_1 := -\langle g^t, x^t - x^* \rangle$ and $J_2 := \|g^t\|^2$ separately.

- Upper bound for J_1 :

$$J_1 = -\langle g^t - \nabla\phi(x^t) + \nabla\phi(x^t), x^t - x^* \rangle = \underbrace{-\langle g^t - \nabla\phi(x^t), x^t - x^* \rangle}_{=: J_3} - \underbrace{\langle \nabla\phi(x^t), x^t - x^* \rangle}_{=: J_4}. \quad (31)$$

We upper bound J_3 and J_4 .

- Upper bound for J_3 : Using Young's inequality, see Remark 4, we have

$$2J_3 \leq \frac{2}{\epsilon} \|g^t - \nabla\phi(x^t)\|^2 + \frac{\epsilon}{2} \|x^t - x^*\|^2, \quad \forall \epsilon > 0. \quad (32)$$

- Upper bound for J_4 : Using the fact that \tilde{F}_i is $\mu_{\tilde{F}}$ -strongly convex, we have

$$J_4 = -\langle \nabla\phi(x^t), x^t - x^* \rangle \leq \phi(x^*) - \phi(x^t) - \frac{\mu_{\tilde{F}}}{2} \|x^t - x^*\|^2. \quad (33)$$

Substituting upper bounds on J_3 and J_4 into (31), we have

$$\begin{aligned} J_1 = J_3 + J_4 &\leq \frac{1}{\epsilon} \|g^t - \nabla\phi(x^t)\|^2 + \frac{\epsilon}{4} \|x^t - x^*\|^2 + \phi(x^*) - \phi(x^t) - \frac{\mu_{\tilde{F}}}{2} \|x^t - x^*\|^2 \\ &= \frac{1}{\epsilon} \|g^t - \nabla\phi(x^t)\|^2 - \left(\frac{\mu_{\tilde{F}}}{2} - \frac{\epsilon}{4} \right) \|x^t - x^*\|^2 + \phi(x^*) - \phi(x^t) \end{aligned} \quad (34)$$

- Upper bound for J_2 :

$$\begin{aligned} J_2 = \|g^t\|^2 &= \|g^t - \nabla\phi(x^t) + \nabla\phi(x^t)\|^2 \\ &\leq 2 \|g^t - \nabla\phi(x^t)\|^2 + 2 \|\nabla\phi(x^t)\|^2 \quad (\text{see Remark 3}) \\ &\leq 2 \|g^t - \nabla\phi(x^t)\|^2 + 4L_{\tilde{F}}(\phi(x^t) - \phi(x^*)), \end{aligned} \quad (35)$$

where in the last line, we used the fact that the average of $L_{\tilde{F}}$ -smooth functions $\tilde{F}_i(\cdot)$ is a $L_{\tilde{F}}$ -smooth function $\phi(x) = \frac{1}{M} \sum_{i=1}^M \tilde{F}_i(x)$, therefore, we can apply Proposition 3 with $x = x^t$, $x' = x^*$, and $\nabla\phi(x^*) = 0$.

Substituting J_1 and J_2 into (30), we can write

$$\begin{aligned} \|x^{t+1} - x^*\|^2 &\leq \|x^t - x^*\|^2 + 2\beta J_1 + \beta^2 J_2 \\ &\leq \|x^t - x^*\|^2 + 2\beta \left(\frac{1}{\epsilon} \left(\|g^t - \nabla\phi\|^2 \right) - \left(\frac{\mu_{\tilde{F}}}{2} - \frac{\epsilon}{4} \right) \|x^t - x^*\|^2 + \phi(x^*) - \phi(x^t) \right) \\ &\quad + \beta^2 \left(2\|g^t - \nabla\phi(x^t)\|^2 + 4L_{\tilde{F}}(\phi(x^t) - \phi(x^*)) \right) \\ &= \left(1 - \beta(\mu_{\tilde{F}} - \frac{\epsilon}{2}) \right) \|x^t - x^*\|^2 - 2\beta(1 - 2\beta L_{\tilde{F}}) (\phi(x^t) - \phi(x^*)) \\ &\quad + 2\beta(\beta + \frac{1}{\epsilon}) \left(\|g^t - \nabla\phi(x^t)\|^2 \right) \\ &\leq \left(1 - \frac{\beta\mu_{\tilde{F}}}{2} \right) \|x^t - x^*\|^2 + 2\beta(\beta + \frac{1}{\mu_{\tilde{F}}}) \left(\|g^t - \nabla\phi(x^t)\|^2 \right) \\ &\leq (1 - \beta) \|x^t - x^*\|^2 + \frac{8}{\mu_{\tilde{F}}^2} \beta(\beta + \frac{1}{2}) \underbrace{\left(\|g^t - \nabla\phi(x^t)\|^2 \right)}_{J_5} \end{aligned} \quad (36)$$

where in the last line we re-defined β with the new $\beta \leq \frac{\mu_{\tilde{F}}}{2} \min \left\{ \frac{1}{2L_{\tilde{F}}}, \frac{2}{\mu_{\tilde{F}}} \right\} = \min \left\{ \frac{\mu_{\tilde{F}}}{4L_{\tilde{F}}}, 1 \right\}$ and chose $\epsilon = \mu_{\tilde{F}}$. Also note that $\mu_{\tilde{F}} \leq L_{\tilde{F}}$ results in $\beta \leq \frac{\mu_{\tilde{F}}}{4L_{\tilde{F}}}$. Let us now bound J_5 using the definitions of g_i^t and the second part of Proposition 1.

$$\begin{aligned}
 J_5 &= \|g^t - \nabla \phi(x^t)\|^2 = \frac{1}{M} \sum_{i=1}^M \|g_i^t - \nabla \tilde{F}_i(x^t)\|^2 \\
 &= \frac{1}{M} \sum_{i=1}^M \|\gamma(x^t - w_i^{t,K}) - \gamma(x^t - \text{prox}_{F_i/\gamma}(x^t))\|^2 \\
 &= \gamma^2 \frac{1}{M} \sum_{i=1}^M \|w_i^{t,K} - \text{prox}_{F_i/\gamma}(x^t)\|^2 \\
 &\leq \gamma^2 \frac{1}{M} \sum_{i=1}^M \nu_i \quad (\text{assumption}) \\
 &=: \gamma^2 \nu
 \end{aligned} \tag{37}$$

where $\nu := \frac{1}{M} \sum_{i=1}^M \nu_i$. Substituting J_5 into (36), we get

$$\|x^{t+1} - x^*\|^2 \leq (1 - \beta) \|x^t - x^*\|^2 + \frac{8}{\mu_{\tilde{F}}^2} \beta \left(\beta + \frac{1}{2} \right) \gamma^2 \nu. \tag{38}$$

Substituting $t = T - 1$ and unrolling (38), we get

$$\begin{aligned}
 \|x^T - x^*\|^2 &\leq (1 - \beta)^T \|x^0 - x^*\|^2 + \frac{8}{\mu_{\tilde{F}}^2} \beta \left(\beta + \frac{1}{2} \right) \gamma^2 \nu \left(\frac{1 - (1 - \frac{\beta \mu_{\tilde{F}}}{2})^T}{1 - (1 - \frac{\beta \mu_{\tilde{F}}}{2})} \right) \\
 &\leq (1 - \beta)^T \|x^0 - x^*\|^2 + \frac{8}{\mu_{\tilde{F}}^2} \beta \left(\beta + \frac{1}{2} \right) \gamma^2 \nu \left(\frac{1}{\frac{\beta \mu_{\tilde{F}}}{2}} \right) \\
 &\leq (1 - \beta)^T \|x^0 - x^*\|^2 + \left(\beta + \frac{1}{2} \right) \frac{16}{\mu_{\tilde{F}}^3} \gamma^2 \nu.
 \end{aligned} \tag{39}$$

We can further simplify (39) using $\beta \leq \frac{\mu_{\tilde{F}}}{4L_{\tilde{F}}} \leq \frac{1}{2}$

$$\|x^T - x^*\|^2 \leq (1 - \beta)^T \|x^0 - x^*\|^2 + \frac{16}{\mu_{\tilde{F}}^3} \gamma^2 \nu. \tag{40}$$

That completes the proof. \square

B.1 Team-level convergence (strongly convex case)

Theorem 4. Consider Problem 6 with Gradient descent steps (9). Let us assume that we have approximate solution to $\text{prox}_{f_{i,j}/\gamma}(\cdot)$ so that we have $\|\text{prox}_{f_{i,j}/\gamma}(w_i^{t,k}) - \theta_{i,j}^{t,k,L}\|^2 \leq \delta_{i,j}$, then

$$\|w_i^{t,K} - \text{prox}_{F_i/\gamma}(x^t)\|^2 \leq \left(1 - \eta_i \frac{\mu_F + \gamma}{2}\right)^K \frac{2L_{\tilde{F}}}{\gamma^2} (\tilde{F}_i(w_i^{t,0}) - \tilde{F}_i(x^*)) + 12 \left(\frac{\lambda}{\mu_F + \gamma}\right)^2 \frac{1}{N_i} \sum_{j=1}^{N_i} \delta_{i,j} := \nu_i \tag{41}$$

where $\eta_i \leq \frac{1}{2(L_F + \gamma)}$.

Proof. Let us re-write (9) as $w_i^{t,k+1} = w_i^{t,k} - \eta_i q_i^{t,k}$, where $q_i^{t,k}$ is the inexact gradient of $p_i(y) := F_i(y) + \frac{\gamma}{2} \|y - x^t\|^2$ at $y = w_i^{t,k}$.

$$\begin{aligned}
 \|w_i^{t,k+1} - w_i^{t,*}\|^2 &= \|w_i^{t,k} - \eta_i q_i^{t,k} - w_i^{t,*}\|^2 \\
 &= \|w_i^{t,k} - w_i^{t,*}\|^2 - \underbrace{2\eta_i \langle q_i^{t,k}, w_i^{t,k} - w_i^{t,*} \rangle}_{J_1} + \underbrace{\eta_i^2 \|q_i^{t,k}\|^2}_{J_2},
 \end{aligned} \tag{42}$$

where $w_i^{t,*}$ is the minimizer of $p_i(\cdot)$. Now, we upper bound J_1 and J_2 .

• **Bound on J_1 :**

$$J_1 = 2\eta_i \left(\underbrace{-\langle q_i^{t,k} - \nabla p_i(w_i^{t,k}), w_i^{t,k} - w_i^{t,*} \rangle}_{J_3} - \underbrace{\langle \nabla p_i(w_i^{t,k}), w_i^{t,k} - w_i^{t,*} \rangle}_{J_4} \right) \quad (43)$$

– **Bound on J_3 :** Note that $q_i^{t,k} = (\lambda + \gamma)w_i^{t,k} - \gamma x^t - \lambda \bar{\theta}_i^{t,k}$ and $\nabla p_i(w_i^{t,k}) = (\lambda + \gamma)w_i^{t,k} - \gamma x^t - \frac{\lambda}{N_i} \sum_{j=1}^{N_i} \text{prox}_{f_{i,j}/\lambda}(w_i^{t,k})$. We have

$$\begin{aligned} J_3 &= -\lambda \left\langle \frac{1}{N_i} \sum_{j=1}^{N_i} \text{prox}_{f_{i,j}/\lambda}(w_i^{t,k}) - \bar{\theta}_i^{t,k}, w_i^{t,k} - w_i^{t,*} \right\rangle \\ &= -\lambda \frac{1}{N_i} \sum_{j=1}^{N_i} \langle \text{prox}_{f_{i,j}/\lambda}(w_i^{t,k}) - \theta_{i,j}^{t,k,L}, w_i^{t,k} - w_i^{t,*} \rangle \quad (\bar{\theta}_i^{t,k} := \frac{1}{N_i} \sum_{j=1}^{N_i} \theta_{i,j}^{t,k,L}). \end{aligned} \quad (44)$$

Using Young's inequality with $\epsilon = (\mu_F + \gamma)/\lambda$, see Remark 4, we get

$$\begin{aligned} 2J_3 &\leq \lambda \frac{1}{N_i} \sum_{j=1}^{N_i} \left(\frac{2\lambda}{\mu_F + \gamma} \|\text{prox}_{f_{i,j}/\lambda}(w_i^{t,k}) - \theta_{i,j}^{t,k,L}\|^2 + \frac{\mu_F + \gamma}{2\lambda} \|w_i^{t,k} - w_i^{t,*}\|^2 \right) \\ &\leq \frac{2\lambda^2}{\mu_F + \gamma} \frac{1}{N_i} \sum_{j=1}^{N_i} \delta_{i,j} + \frac{\mu_F + \gamma}{2} \|w_i^{t,k} - w_i^{t,*}\|^2. \end{aligned} \quad (45)$$

– **Bound on J_4 :** Note that $p_i(\cdot)$ is $(\mu_F + \gamma)$ -strongly convex, therefore we have

$$J_4 \leq p_i(w_i^{t,*}) - p_i(w_i^{t,k}) - \frac{\mu_F + \gamma}{2} \|w_i^{t,k} - w_i^{t,*}\|^2. \quad (46)$$

Substituting upper bounds on J_3 and J_4 into (43), we have

$$J_1 \leq 2\eta_i \left(\frac{\lambda^2}{\mu_F + \gamma} \frac{1}{N_i} \sum_{j=1}^{N_i} \delta_{i,j} + p_i(w_i^{t,*}) - p_i(w_i^{t,k}) - \frac{\mu_F + \gamma}{4} \|w_i^{t,k} - w_i^{t,*}\|^2 \right). \quad (47)$$

• **Upper bound for J_2**

$$\begin{aligned} J_2 &= \|q_i^{t,k}\|^2 = \|q_i^{t,k} - \nabla p_i(w_i^{t,k}) + \nabla p_i(w_i^{t,k})\|^2 \\ &\leq 2(\|q_i^{t,k} - \nabla p_i(w_i^{t,k})\|^2 + \|\nabla p_i(w_i^{t,k})\|^2) \quad (\text{see Remark 3}) \\ &= 2(\lambda^2 \|\frac{1}{N_i} \sum_{j=1}^{N_i} \text{prox}_{f_{i,j}/\lambda}(w_i^{t,k}) - \theta_{i,j}^{t,k,L}\|^2 + \|\nabla p_i(w_i^{t,k})\|^2) \\ &\leq 2\lambda^2 \frac{1}{N_i} \sum_{j=1}^{N_i} \|\text{prox}_{f_{i,j}/\lambda}(w_i^{t,k}) - \theta_{i,j}^{t,k,L}\|^2 + 2\|\nabla p_i(w_i^{t,k})\|^2 \quad (\text{see Remark 3}) \\ &\leq 2\lambda^2 \frac{1}{N_i} \sum_{j=1}^{N_i} \delta_{i,j} + 4(L_F + \gamma)(p_i(w_i^{t,k}) - p_i(w_i^{t,*})) \quad (p_i(\cdot) \text{ is } (L_F + \gamma)\text{-Smooth}) \end{aligned} \quad (48)$$

Substituting J_1 and J_2 into (42), we can write

$$\begin{aligned}
 \|w_i^{t,k+1} - w_i^{t,*}\|^2 &\leq \|w_i^{t,k} - w_i^{t,*}\|^2 + 2\eta_i \left(\frac{\lambda^2}{\mu_F + \gamma} \frac{1}{N_i} \sum_{j=1}^{N_i} \delta_{i,j} + p_i(w_i^{t,k}) - p_i(w_i^{t,*}) - \frac{\mu_F + \gamma}{4} \|w_i^{t,k} - w_i^{t,*}\|^2 \right) \\
 &\quad + 2\eta_i^2 \lambda^2 \frac{1}{N_i} \sum_{j=1}^{N_i} \delta_{i,j} + 4\eta_i^2 (L_{\tilde{f}} + \gamma) (p_i(w_i^{t,k}) - p_i(w_i^{t,*})) \\
 &= (1 - \eta_i \frac{\mu_F + \gamma}{2}) \|w_i^{t,k} - w_i^{t,*}\|^2 - 2\eta_i (1 - 2\eta_i (L_F + \gamma)) (p_i(w_i^{t,k}) - p_i(w_i^{t,*})) \\
 &\quad + 2\eta_i \lambda^2 \left(\eta_i + \frac{1}{\mu_F + \gamma} \right) \frac{1}{N_i} \sum_{j=1}^{N_i} \delta_{i,j} \\
 &\leq (1 - \eta_i \frac{\mu_F + \gamma}{2}) \|w_i^{t,k} - w_i^{t,*}\|^2 + 2\eta_i \lambda^2 \left(\eta_i + \frac{1}{\mu_F + \gamma} \right) \frac{1}{N_i} \sum_{j=1}^{N_i} \delta_{i,j} \quad (\eta_i \leq \frac{1}{2(L_F + \gamma)}) \\
 &\leq (1 - \eta_i \frac{\mu_F + \gamma}{2}) \|w_i^{t,k} - w_i^{t,*}\|^2 + \left(\frac{6\eta_i \lambda^2}{\mu_F + \gamma} \right) \frac{1}{N_i} \sum_{j=1}^{N_i} \delta_{i,j} \quad (\eta_i \leq \frac{2}{(\mu_F + \gamma)}). \tag{49}
 \end{aligned}$$

Substituting $k = K - 1$ and unrolling (49), we get

$$\begin{aligned}
 \|w_i^{t,K} - w_i^{t,*}\|^2 &\leq \left(1 - \eta_i \frac{\mu_F + \gamma}{2}\right)^K \|w_i^{t,0} - w_i^{t,*}\|^2 + \left(\frac{6\eta_i \lambda^2}{\mu_F + \gamma}\right) \frac{1}{N_i} \sum_{j=1}^{N_i} \delta_{i,j} \left(\frac{1 - (1 - \eta_i \frac{\mu_F + \gamma}{2})^K}{1 - (1 - \eta_i \frac{\mu_F + \gamma}{2})} \right) \\
 &\leq \left(1 - \eta_i \frac{\mu_F + \gamma}{2}\right)^K \|w_i^{t,0} - w_i^{t,*}\|^2 + 12 \left(\frac{\lambda}{\mu_F + \gamma}\right)^2 \frac{1}{N_i} \sum_{j=1}^{N_i} \delta_{i,j}. \tag{50}
 \end{aligned}$$

Substituting $w_i^{t,*} = \text{prox}_{F_i/\gamma}(x^t)$ and $w_i^{t,0} = x^t$ into the equation above, we can write

$$\begin{aligned}
 \|w_i^{t,K} - \text{prox}_{F_i/\gamma}(x^t)\|^2 &\leq \left(1 - \eta_i \frac{\mu_F + \gamma}{2}\right)^K \|x^t - \text{prox}_{F_i/\gamma}(x^t)\|^2 + 12 \left(\frac{\lambda}{\mu_F + \gamma}\right)^2 \frac{1}{N_i} \sum_{j=1}^{N_i} \delta_{i,j} \\
 &= \left(1 - \eta_i \frac{\mu_F + \gamma}{2}\right)^K \frac{1}{\gamma^2} \|\nabla \tilde{F}_i(x^t)\|^2 + 12 \left(\frac{\lambda}{\mu_F + \gamma}\right)^2 \frac{1}{N_i} \sum_{j=1}^{N_i} \delta_{i,j} \\
 &\leq \left(1 - \eta_i \frac{\mu_F + \gamma}{2}\right)^K \frac{2L_{\tilde{F}}}{\gamma^2} (\tilde{F}_i(x^t) - \tilde{F}_i(x^*)) + 12 \left(\frac{\lambda}{\mu_F + \gamma}\right)^2 \frac{1}{N_i} \sum_{j=1}^{N_i} \delta_{i,j} \\
 &= \left(1 - \eta_i \frac{\mu_F + \gamma}{2}\right)^K \frac{2L_{\tilde{F}}}{\gamma^2} (\tilde{F}_i(w_i^{t,0}) - \tilde{F}_i(x^*)) + 12 \left(\frac{\lambda}{\mu_F + \gamma}\right)^2 \frac{1}{N_i} \sum_{j=1}^{N_i} \delta_{i,j} \\
 &:= \nu_i \tag{51}
 \end{aligned}$$

where in the second line, we used $\nabla \tilde{F}_i(x^t) = \gamma(x^t - \text{prox}_{F_i/\gamma}(x^t))$, and in the third line we used the smoothness of $\tilde{F}_i(\cdot)$. Note also that the last two lines of (49) require $\eta_i \leq \min\{\frac{1}{2(L_F + \gamma)}, \frac{2}{(\mu_F + \gamma)}\}$ that can be reduced to $\eta_i \leq \frac{1}{2(L_F + \gamma)}$ because we always have $\mu_F \leq L_F$. \square

B.2 Client-level convergence (strongly convex case)

Theorem 5. Let $f_{i,j}$ be μ_f -strongly convex and L_f -smooth functions. Consider Problem 3 with Gradient descent steps (4), we have

$$\|\theta_{i,j}^{t,k,L} - \text{prox}_{f_{i,j}/\lambda}(w_i^{t,k})\|^2 \leq (1 - \alpha\mu_f)^L \frac{1}{\lambda^2} \|\nabla \tilde{f}_{i,j}(\theta_{i,j}^{t,k,0})\|^2 =: \delta_{i,j}, \tag{52}$$

where $\alpha \leq \frac{1}{L_f + \lambda}$.

Proof. Let us define $p_{i,j}(y) := f_{i,j}(y) + \frac{\lambda}{2}\|y - w_i^{t,k}\|^2$. Note that $p_{i,j}(\cdot)$ is $(\mu_f + \lambda)$ -strongly convex and $(L_f + \lambda)$ -smooth. We use (4), and write

$$\begin{aligned}
 \|\theta_{i,j}^{t,k,l+1} - \theta_{i,j}^{t,k,*}\|^2 &= \|\theta_{i,j}^{t,k,l} - \alpha \nabla p_{i,j}(\theta_{i,j}^{t,k,l}) - \theta_{i,j}^{t,k,*}\|^2 \\
 &= \|\theta_{i,j}^{t,k,l} - \theta_{i,j}^{t,k,*}\|^2 - 2\alpha \langle \nabla p_{i,j}(\theta_{i,j}^{t,k,l}), \theta_{i,j}^{t,k,l} - \theta_{i,j}^{t,k,*} \rangle + \alpha^2 \|\nabla p_{i,j}(\theta_{i,j}^{t,k,l})\|^2 \\
 &\leq \|\theta_{i,j}^{t,k,l} - \theta_{i,j}^{t,k,*}\|^2 + 2\alpha \left(p_{i,j}(\theta_{i,j}^{t,k,*}) - p_{i,j}(\theta_{i,j}^{t,k,l}) - \frac{\mu_f + \lambda}{2} \|\theta_{i,j}^{t,k,l} - \theta_{i,j}^{t,k,*}\|^2 \right) + \alpha^2 \|\nabla p_{i,j}(\theta_{i,j}^{t,k,l})\|^2 \\
 &\leq (1 - \alpha(\mu_f + \lambda)) \|\theta_{i,j}^{t,k,l} - \theta_{i,j}^{t,k,*}\|^2 - 2\alpha (p_{i,j}(\theta_{i,j}^{t,k,l}) - p_{i,j}(\theta_{i,j}^{t,k,*})) + 2\alpha^2 (L_f + \lambda) (p_{i,j}(\theta_{i,j}^{t,k,l}) - p_{i,j}(\theta_{i,j}^{t,k,*})) \\
 &\leq (1 - \alpha(\mu_f + \lambda)) \|\theta_{i,j}^{t,k,l} - \theta_{i,j}^{t,k,*}\|^2 - 2\alpha(1 - \alpha(L_f + \lambda)) (p_{i,j}(\theta_{i,j}^{t,k,l}) - p_{i,j}(\theta_{i,j}^{t,k,*})) \\
 &\leq (1 - \alpha(\mu_f + \lambda)) \|\theta_{i,j}^{t,k,l} - \theta_{i,j}^{t,k,*}\|^2 \quad (\alpha \leq \frac{1}{L_f + \lambda})
 \end{aligned} \tag{53}$$

In the third and fourth lines, we used strong convexity of $p_{i,j}$ and Proposition 3. Substituting $l = L - 1$, $\theta_{i,j}^{t,k,0} = w_i^{t,k}$, and $\theta_{i,j}^{t,k,*} = \text{prox}_{f_{i,j}/\lambda}(w_i^{t,k})$, we get

$$\begin{aligned}
 \|\theta_{i,j}^{t,k,L} - \text{prox}_{f_{i,j}/\lambda}(w_i^{t,k})\|^2 &\leq (1 - \alpha(\mu_f + \lambda))^L \|w_i^{t,k} - \text{prox}_{f_{i,j}/\lambda}(w_i^{t,k})\|^2 \\
 &= (1 - \alpha(\mu_f + \lambda))^L \frac{1}{\lambda^2} \|\nabla \tilde{f}_{i,j}(w_i^{t,k})\|^2 \\
 &= (1 - \alpha(\mu_f + \lambda))^L \frac{1}{\lambda^2} \|\nabla \tilde{f}_{i,j}(\theta_{i,j}^{t,k,0})\|^2 \quad (\theta_{i,j}^{t,k,0} = w_i^{t,k}) \\
 &=: \delta_{i,j}.
 \end{aligned} \tag{54}$$

Note that we require $\alpha \leq \min\{\frac{1}{L_f + \lambda}, \frac{1}{\mu_f + \lambda}\}$ that can be reduced to $\alpha \leq \frac{1}{L_f + \lambda}$ since we always have $\mu_f \leq L_f$. That completes the proof. \square

B.3 Discussion on error bounds (strongly convex case)

In this section we discuss the relation between L , K , and T in the strongly convex setup.

B.3.1 How to choose L

Let us start with (41)

$$\begin{aligned}
 \|w_i^{t,K} - \text{prox}_{F_i/\gamma}(x^t)\|^2 &\leq (1 - \eta_i \frac{\mu_F + \gamma}{2})^K \frac{2L_{\tilde{F}}}{\gamma^2} (\tilde{F}_i(w_i^{t,0}) - \tilde{F}_i(x^*)) + 12 \left(\frac{\lambda}{\mu_F + \gamma} \right)^2 \frac{1}{N_i} \sum_{j=1}^{N_i} \delta_{i,j} \\
 &\leq (1 - \eta_i \frac{\mu_F + \gamma}{2})^K \frac{\Gamma_i^{(1)}}{2} + \Gamma^{(2)} \delta_i
 \end{aligned} \tag{55}$$

where $\Gamma_i^{(1)} := 4 \frac{L_{\tilde{F}}}{\gamma^2} (\tilde{F}_i(w_i^{t,0}) - \tilde{F}_i(x^*))$ and $\Gamma^{(2)} := 12 \left(\frac{\lambda}{\mu_F + \gamma} \right)^2$. We require $\delta_i = (1 - \eta_i \frac{\mu_F + \gamma}{2})^K \frac{\Gamma_i^{(1)}}{2\Gamma^{(2)}}$, then

$$\|w_i^{t,K} - \text{prox}_{F_i/\gamma}(x^t)\|^2 \leq (1 - \eta_i \frac{\mu_F + \gamma}{2})^K \Gamma_i^{(1)} =: \nu_i. \tag{56}$$

Note also that from (52)

$$(1 - \alpha\mu_f)^L \frac{1}{\lambda^2} \|\nabla \tilde{f}_{i,j}(\theta_{i,j}^{t,k,0})\|^2 \leq \delta_{i,j} \rightarrow (1 - \alpha\mu_f)^L \frac{1}{\lambda^2} \frac{1}{N_i} \sum_{j=1}^{N_i} \|\nabla \tilde{f}_{i,j}(\theta_{i,j}^{t,k,0})\|^2 \leq \delta_i. \tag{57}$$

Using the equation above and $\delta_i = (1 - \eta_i \frac{\mu_F + \gamma}{2})^K \frac{\Gamma_i^{(1)}}{2\Gamma^{(2)}}$, we write

$$(1 - \alpha\mu_f)^L \Gamma_i^{(3)} \leq (1 - \eta_i \frac{\mu_F + \gamma}{2})^K \frac{\Gamma_i^{(1)}}{2\Gamma^{(2)}} \rightarrow L \geq \frac{\ln(1 - \eta_i \frac{\mu_F + \gamma}{2})}{\ln(1 - \alpha\mu_f)} K + \frac{1}{\ln(1 - \alpha\mu_f)} \ln \left(\frac{\Gamma_i^{(1)}}{2\Gamma^{(3)}\Gamma^{(2)}} \right) \tag{58}$$

where $\Gamma_i^{(3)} := \frac{1}{\lambda^2} \frac{1}{N_i} \sum_{j=1}^{N_i} \|\nabla \tilde{f}_{i,j}(\theta_{i,j}^{t,k,0})\|^2$. Note that (58) allows different teams to have a different number of loops to provide the needed accuracy.

B.3.2 How to choose K

Consider (29)

$$\begin{aligned}\|x^T - x^*\|^2 &\leq (1 - \frac{\beta\mu_{\tilde{F}}}{2})^T \|x^0 - x^*\|^2 + \frac{6\gamma^2\nu}{\mu_{\tilde{F}}^2} \\ &= 2(1 - \frac{\beta\mu_{\tilde{F}}}{2})^T \|x^0 - x^*\|^2\end{aligned}\quad (59)$$

where in the last line we require $\nu = \frac{\mu_{\tilde{F}}^2}{6\gamma^2}(1 - \frac{\beta\mu_{\tilde{F}}}{2})^T \|x^0 - x^*\|^2$. Also note that from (56) we can write

$$(1 - \eta_i \frac{\mu_F + \gamma}{2})^K \Gamma_i^{(1)} = \nu_i \rightarrow (1 - \eta_i \frac{\mu_F + \gamma}{2})^K \frac{1}{M} \sum_{i=1}^M \Gamma_i^{(1)} \leq (1 - \eta_{\min} \frac{\mu_F + \gamma}{2})^K \frac{1}{M} \sum_{i=1}^M \Gamma_i^{(1)} = \frac{1}{M} \sum_{i=1}^M \nu_i = \nu, \quad (60)$$

where $\eta_{\min} = \min_i \{\eta_i\}$. Finally, we can write

$$(1 - \eta_{\min} \frac{\mu_F + \gamma}{2})^K \Gamma^{(4)} \leq \Gamma^{(5)} (1 - \frac{\beta\mu_{\tilde{F}}}{2})^T \rightarrow K \geq \frac{\ln(1 - \frac{\beta\mu_{\tilde{F}}}{2})}{\ln(1 - \eta_{\min} \frac{\mu_F + \gamma}{2})} T + \frac{1}{\ln(1 - \eta_{\min} \frac{\mu_F + \gamma}{2})} \ln\left(\frac{\Gamma^{(5)}}{\Gamma^{(4)}}\right), \quad (61)$$

where $\Gamma^{(4)} := \frac{1}{M} \sum_{i=1}^M \Gamma_i^{(1)}$ and $\Gamma^{(5)} := \frac{\mu_{\tilde{F}}^2}{6\gamma^2} \|x^0 - x^*\|^2$.

B.3.3 Combining Theorem 3, Theorem 4, and Theorem 5

Assuming (58) and (61) are in force, we can derive (59)

$$\|x^T - x^*\|^2 \leq 2(1 - \frac{\beta\mu_{\tilde{F}}}{2})^T \|x^0 - x^*\|^2. \quad (62)$$

This completes the proof of Theorem 1.

C Convergence of PerMFL (non-convex case)

Let us consider the team-level update as in Algorithm 2. We analyze the convergence of this algorithm when objectives are non-convex and smooth. We assume that we have access to the approximate solution to the $\text{prox}_{F_i/\gamma}(\cdot)$.

Theorem 6. *Suppose that the sequence $\{x^t\}$ is generated by PerMFL. Further assume that $w_i^{t,k*}$ is an approximate solution to $\text{prox}_{F_i/\gamma}(x^t)$ such that $\|w_i^{t,k*} - \text{prox}_{F_i/\gamma}(x^t)\|^2 \leq \nu_i$. Then, we have*

$$\mathbb{E}[\|\nabla\phi(x^{\tilde{t}})\|^2] \leq 2 \frac{\phi(x^0) - \phi(x^*)}{\beta T} + \gamma^2 \nu. \quad (63)$$

where $\beta \leq \frac{1}{L_{\tilde{F}}}$, $\nu := \frac{1}{M} \sum_{i=1}^M \nu_i$ and \tilde{t} is uniformly sampled from $[0, T-1]$.

Proof. Using smoothness of F , we can write

$$\begin{aligned}\phi(x^{t+1}) - \phi(x^t) &\leq \langle \nabla\phi(x^t), x^{t+1} - x^t \rangle + \frac{L_{\tilde{F}}}{2} \|x^{t+1} - x^t\|^2 \\ &= -\beta \langle \nabla\phi(x^t), g^t \rangle + \beta^2 \frac{L_{\tilde{F}}}{2} \|g^t\|^2 \quad (\text{see (28)}) \\ &= -\beta \langle \nabla\phi(x^t), g^t \rangle + \frac{\beta}{2} \|g^t\|^2 + \frac{\beta}{2} (\beta L_{\tilde{F}} - 1) \|g^t\|^2 \\ &\leq -\beta \langle \nabla\phi(x^t), g^t \rangle + \frac{\beta}{2} \|g^t\|^2 \quad (\text{by choosing } \beta \leq 1/L_{\tilde{F}}) \\ &= -\frac{\beta}{2} \|\nabla\phi(x^t)\|^2 + \frac{\beta}{2} \underbrace{\|g^t - \nabla\phi(x^t)\|^2}_{J_1},\end{aligned}\quad (64)$$

where in the last line, we used $2\langle a, b \rangle = \|a\|^2 + \|b\|^2 - \|a - b\|^2$.

We bound J_1 as follows:

• **Upper bound on J_1 :**

$$\begin{aligned}
 J_1 &= \|g^t - \nabla \phi(x^t)\|^2 \\
 &= \left\| \frac{1}{M} \sum_{i=1}^M (g_i^t - \nabla \tilde{F}_i(x^t)) \right\|^2 \\
 &\leq \frac{1}{M} \sum_{i=1}^M \|g_i^t - \nabla \tilde{F}_i(x^t)\|^2 \quad (\text{see: Remark 3}) \\
 &= \frac{1}{M} \sum_{i=1}^M \|\gamma(x^t - w_i^{t,k*}) - \gamma(x^t - \text{prox}_{F_i/\gamma}(x^t))\|^2 \\
 &= \gamma^2 \frac{1}{M} \sum_{i=1}^M \|w_i^{t,k*} - \text{prox}_{F_i/\gamma}(x^t)\|^2 \\
 &\leq \gamma^2 \frac{1}{M} \sum_{i=1}^M \nu_i \\
 &= \gamma^2 \nu
 \end{aligned} \tag{65}$$

Substituting J_1 into (64), we have

$$\phi(x^{t+1}) - \phi(x^t) \leq -\frac{\beta}{2} \|\nabla \phi(x^t)\|^2 + \frac{\beta}{2} \gamma^2 \nu. \tag{66}$$

(66), can be re-written as

$$\|\nabla \phi(x^t)\|^2 \leq \frac{2}{\beta} (\phi(x^t) - \phi(x^{t+1})) + \gamma^2 \nu \tag{67}$$

Averaging (67) over t , we get

$$\begin{aligned}
 \frac{1}{T} \sum_{t=0}^{T-1} \|\nabla \phi(x^t)\|^2 &\leq \frac{1}{T} \sum_{t=0}^{T-1} \frac{2}{\beta} (\phi(x^t) - \phi(x^{t+1})) + \gamma^2 \nu \\
 &= 2 \frac{\phi(x^0) - \phi(x^T)}{\beta T} + \gamma^2 \nu \\
 &\leq 2 \frac{\phi(x^0) - \phi(x^*)}{\beta T} + \gamma^2 \nu \quad (\text{since } \phi(x^T) \geq \phi(x^*))
 \end{aligned} \tag{68}$$

Assume \tilde{t} is sampled uniformly at random from $[0, T-1]$, then we can write

$$\mathbb{E}[\|\nabla \phi(x^{\tilde{t}})\|^2] \leq 2 \frac{\phi(x^0) - \phi(x^*)}{\beta T} + \gamma^2 \nu. \tag{69}$$

□

C.1 Team-level convergence (non-convex case)

Theorem 7. Consider Problem 6 with gradient descent steps (9), and assume that we have $\|\text{prox}_{f_{i,j}/\lambda}(w_i^{t,k}) - \theta_{i,j}^{t,k,L}\|^2 \leq \delta_{i,j}$. We can write

$$\|w_i^{t,k*} - \text{prox}_{F_i/\gamma}(x^t)\|^2 \leq \frac{1}{(\gamma - L_{\tilde{f}})^2} \left(\frac{2}{K\eta_i} (F_i(x^t) - \text{prox}_{F_i/\gamma}(x^t)) + \lambda^2 \frac{1}{N_i} \sum_{j=1}^{N_i} \delta_{i,j} \right) =: \nu_i \tag{70}$$

where $\eta_i \leq \frac{1}{(L_{\tilde{f}} + \gamma)}$, $\gamma > L_{\tilde{f}}$, and $w_i^{t,k*} = \arg \min_k \{\|\nabla p_i(w_i^{t,k})\|^2\}$.

Proof. Let us define $p_i(y) := F_i(y) + \frac{\gamma}{2} \|y - x^t\|^2$. Since $\tilde{f}_{i,j}(\cdot)$ is $L_{\tilde{f}}$ -Smooth therefore $F_i(\cdot) = \frac{1}{N_i} \sum_{j=1}^{N_i} \tilde{f}_{i,j}(\cdot)$ and $p_i(\cdot)$ are $L_{\tilde{f}}$ -Smooth and $(L_{\tilde{f}} + \gamma)$ -Smooth, respectively. Using smoothness, we have

$$p_i(w_i^{t,k+1}) - p_i(w_i^{t,k}) \leq \langle \nabla p_i(w_i^{t,k}), w_i^{t,k+1} - w_i^{t,k} \rangle + \frac{L_{\tilde{f}} + \gamma}{2} \|w_i^{t,k+1} - w_i^{t,k}\|^2 \tag{71}$$

Now, let us re-write (9) as $w_i^{t,k+1} = w_i^{t,k} - \eta_i q_i^{t,k}$, where $q_i^{t,k}$ is the inexact gradient of $p_i(y) := F_i(y) + \frac{\gamma}{2}\|y - x^t\|^2$ at $y = w_i^{t,k}$.

$$\begin{aligned}
 p_i(w_i^{t,k+1}) - p_i(w_i^{t,k}) &\leq \langle \nabla p_i(w_i^{t,k}), w_i^{t,k+1} - w_i^{t,k} \rangle + \eta_i^2 \frac{L_{\bar{f}} + \gamma}{2} \|q_i^{t,k}\|^2 \\
 &= -\eta_i \langle \nabla p_i(w_i^{t,k}), q_i^{t,k} \rangle + \eta_i^2 \frac{L_{\bar{f}} + \gamma}{2} \|q_i^{t,k}\|^2 \\
 &= -\frac{\eta_i}{2} \|\nabla p_i(w_i^{t,k})\|^2 - \frac{\eta_i}{2} \|q_i^{t,k}\|^2 + \frac{\eta_i}{2} \|q_i^{t,k} - \nabla p_i(w_i^{t,k})\|^2 + \eta_i^2 \frac{L_{\bar{f}} + \gamma}{2} \|q_i^{t,k}\|^2 \\
 &= -\frac{\eta_i}{2} \|\nabla p_i(w_i^{t,k})\|^2 - \frac{\eta_i}{2} \left(1 - \eta_i(L_{\bar{f}} + \gamma)\right) \|q_i^{t,k}\|^2 + \frac{\eta_i}{2} \|q_i^{t,k} - \nabla p_i(w_i^{t,k})\|^2 \\
 &= -\frac{\eta_i}{2} \|\nabla p_i(w_i^{t,k})\|^2 + \frac{\eta_i}{2} \|q_i^{t,k} - \nabla p_i(w_i^{t,k})\|^2
 \end{aligned} \tag{72}$$

where in the third line, we used $2\langle a, b \rangle = \|a\|^2 + \|b\|^2 - \|a - b\|^2$ and in the last line we used $\eta_i \leq \frac{1}{L_{\bar{f}} + \gamma}$.

Re-arranging and averaging over k , we get

$$\begin{aligned}
 \frac{1}{K} \sum_{k=0}^{K-1} \left(\|\nabla p_i(w_i^{t,k})\|^2 - \|q_i^{t,k} - \nabla p_i(w_i^{t,k})\|^2 \right) &\leq \frac{2}{K\eta_i} (p_i(w_i^{t,0}) - p_i(w_i^{t,K})) \\
 &\leq \frac{2}{K\eta_i} (p_i(x^t) - p_i(w_i^{t,K})) \\
 &\leq \frac{2}{K\eta_i} (p_i(x^t) - p_i(w_i^{t,*})) \\
 &\leq \frac{2}{K\eta_i} (F_i(x^t) - \text{prox}_{F_i/\gamma}(x^t)).
 \end{aligned} \tag{73}$$

Substituting the assumption $\|\text{prox}_{f_{i,j}/\lambda}(w_i^{t,k}) - \theta_{i,j}^{t,k,L}\|^2 \leq \delta_{i,j}$, we get

$$\begin{aligned}
 \frac{1}{K} \sum_{k=0}^{K-1} \|\nabla p_i(w_i^{t,k})\|^2 &\leq \frac{2}{K\eta_i} (F_i(x^t) - \text{prox}_{F_i/\gamma}(x^t)) + \frac{1}{K} \sum_{k=0}^{K-1} \|q_i^{t,k} - \nabla p_i(w_i^{t,k})\|^2 \\
 &\leq \frac{2}{K\eta_i} (F_i(x^t) - \text{prox}_{F_i/\gamma}(x^t)) + \lambda^2 \frac{1}{K} \sum_{k=0}^{K-1} \left\| \frac{1}{N_i} \sum_{j=1}^{N_i} (\text{prox}_{f_{i,j}/\lambda}(w_i^{t,k}) - \theta_{i,j}^{t,k,L}) \right\|^2 \\
 &\leq \frac{2}{K\eta_i} (F_i(x^t) - \text{prox}_{F_i/\gamma}(x^t)) + \lambda^2 \frac{1}{K} \sum_{k=0}^{K-1} \frac{1}{N_i} \sum_{j=1}^{N_i} \|(\text{prox}_{f_{i,j}/\lambda}(w_i^{t,k}) - \theta_{i,j}^{t,k,L})\|^2 \\
 &\leq \frac{2}{K\eta_i} (F_i(x^t) - \text{prox}_{F_i/\gamma}(x^t)) + \lambda^2 \frac{1}{N_i} \sum_{j=1}^{N_i} \delta_{i,j}
 \end{aligned} \tag{74}$$

Let us define $w_i^{t,k*} = \arg \min_k \{\|\nabla p_i(w_i^{t,k})\|^2\}$, then we can write

$$\frac{1}{K} \sum_{k=0}^{K-1} \|\nabla p_i(w_i^{t,k})\|^2 \geq \|\nabla p_i(w_i^{t,k*})\|^2 \geq (\gamma - L_{\bar{f}})^2 \|w_i^{t,k*} - w_i^{t,*}\|^2 \geq (\gamma - L_{\bar{f}})^2 \|w_i^{t,k*} - \text{prox}_{F_i/\gamma}(x^t)\|^2 \tag{75}$$

where we used (18) because $p_i(\cdot)$ is $(\gamma - L_{\bar{f}})$ -strongly convex. Finally, we can combine (74) and (75)

$$\|w_i^{t,k*} - \text{prox}_{F_i/\gamma}(x^t)\|^2 \leq \frac{1}{(\gamma - L_{\bar{f}})^2} \left(\frac{2}{K\eta_i} (F_i(x^t) - \text{prox}_{F_i/\gamma}(x^t)) + \lambda^2 \frac{1}{N_i} \sum_{j=1}^{N_i} \delta_{i,j} \right) =: \nu_i \tag{76}$$

□

C.2 Client-level convergence (non-convex case)

Theorem 8. Let $f_{i,j}$ be L_f -smooth functions. Consider Problem 3 with gradient descent steps (4), we have

$$\|\theta_{i,j}^{t,k,*} - \text{prox}_{f_{i,j}/\lambda}(w_i^{t,k})\|^2 \leq \frac{1}{L\alpha(1 - \frac{L_F + \lambda}{2}\alpha)(\gamma - L_{\bar{f}})^2} (f_{i,j}(\theta_{i,j}^{t,k,0}) - \tilde{f}_{i,j}(\theta_{i,j}^{t,k,0})) =: \delta_{i,j} \tag{77}$$

where $\alpha \leq \frac{2}{L_F + \lambda}$ and $\theta_{i,j}^{t,k,l*} = \arg \min_l \{\|\nabla p_{i,j}(\theta_{i,j}^{t,k,l})\|^2\}$.

Proof. Let us define $p_{i,j}(y) := f_{i,j}(y) + \frac{\lambda}{2}\|y - w_i^{t,k}\|^2$. Note that $p_{i,j}(\cdot)$ is $(L_f + \lambda)$ -smooth. Using smoothness, we have

$$\begin{aligned} p_{i,j}(\theta_{i,j}^{t,k,l+1}) - p_{i,j}(\theta_{i,j}^{t,k,l}) &\leq \langle \nabla p_{i,j}(\theta_{i,j}^{t,k,l}), \theta_{i,j}^{t,k,l+1} - \theta_{i,j}^{t,k,l} \rangle + \frac{L_F + \lambda}{2} \|w_i^{t,k+1} - w_i^{t,k}\|^2 \\ &= \langle \nabla p_{i,j}(\theta_{i,j}^{t,k,l}), -\alpha \nabla p_{i,j}(\theta_{i,j}^{t,k,l}) \rangle + \frac{L_F + \lambda}{2} \alpha^2 \|\nabla p_{i,j}(\theta_{i,j}^{t,k,l})\|^2 \quad (\text{see (4)}) \\ &= -\alpha(1 - \alpha \frac{L_F + \lambda}{2}) \|\nabla p_{i,j}(\theta_{i,j}^{t,k,l})\|^2. \end{aligned} \quad (78)$$

Averaging over l and assuming $\alpha \leq \frac{2}{L_F + \lambda}$, we get

$$\begin{aligned} \frac{1}{L} \sum_{l=0}^{L-1} \|\nabla p_{i,j}(\theta_{i,j}^{t,k,l})\|^2 &\leq \frac{1}{L\alpha(1 - \frac{L_F + \lambda}{2}\alpha)} (p_{i,j}(\theta_{i,j}^{t,k,0}) - p_{i,j}(\theta_{i,j}^{t,k,L})) \\ &\leq \frac{1}{L\alpha(1 - \frac{L_F + \lambda}{2}\alpha)} (p_{i,j}(w_i^{t,k}) - p_{i,j}(\theta_{i,j}^{t,k,*})) \quad (\theta_{i,j}^{t,k,0} = w_i^{t,k}, p_{i,j}(\theta_{i,j}^{t,k,L}) \geq p_{i,j}(\theta_{i,j}^{t,k,*})) \\ &= \frac{1}{L\alpha(1 - \frac{L_F + \lambda}{2}\alpha)} (f_{i,j}(w_i^{t,k}) - \tilde{f}_{i,j}(w_i^{t,k})) \quad (\theta_{i,j}^{t,k,*} = \text{prox}_{f_{i,j}/\lambda}(w_i^{t,k})) \\ &\leq \frac{1}{L\alpha(1 - \frac{L_F + \lambda}{2}\alpha)} (f_{i,j}(\theta_{i,j}^{t,k,0}) - \tilde{f}_{i,j}(\theta_{i,j}^{t,k,0})) \end{aligned} \quad (79)$$

Let us define $\theta_{i,j}^{t,k,l*} = \arg \min_l \{\|\nabla p_{i,j}(\theta_{i,j}^{t,k,l})\|^2\}$, then we can write

$$\frac{1}{L} \sum_{l=0}^{L-1} \|\nabla p_{i,j}(\theta_{i,j}^{t,k,l})\|^2 \geq \|\nabla p_{i,j}(\theta_{i,j}^{t,k,l*})\|^2 \geq (\gamma - L_{\tilde{f}})^2 \|\theta_{i,j}^{t,k,l*} - \theta_{i,j}^{t,k,*}\|^2 \geq (\gamma - L_{\tilde{f}})^2 \|\theta_{i,j}^{t,k,l*} - \text{prox}_{f_{i,j}/\lambda}(w_i^{t,k})\|^2 \quad (80)$$

where we used (18) with $x = \theta_{i,j}^{t,k,l*}$, $y = \theta_{i,j}^{t,k,*}$, $\nabla p_{i,j}(\theta_{i,j}^{t,k,*}) = 0$ because $p_{i,j}(\cdot)$ is $(\gamma - L_{\tilde{f}})$ -strongly convex. Finally, we can combine (79) and (80)

$$\|\theta_{i,j}^{t,k,l*} - \text{prox}_{f_{i,j}/\lambda}(w_i^{t,k})\|^2 \leq \frac{1}{L\alpha(1 - \frac{L_F + \lambda}{2}\alpha)(\gamma - L_{\tilde{f}})^2} (f_{i,j}(\theta_{i,j}^{t,k,0}) - \tilde{f}_{i,j}(\theta_{i,j}^{t,k,0})) =: \delta_{i,j} \quad (81)$$

□

C.3 Discussion on error bounds (non-convex case)

In this section, we discuss the relation between L , K , and T in the non-convex setup.

C.4 How to choose L

From (70), we have

$$\begin{aligned} \|w_i^{t,k*} - \text{prox}_{F_i/\gamma}(x^t)\|^2 &\leq \frac{1}{(\gamma - L_{\tilde{f}})^2} \left(\frac{2}{K\eta_i} (F_i(x^t) - \text{prox}_{F_i/\gamma}(x^t)) + \lambda^2 \frac{1}{N_i} \sum_{j=1}^{N_i} \delta_{i,j} \right) \\ &= \frac{1}{(\gamma - L_{\tilde{f}})^2} \left(\frac{2}{K\eta_i} (F_i(x^t) - \text{prox}_{F_i/\gamma}(x^t)) + \lambda^2 \delta_i \right) \\ &\leq \frac{B_i^1}{K} = \nu_i \end{aligned} \quad (82)$$

where $B_i^1 = \frac{4}{\eta_i(\gamma - L_{\tilde{f}})^2} (F_i(x^t) - \text{prox}_{F_i/\gamma}(x^t))$ by requiring $\delta_i \leq \frac{2}{\lambda^2 \eta_i K} (F_i(x^t) - \text{prox}_{F_i/\gamma}(x^t))$. Note that, from (81), we can write

$$\frac{1}{L_i\alpha(1 - \frac{L_F + \lambda}{2}\alpha)(\gamma - L_{\tilde{f}})^2} \frac{1}{N_i} \sum_{j=1}^{N_i} (f_{i,j}(\theta_{i,j}^{t,k,0}) - \tilde{f}_{i,j}(\theta_{i,j}^{t,k,0})) = \frac{1}{N_i} \sum_{j=1}^{N_i} \delta_{i,j} = \delta_i, \quad (83)$$

and therefore

$$\frac{1}{L_i \alpha (1 - \frac{L_F + \lambda}{2} \alpha) (\gamma - L_{\tilde{f}})^2} \frac{1}{N_i} \sum_{j=1}^{N_i} (f_{i,j}(\theta_{i,j}^{t,k,0}) - \tilde{f}_{i,j}(\theta_{i,j}^{t,k,0})) = \delta_i \leq \frac{2}{\lambda^2 \eta_i K} (F_i(x^t) - \text{prox}_{F_i/\gamma}(x^t)). \quad (84)$$

This leads to

$$L_i \geq B_i^2 K \quad (85)$$

where $B_i^2 = \frac{\lambda^2 \eta_i}{2\alpha(1 - \frac{L_F + \lambda}{2} \alpha) (\gamma - L_{\tilde{f}})^2} \frac{1}{N_i} \sum_{j=1}^{N_i} (\frac{f_{i,j}(\theta_{i,j}^{t,k,0}) - \tilde{f}_{i,j}(\theta_{i,j}^{t,k,0})}{F_i(x^t) - \text{prox}_{F_i/\gamma}(x^t)})$. Note that (85) allows different teams to have a different number of loops to provide the needed accuracy.

C.5 How to choose K

From (63), we have

$$\begin{aligned} \mathbb{E}[\|\nabla \phi(x^t)\|^2] &\leq 2 \frac{\phi(x^0) - \phi(x^*)}{\beta T} + \beta L_{\tilde{F}} \gamma^2 \nu \\ &\leq \frac{B^3}{T} \end{aligned} \quad (86)$$

where $B^3 = 4 \frac{\phi(x^0) - \phi(x^*)}{\beta}$ by requiring $\nu \leq 2 \frac{\phi(x^0) - \phi(x^*)}{\beta^2 \gamma^2 L_{\tilde{F}} T}$. Using equation above and (82), we get

$$\frac{1}{K} \frac{1}{M} \sum_{i=1}^M B_i^1 = \frac{1}{M} \sum_{i=1}^M \nu_i = \nu \leq 2 \frac{\phi(x^0) - \phi(x^*)}{\beta^2 \gamma^2 L_{\tilde{F}} T}. \quad (87)$$

That leads to

$$K \geq B^4 T \quad (88)$$

where $B^4 := \frac{\beta^2 \gamma^2 L_{\tilde{F}} T}{2(\phi(x^0) - \phi(x^*))} \frac{1}{M} \sum_{i=1}^M B_i^1$.

C.6 Combining Theorem 6, Theorem 7, and Theorem 8

Assuming (85) and (88) are in force, we can derive (86)

$$\mathbb{E}_t[\|\nabla \phi(x^t)\|^2] \leq 4 \frac{\phi(x^0) - \phi(x^*)}{\beta} \frac{1}{T} = \mathcal{O}\left(\frac{1}{T}\right). \quad (89)$$

This can be translated to

$$\mathbb{E}_t[\|\nabla \phi(x^t)\|] \leq \mathcal{O}\left(\frac{1}{\sqrt{T}}\right). \quad (90)$$

D Experiments

We studied classification problems to validate PerMFL using both image (MNIST [31], FMNIST [32] EMNIST [33] with 10 classes and 62 classes, CIFAR100 [34]) and non-image synthetic datasets, but PerMFL is not limited to these two categories of data. Data distributions are heterogeneous and non-iid. The distribution of the EMNIST dataset with 62 classes exhibits non-iid characteristics similar to the FEMNIST dataset. Consequently, we will distinguish EMNIST with 10 classes as 'EMNIST' and EMNIST with 62 classes as 'FEMNIST'. In the case of MNIST, FMNIST, EMNIST, and synthetic datasets, each device contains data for 2 classes. However, for FEMNIST and CIFAR100 datasets, each device carries data for 3 classes. There are no overlapping samples among devices. This supplementary material provides the following experiments and analysis to validate the PerMFL.

1. A detailed empirical study to investigate the impact of hyperparameters β , λ , and γ on the convergence of PerMFL (see Appendix D.4).
2. An ablation study to analyze the influence of team and device participation (see Appendix D.5).
3. An ablation study to explore team formation, i.e., the performance of PerMFL on worst-case and average-case team formation (see Section 4.1.4).
4. An ablation study that explores the effects of team iterations on the convergence of PerMFL (see Appendix D.6).
5. Convergence analysis on MNIST and synthetic datasets with the multi-tier SOTA such as (AL2GD[18], h-SGD [5], [19]) (see Appendix D.7).
6. Performance analysis of PerMFL on FEMNIST and CIFAR100 datasets (see Appendix D.8).

Each experiments ran 10 times, from there we produced mean and standard deviation.

D.1 Hardware specification

The experiments were conducted using an NVIDIA DGX-A100 GPU with 40 GB of RAM. The DGX-A100 is based on the NVIDIA A100 Tensor Core GPU architecture, and each A100 GPU in the system has 40 GB of high-bandwidth memory (HBM2). The standard configuration of the DGX-A100 includes eight A100 GPUs connected via NVLink, providing a total of 320 GB of GPU memory (40 GB per GPU \times 8 GPUs). However, we could utilize only one GPU at a time for our experiments, which allowed us to utilize 40 GB of GPU memory per experiment.

D.2 Dataset description

We conducted our experiments using MNIST, FMNIST, EMNIST, FEMNIST, CIFAR100 and Synthetic datasets. FEMNIST, CIFAR100, and synthetic datasets are considered to create larger and more complicated scenarios from these datasets. The description of the datasets is given below.

D.2.1 MNIST

The primary purpose of the MNIST dataset is to serve as a widely used benchmark for evaluating and comparing the performance of various models in image classification tasks. It consists of a total of 70,000 examples, with 60,000 examples used for training and 10,000 examples used for testing. Each example is a grayscale image measuring 28x28 pixels, representing a handwritten digit ranging from 0 to 9. Every image in the dataset is associated with a label that denotes the correct digit it represents. The labels themselves are integers ranging from 0 to 9, corresponding to the handwritten digits in the images.

D.2.2 FMNIST

The FMNIST dataset serves the purpose of evaluating and benchmarking machine learning algorithms, particularly in the areas of image classification and pattern recognition. It differs from the original MNIST dataset by focusing on fashion-related images rather than handwritten digits, providing a more complex task. The dataset consists of 70,000 grayscale images with dimensions of 28x28 pixels. These images are split into 60,000 training examples and 10,000 testing examples. They depict various fashion items, including clothing, shoes, bags, and accessories. Each image in the FMNIST dataset is associated with a label representing the corresponding fashion item category. There are a total of 10 classes representing different types of clothing and fashion accessories such as T-shirt/top, Trouser, Pullover, Dress, Coat, Sandal, Shirt, Sneaker, Bag, and Ankle boot. Compared to the MNIST dataset, FMNIST presents a more significant challenge due to the diversity of clothing types and the increased complexity of the images. These datasets are often utilized to assess the robustness and generalization capabilities of machine learning models.

D.2.3 EMNIST

The dataset is a collection of handwritten characters, including lowercase and uppercase letters and digits. It consists of six different splits or variations, each representing a different task or scenario. The first split, called EMNIST ByClass, contains a total of 814,255 images representing 62 character classes. These classes include 26 uppercase letters, 26 lowercase letters, and 10 digits. The second split, EMNIST ByMerge, merges similar characters into a single class, resulting in 47 classes. This split is useful and challenging for scenarios where distinguishing between similar characters, such as uppercase and lowercase letters. The third split, EMNIST Balanced, aims to balance the number of samples per class. It provides a balanced dataset with 131,600 images representing 47 classes. The fourth split, EMNIST Letters, focuses exclusively on uppercase and lowercase letters. It consists of 145,600 images representing 26 classes of letters. The fifth split, EMNIST Digits, contains only the digits from 0 to 9. It consists of 280,000 images representing the 10-digit classes. Lastly, the sixth split follows the structure of the original MNIST dataset that contains 70,000 images of digits from 0 to 9. Each image in the dataset is associated with a label indicating the corresponding character class that provided information about the specific representative character or digit. Here for all the experiments, we considered split by digits.

D.2.4 FEMNIST

It is a Federated EMNIST dataset. It is a ByClass split over the EMNIST dataset containing 814,255 images representing 62 character classes (0-9, A-Z, and a-z). The data are distributed among 3500 devices in an unbalanced manner, where each device has access to a maximum of 3 classes. FEMNIST is similar to [35].

D.2.5 CIFAR100

This dataset is a collection of 60,000 32x32 colour images in 100 classes, with 600 images per class. The dataset is distributed among 350 clients in an unbalanced manner where each client can access 3 classes.

D.2.6 Synthetic

We generate a synthetic dataset with $\bar{\alpha} = 0.5$ and $\bar{\beta} = 0.5$. The synthetic dataset is a tabular dataset. It has 60 features and 10 classes. The sample size of each client ranges from 250 to 25810, and each client has almost 2 classes. Finally, we distribute the data to N devices according to the power law in [36].

D.2.7 Data division

MNIST, FMNIST, EMNIST, and synthetic datasets have ten different class labels representing distinct data distributions. The data was divided among multiple devices in a non-iid manner that ensured each device had information from two classes. To ensure each device has two classes, first, we gave specific data from each of these two classes to that device and then randomly distributed the remaining samples from these two classes. A similar approach is taken for the other devices. Following that, the devices were further divided into teams randomly. In the experiments, teams have an equal number of devices.

D.3 Learning models

Our study examined different scenarios and used specific models to handle them. We employed a multi-nomial logistic regression (MLR) model with l_2 regularization and a softmax activation function for strongly convex scenarios. To handle non-convex scenarios, we adopted different approaches depending on the dataset. For synthetic datasets, we constructed deep neural networks with two hidden layers. On the other hand, for the MNIST, FMNIST, and EMNIST datasets, which also involve non-convex scenarios, we built three two-layered convolutional neural networks (CNNs).

Throughout our experiments, we used the abbreviations (PM) and (GM) to refer to the personalized model and global model, respectively.

D.4 Effect of hyperparameters

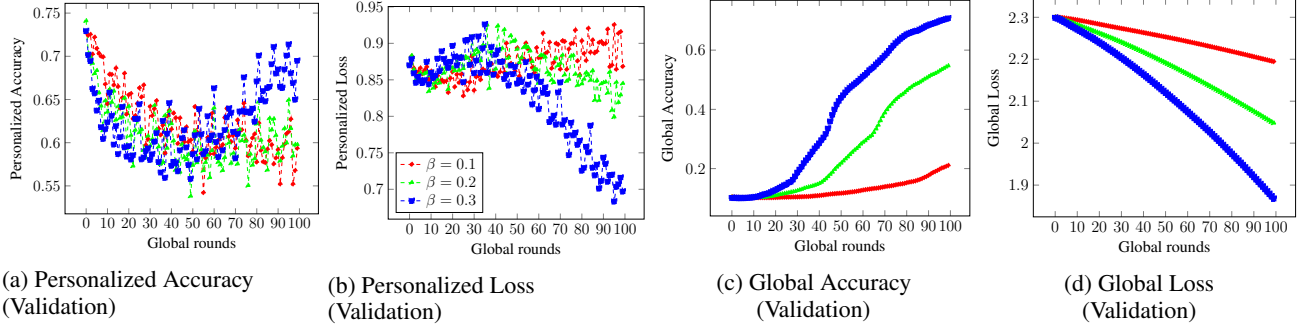
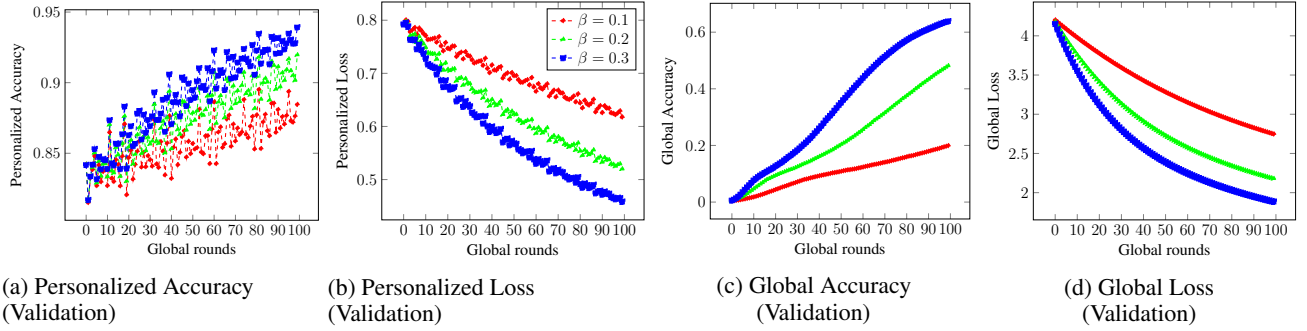
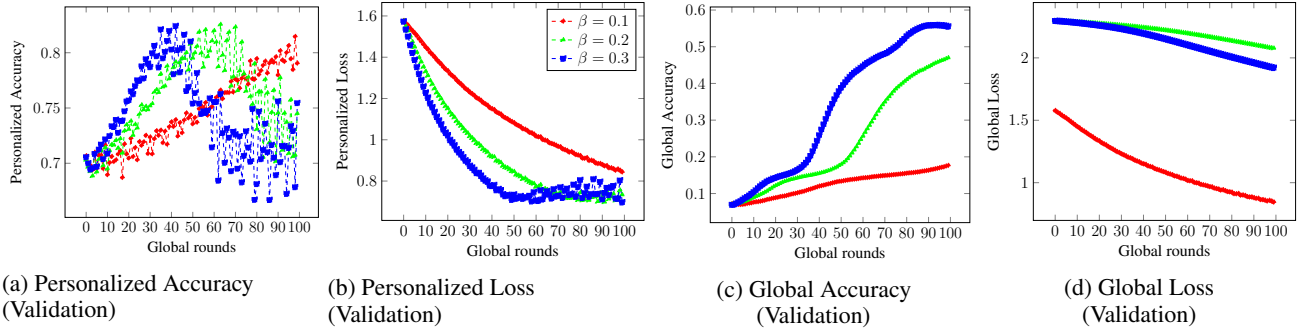
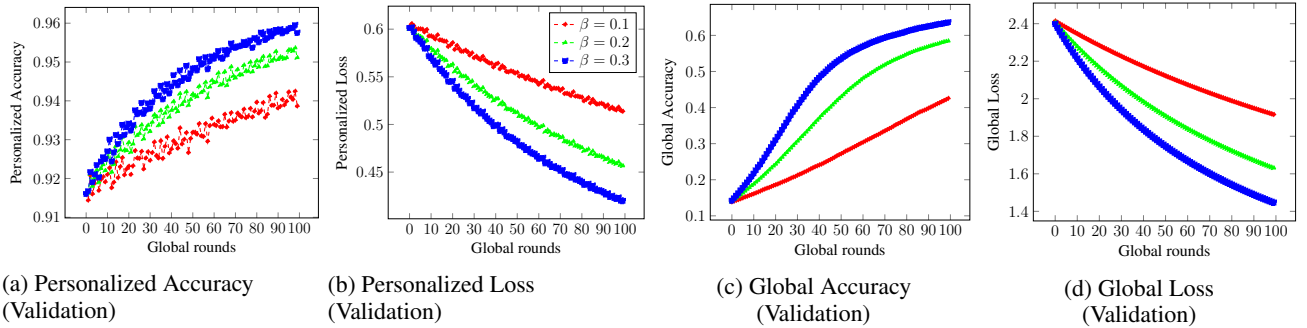
A series of tests were conducted on the MNIST, FMNIST, and Synthetic datasets to examine the impact of various hyperparameters, including λ , γ , and β , on the convergence of PerMFL. These tests were performed for both smooth strongly convex and smooth non-convex scenarios. The entire experiment is performed with the full participation of teams and devices for each global rounds. The number of teams is four, and each team has ten devices.

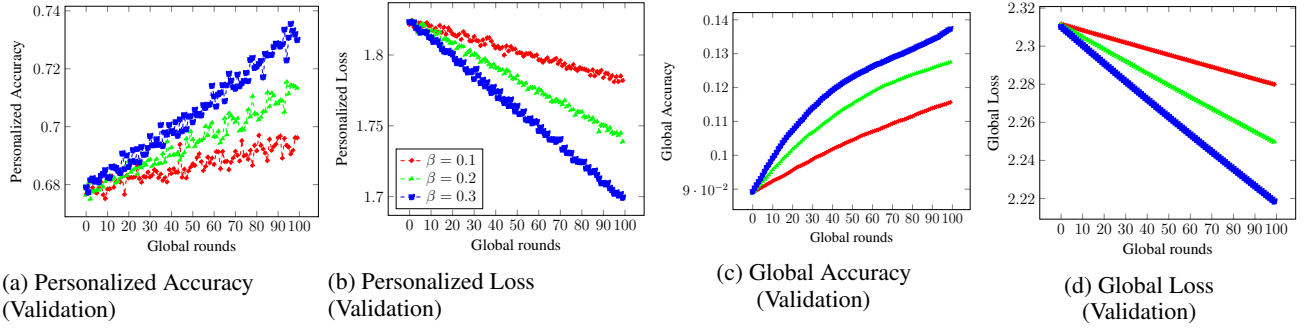
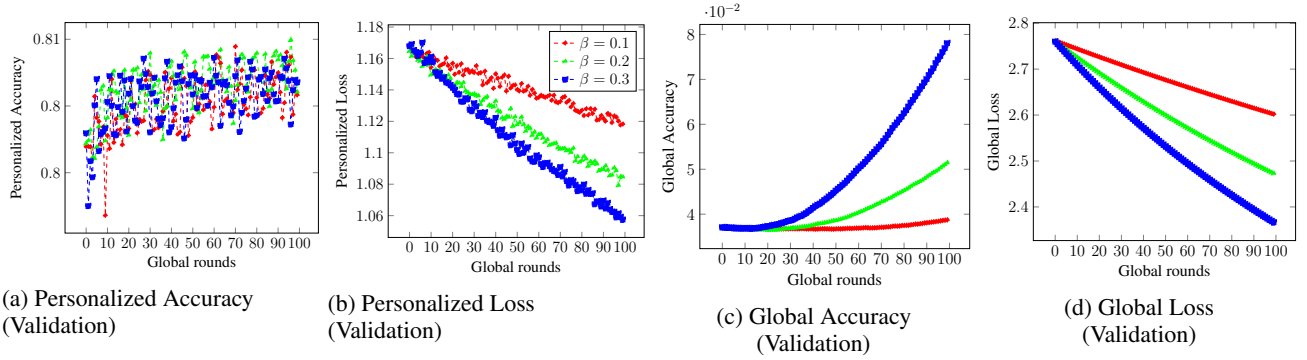
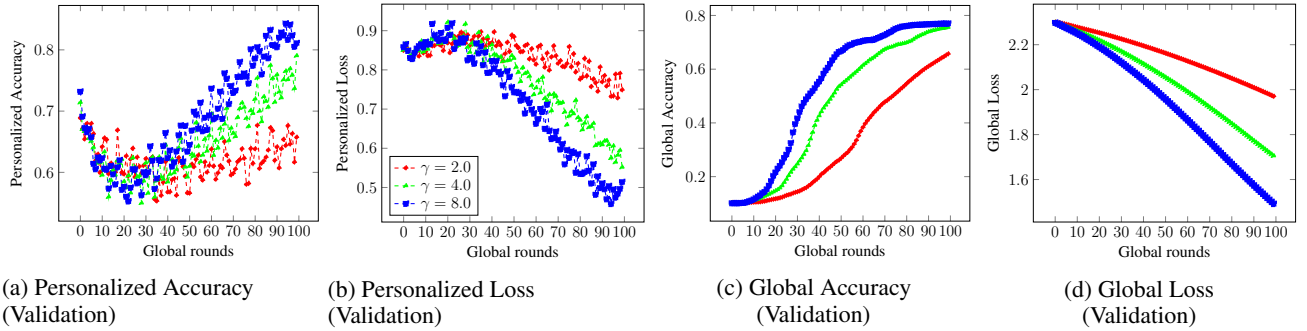
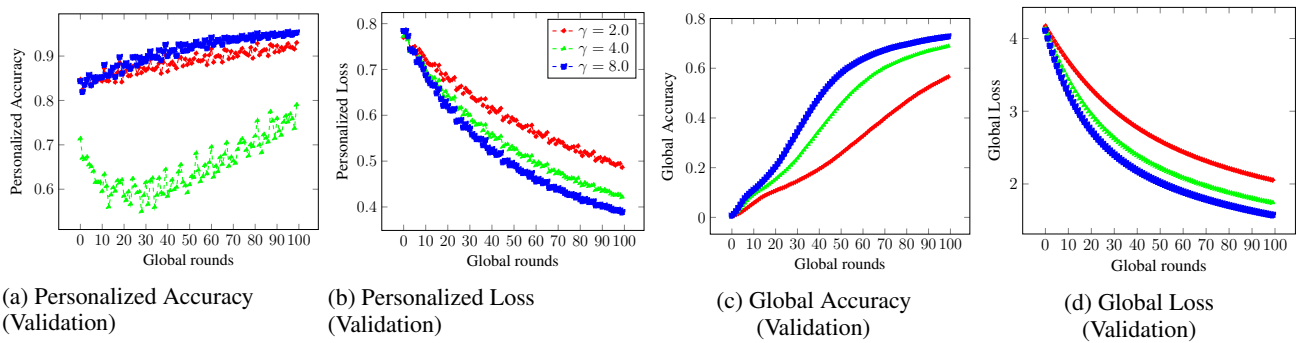
Effect of β : In this study, we made the following observation: when we increased the value of β (see Figure 5 to Figure 10) while other hyperparameters λ , and γ remains constant, both personalized and global model of PerMFL exhibited faster convergence. This behaviour was consistent in both convex and non-convex settings. Very low values of β do not generalize the global model well and delay the convergence of personalized and global models. A high value of β better generalizes the global model and the convergence faster. In all experiments from Figure 5 to Figure 10, we set the value of $\gamma = 3.0$ and $\lambda = 0.5$, $\eta = 0.03$, and $\alpha = 0.01$.

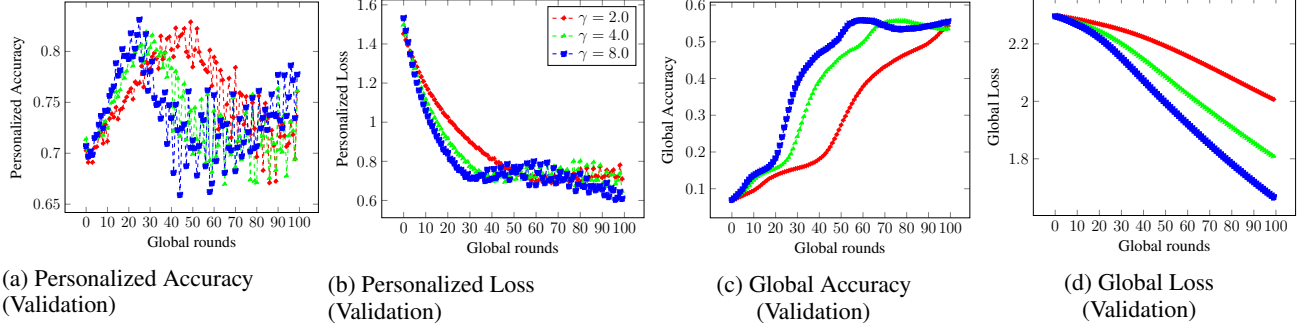
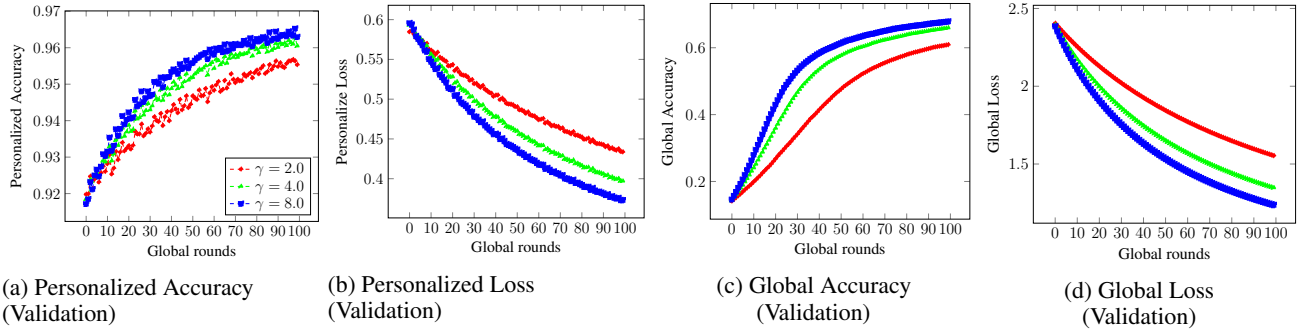
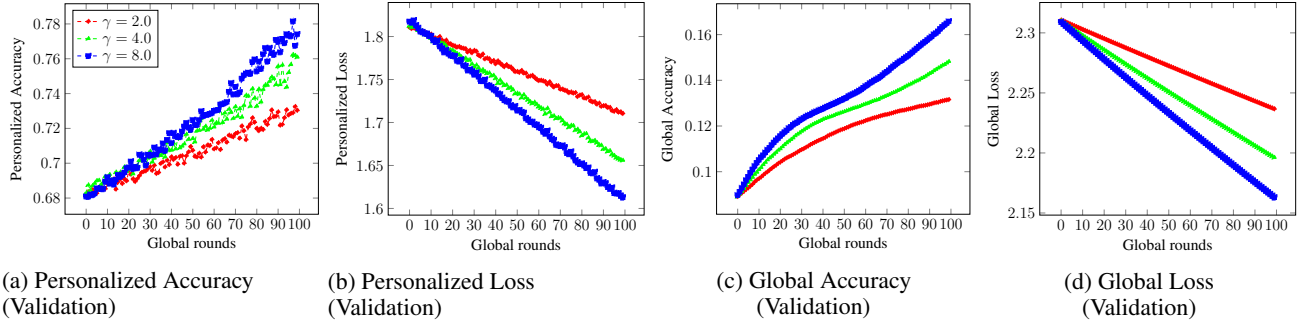
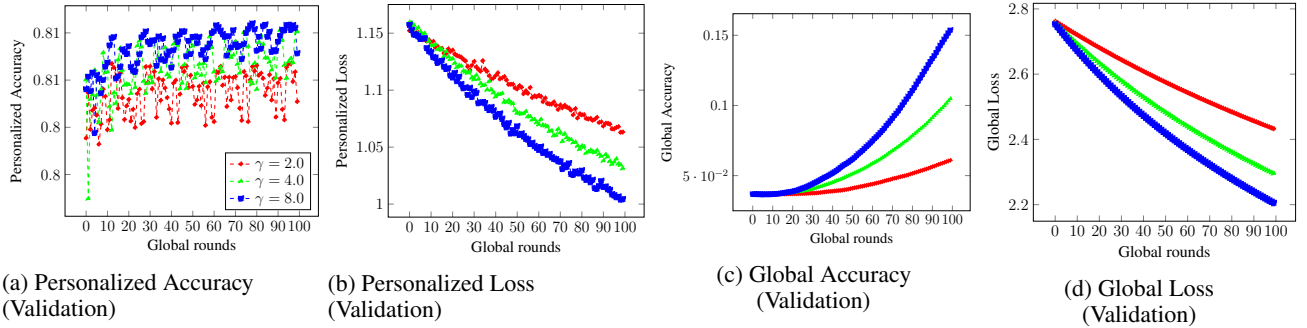
Effect of γ : In this study, we examined the influence of the hyperparameter γ on the convergence of PerMFL. From Figure 11 to Figure 16, we observed that increasing the value of γ led to faster convergence of PerMFL PM and GM. Like β , a low value of γ does not generalize the model well and slows the convergence speed of personalized and global models. Increasing the value of γ results in a better generalization with a faster convergence. In all experiments from Figure 11 to Figure 16, we set the value of $\lambda = 1.5$ and $\beta = 0.1$, $\eta = 0.03$, and $\alpha = 0.01$.

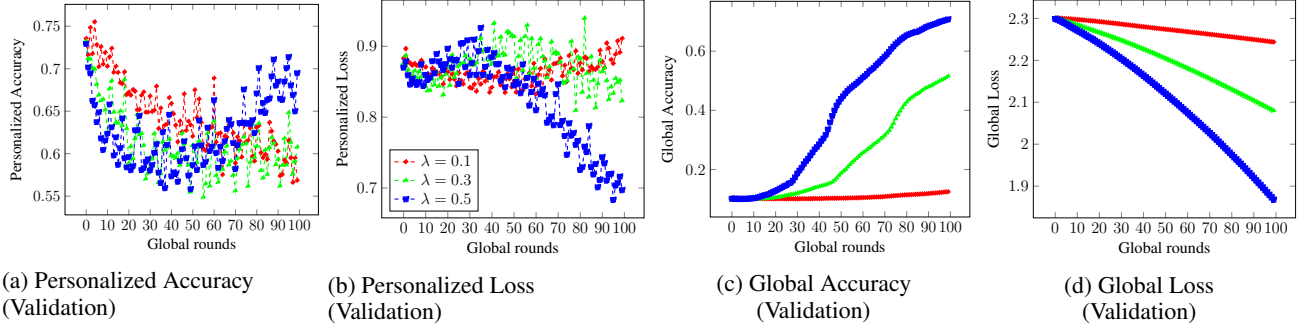
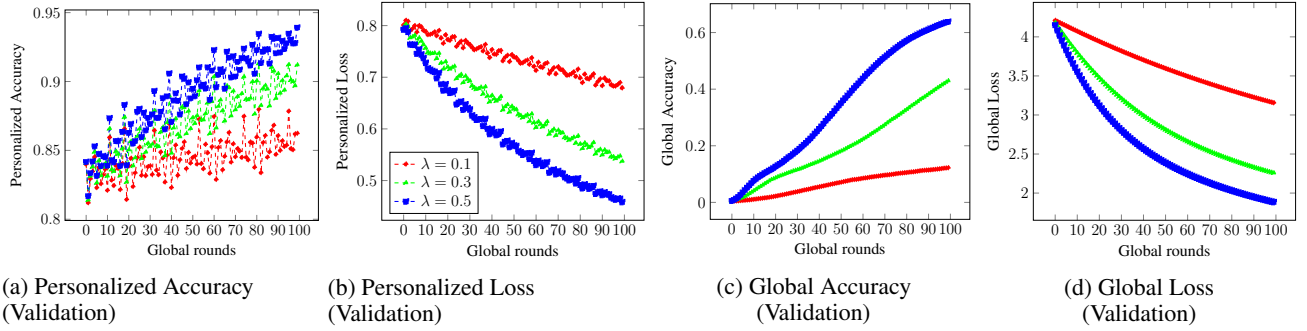
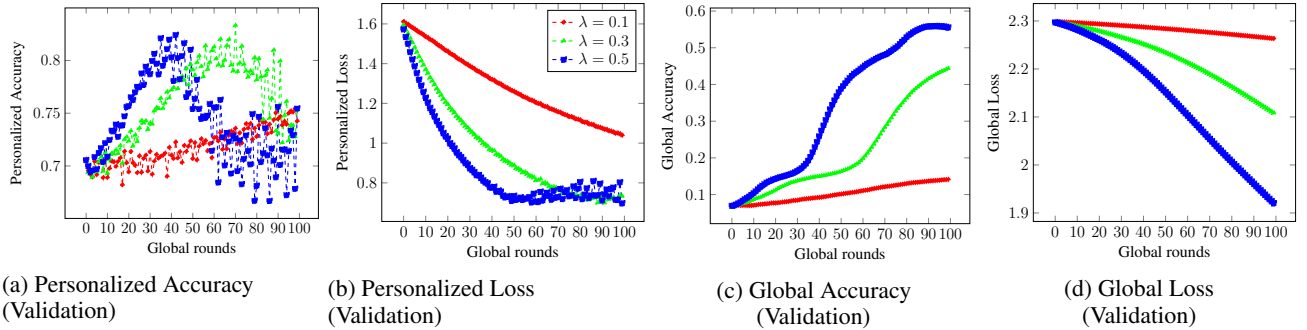
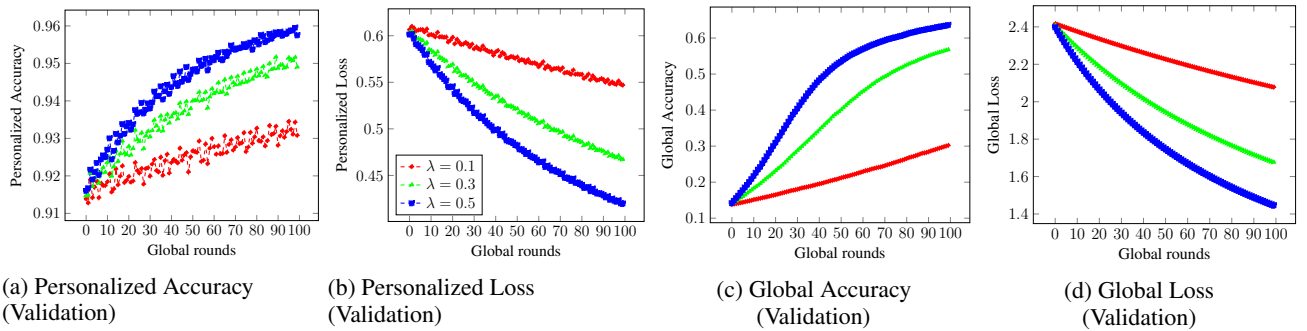
Effect of λ : Here, we examined the influence of the hyperparameter λ on the convergence of PerMFL. From the experimental results (see Figure 17 to Figure 21), we found that a low value of λ tended to impede the convergence process of both the personalized and global models. However, by increasing the value of λ , we observed a significant improvement in convergence. All the experiments from Figure 17 to Figure 21, we set the value of $\beta = 0.3$ and $\gamma = 3.0$, $\eta = 0.03$, and $\alpha = 0.01$.

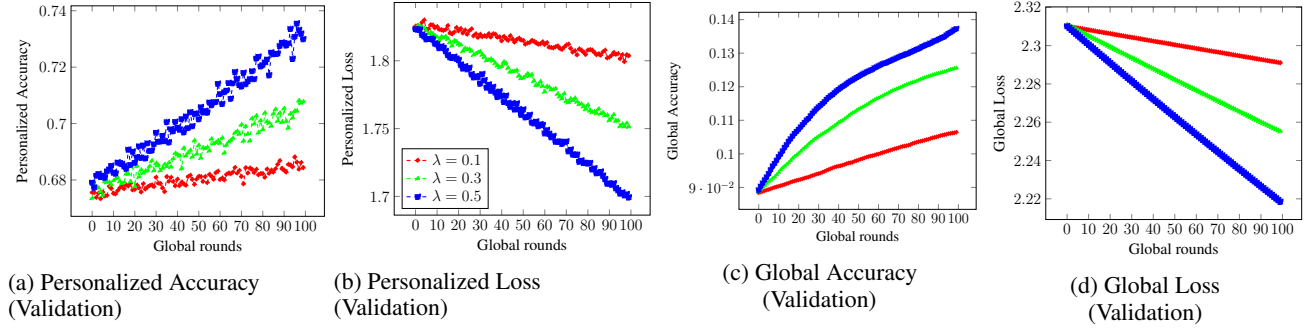
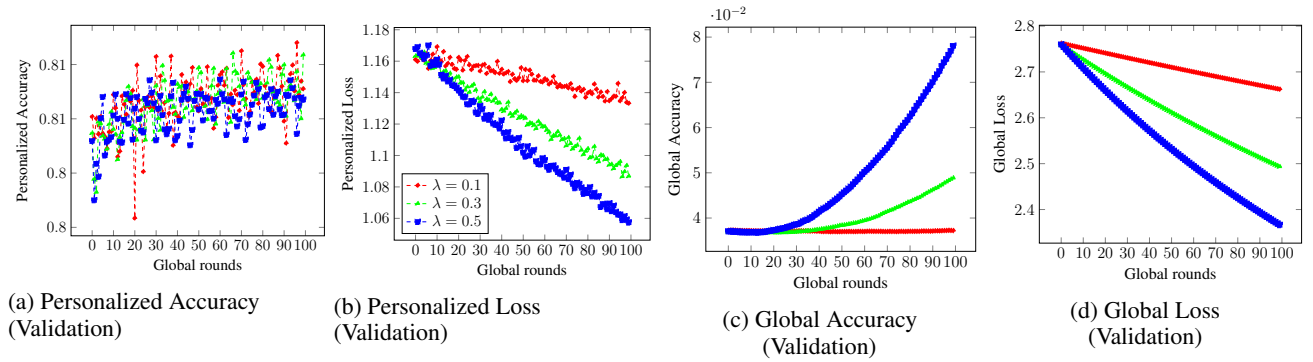
Discussions : The hyperparameters β , γ , and λ exhibit interdependencies that should be taken into consideration. Modifying the value of a single hyperparameter can significantly influence the learning of both the personalized and global models. Consequently, it is crucial to recognize the intricate relationship among these hyperparameters, as changes in one hyperparameter can have consequential effects on the overall learning process. Therefore, thoroughly evaluating these hyperparameters is essential to achieve optimal model performance and convergence.


 Figure 5: Effect of β on convergence of PerMFL in non-convex settings (CNN) using MNIST dataset

 Figure 6: Effect of β on convergence of PerMFL in strongly convex settings (MCLR) using MNIST dataset

 Figure 7: Effect of β on convergence of PerMFL in non-convex settings (CNN) using FMNIST dataset

 Figure 8: Effect of β on convergence of PerMFL in strongly convex settings (MCLR) using FMNIST dataset


 Figure 9: Effect of β on convergence of PerMFL in non-convex settings (DNN) using Synthetic dataset

 Figure 10: Effect of β on convergence of PerMFL in strongly convex settings (MCLR) using Synthetic dataset

 Figure 11: Effect of γ on convergence of PerMFL in non-convex settings (CNN) using MNIST dataset

 Figure 12: Effect of the hyperparameter γ on convergence of PerMFL in strongly convex settings (MCLR) using MNIST dataset


 Figure 13: Effect of γ on convergence of PerMFL in non-convex settings (CNN) using FMNIST dataset

 Figure 14: Effect of γ on convergence of PerMFL in strongly convex settings (MCLR) using FMNIST dataset

 Figure 15: Effect of γ on convergence of PerMFL in non-convex settings (DNN) using Synthetic dataset

 Figure 16: Effect of γ on convergence of PerMFL in strongly convex settings (MCLR) using Synthetic dataset


 Figure 17: Effect of λ on convergence of PerMFL in non-convex settings (CNN) using MNIST dataset

 Figure 18: Effect of λ on convergence of PerMFL in strongly convex settings (MCLR) using MNIST dataset

 Figure 19: Effect of λ on convergence of PerMFL in non-convex settings (CNN) using FMNIST dataset

 Figure 20: Effect of λ on convergence of PerMFL in strongly convex settings (MCLR) using FMNIST dataset


 Figure 21: Effect of λ on convergence of PerMFL in non-convex settings (DNN) using Synthetic dataset

 Figure 22: Effect of λ on convergence of PerMFL in strongly convex settings (MCLR) using Synthetic dataset

D.5 Ablation study on the effect of teams and devices participation on PerMFL

In a multi-tier architecture, teams and devices can be constituted in four ways: (1) Both teams and devices within teams have full participation (see Figure 23 to Figure 30), (2) Teams have full participation, but devices within teams are partially participating (see Figure 31 to Figure 42), (3) Teams have partial participation, but all devices within teams are participating (see Figure 43 to Figure 48), and (4) Teams and devices both have partial participation (see Figure 49 to Figure 51). In these experiments, we observed how well PerMFL performs and converges in various team combinations. We are also studying how PerMFL behaves when the number of participating teams and devices is limited.

D.5.1 Full participation of Teams and Devices

We conducted experiments in both convex (see Figure 24, Figure 26, Figure 28, Figure 30) and non-convex (See Figure 23, Figure 25, Figure 27, Figure 29) settings using MNIST, FMNIST, EMNIST, and Synthetic datasets. Our findings indicate that when it comes to team and device selection strategies, having full participation of teams and devices yields the best results compared to the other three types of participation strategies. Increasing the number of teams does not negatively impact the performance of the personalized model. However, in some cases, such as those depicted in Figure 29a and Figure 29b, increasing the number of teams can lead to a decrease in the convergence of the global model.

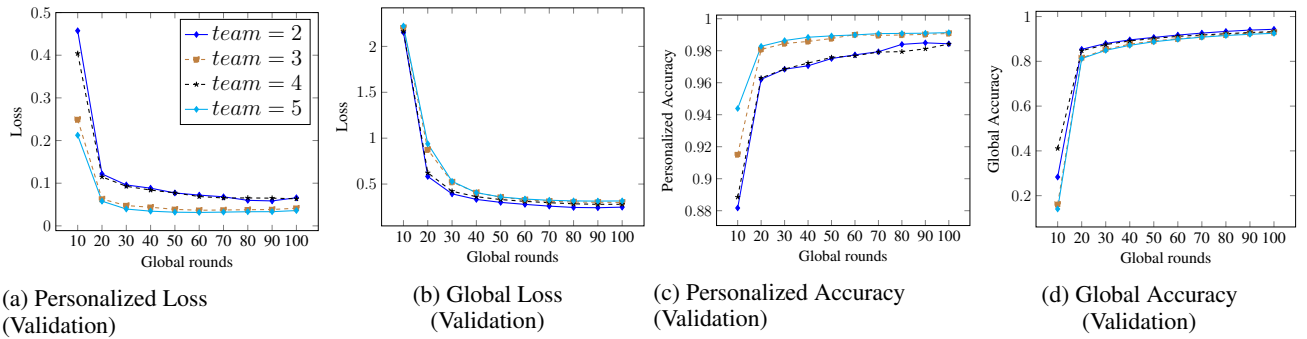


Figure 23: Full participation teams and devices on MNIST datasets in non-convex settings (CNN)

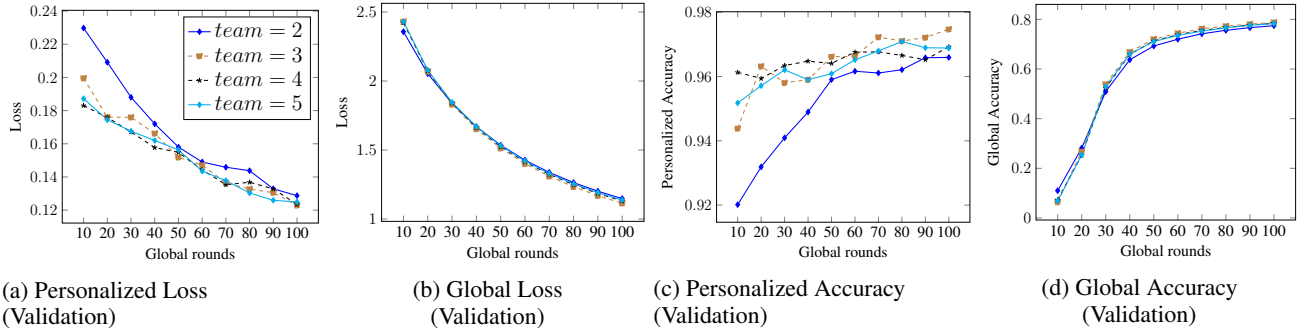


Figure 24: Full participation teams and devices on MNIST datasets in convex settings (MCLR)

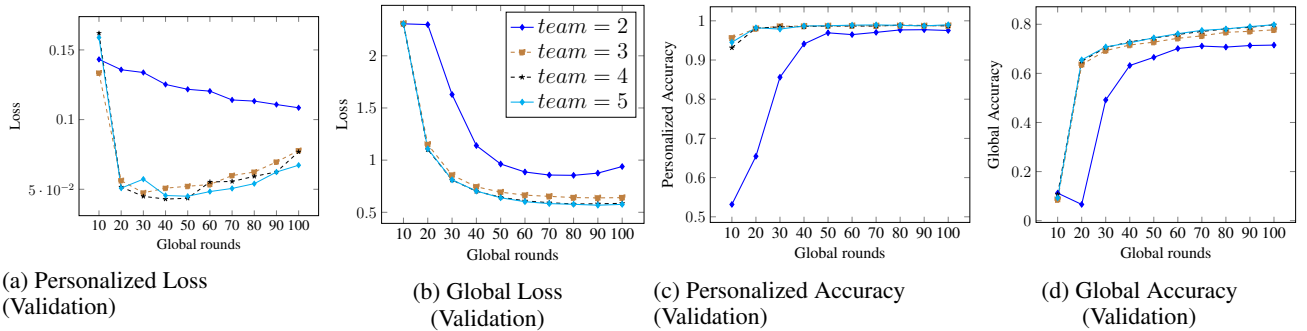


Figure 25: Full participation teams and devices on FMNIST datasets in non-convex settings (CNN)

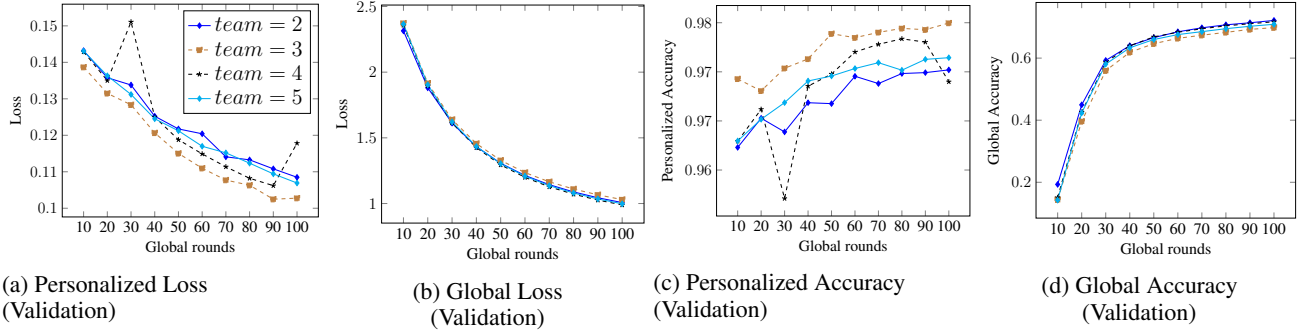


Figure 26: Full participation teams and devices on FMNIST datasets in convex settings (MCLR)

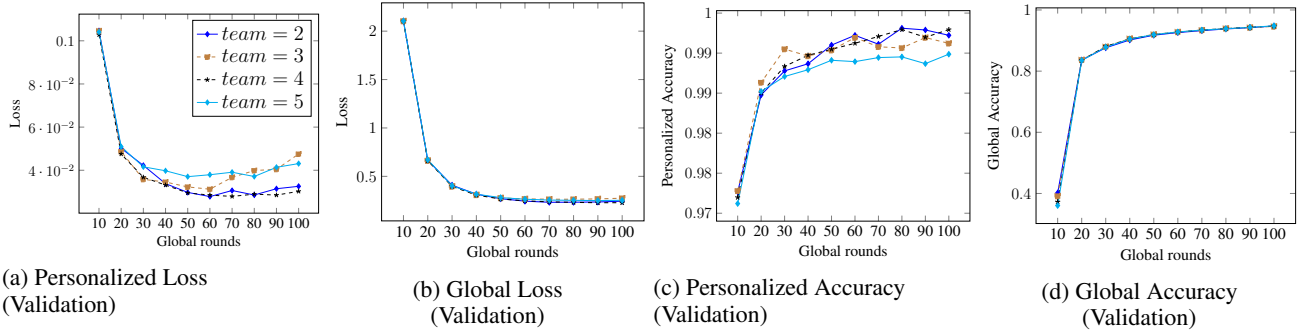


Figure 27: Full participation teams and devices on EMNIST datasets in non-convex settings (CNN)

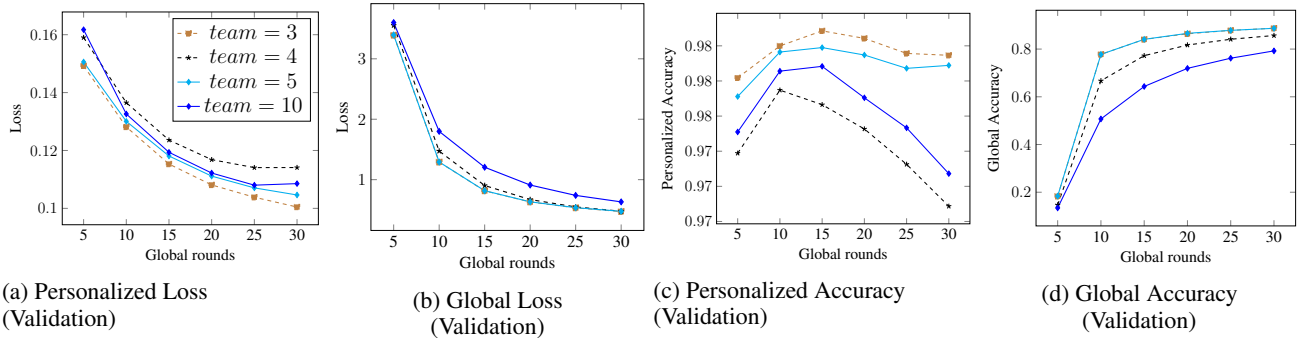


Figure 28: Full participation teams and devices on EMNIST datasets in convex settings (MCLR)

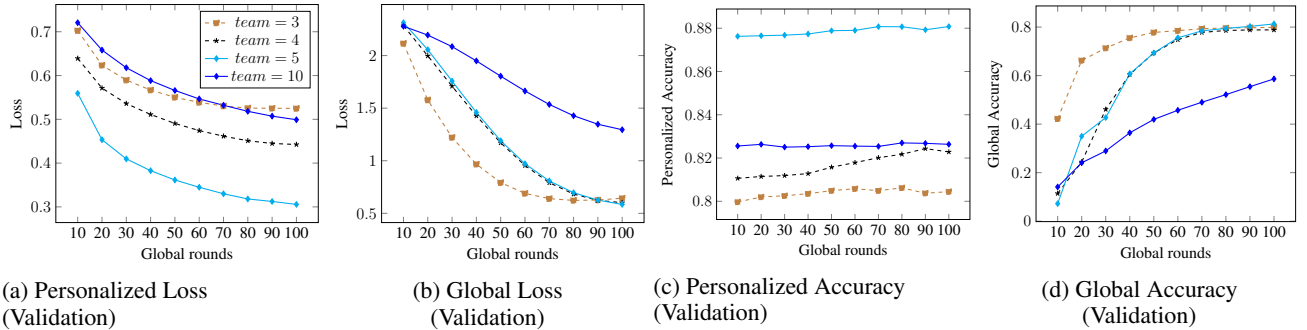


Figure 29: Full participation teams and devices on Synthetic datasets in non-convex settings (DNN)

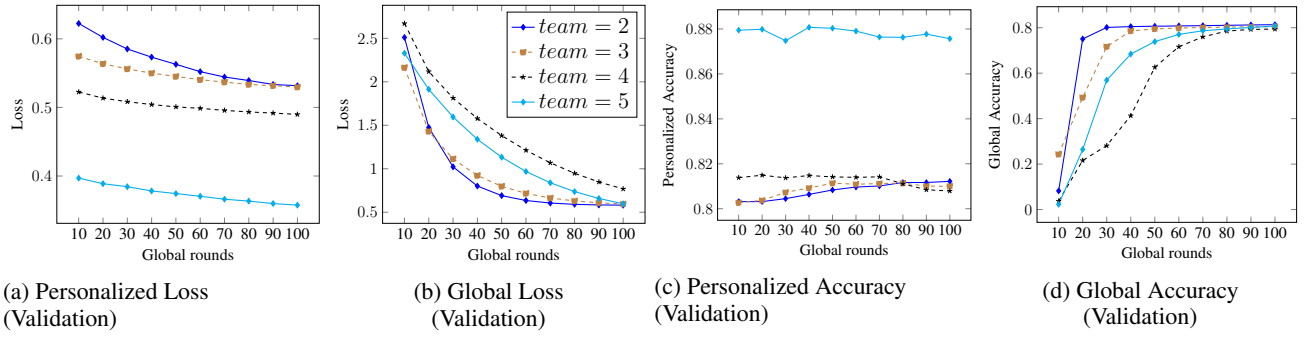


Figure 30: Full participation teams and devices on Synthetic datasets in convex settings (MCLR)

D.5.2 Full participation of Teams and partial participation of Devices

Here, we conducted experiments in convex settings using the MCLR approach; we observed that PerMFL with a low percentage of device participation converges slower compared to a high percentage of device participation (see Figure 31 to Figure 42). Increasing the number of participating devices resulted in faster convergence of the global model. Therefore, to achieve a better global model with faster convergence, it is recommended to increase the number of device participants per team iteration.

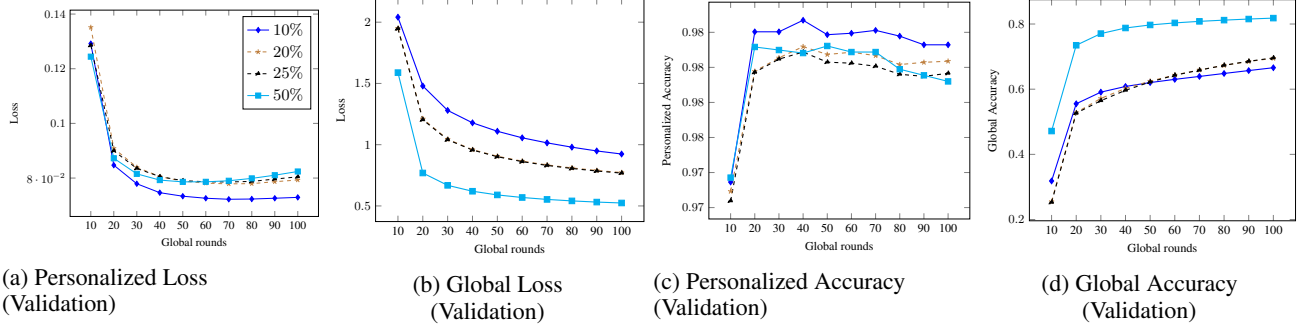


Figure 31: Full team participation (5 teams) but partial devices participation on FMNIST datasets in convex settings (MCLR)

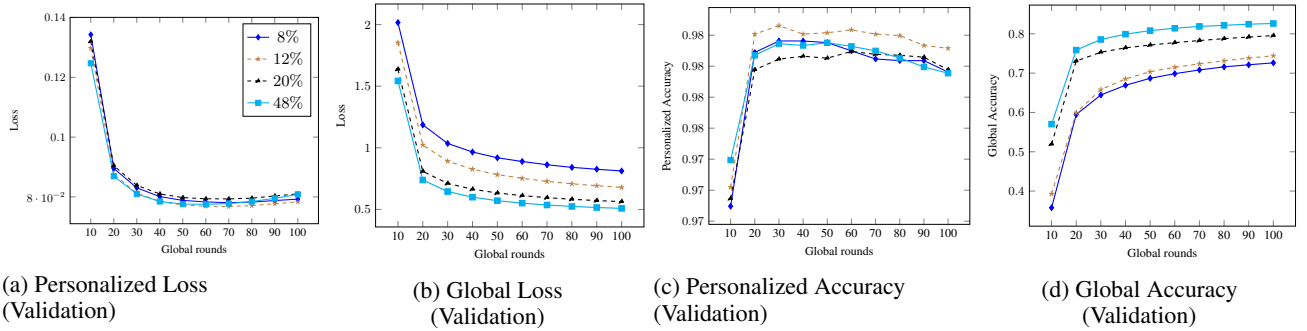


Figure 32: Full team participation (4 teams) but partial devices participation on FMNIST datasets in convex settings (MCLR)

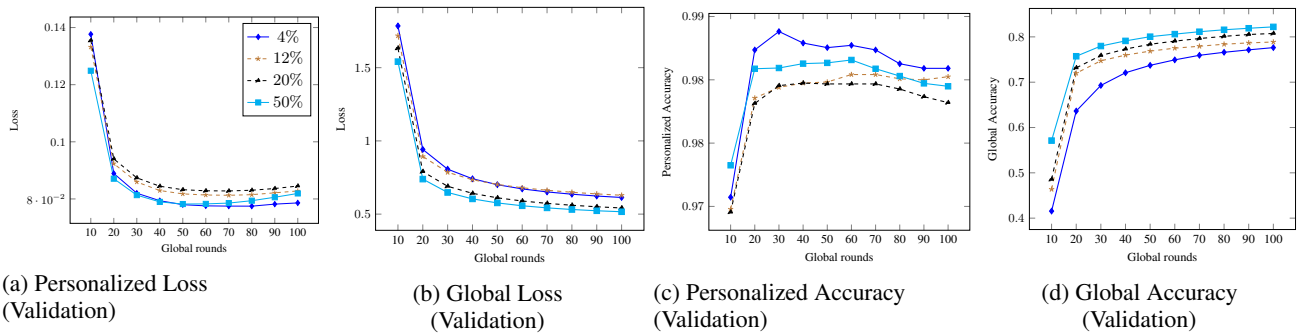


Figure 33: Full team participation (2 teams) but partial devices participation on FMNIST datasets in convex settings (MCLR)

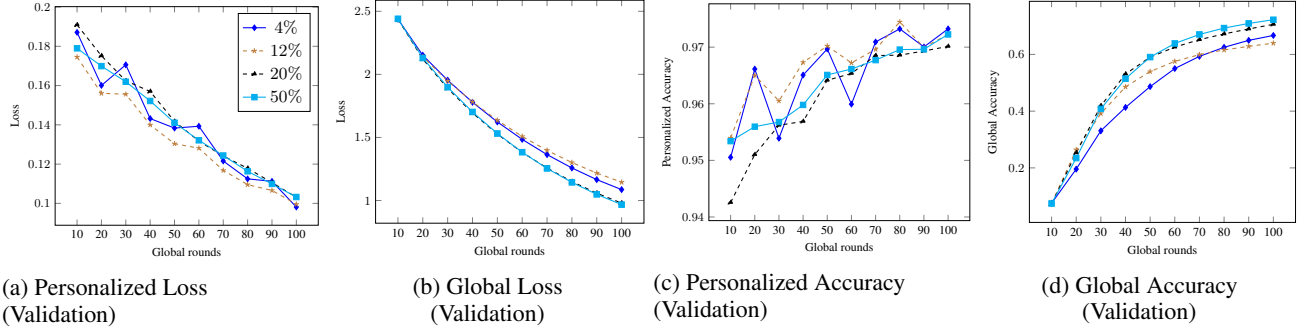


Figure 34: Full team participation (2 teams) but partial devices participation on MNIST datasets in convex settings (MCLR)

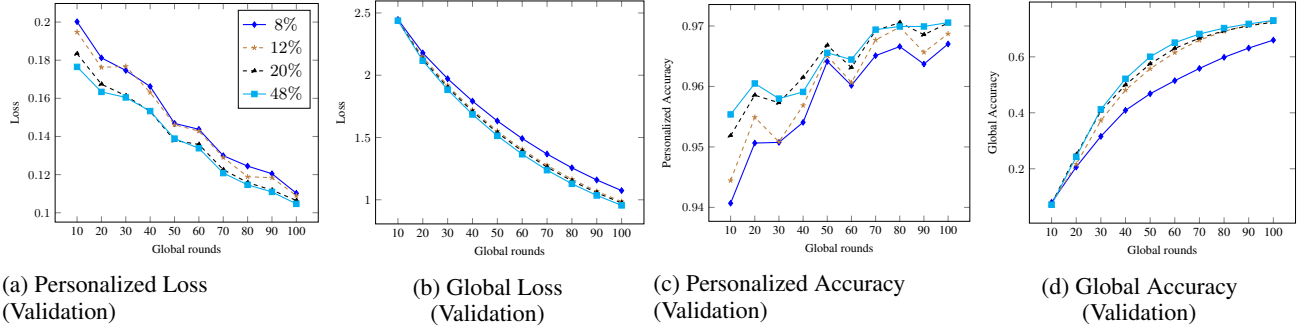


Figure 35: Full team participation (4 teams) but partial devices participation on MNIST datasets in convex settings (MCLR)

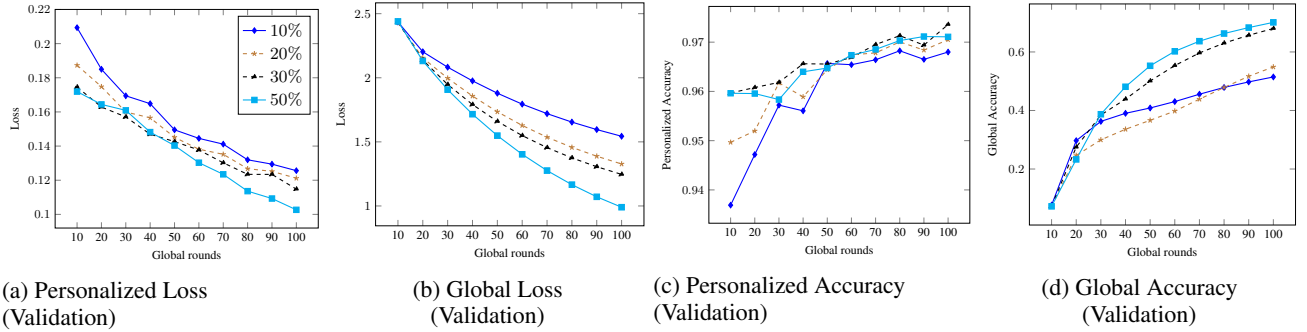


Figure 36: Full team participation (5 teams) but partial devices participation on MNIST datasets in convex settings (MCLR)

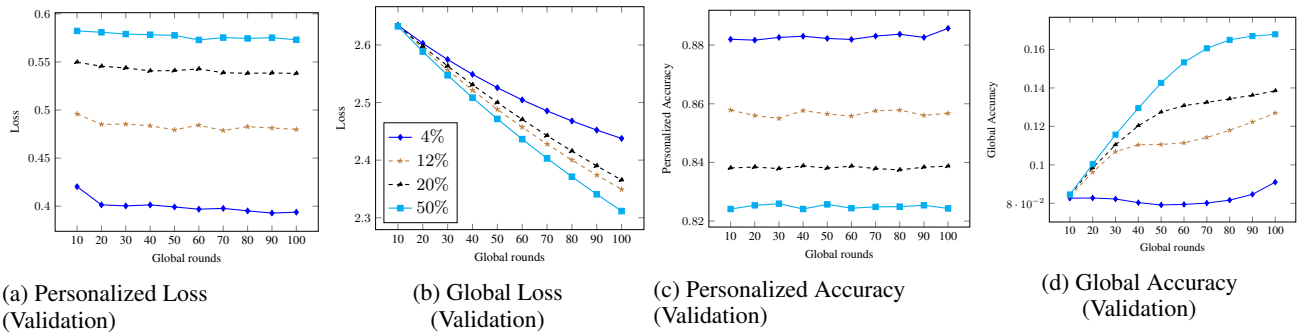


Figure 37: Full team participation (2 teams) but partial devices participation on Synthetic datasets in convex settings (MCLR)

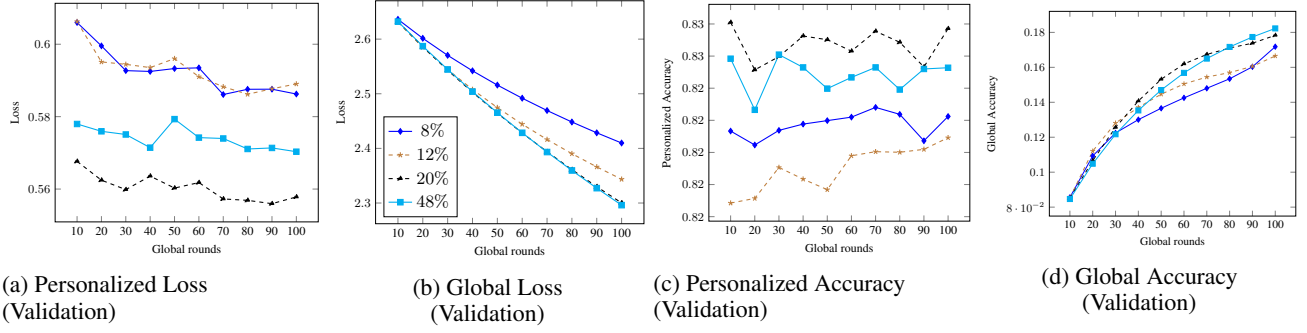


Figure 38: Full team participation (4 teams) but partial devices participation on Synthetic datasets in convex settings (MCLR)

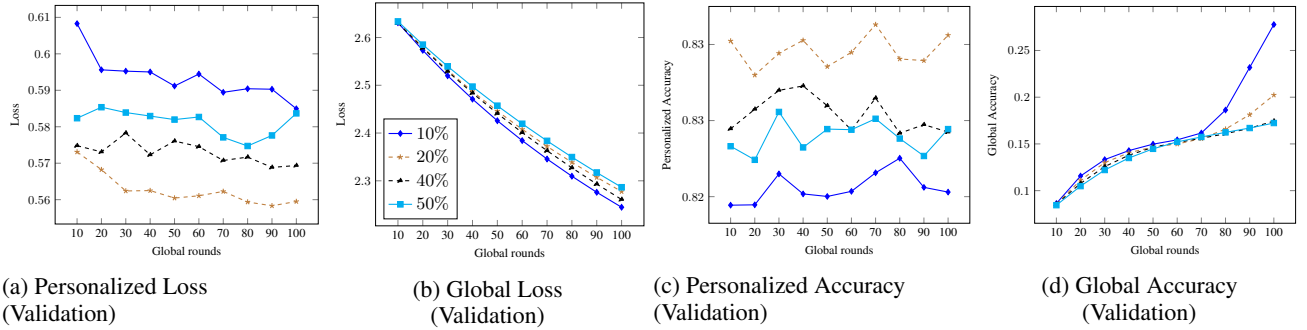


Figure 39: Full team participation (5 teams) but partial devices participation on Synthetic datasets in convex settings (MCLR)

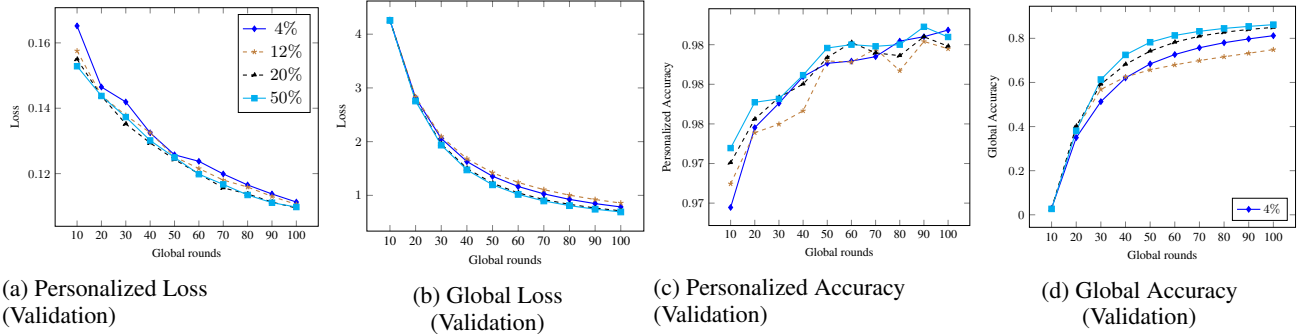


Figure 40: Full team participation (2 teams) but partial devices participation on EMNIST datasets in convex settings (MCLR)

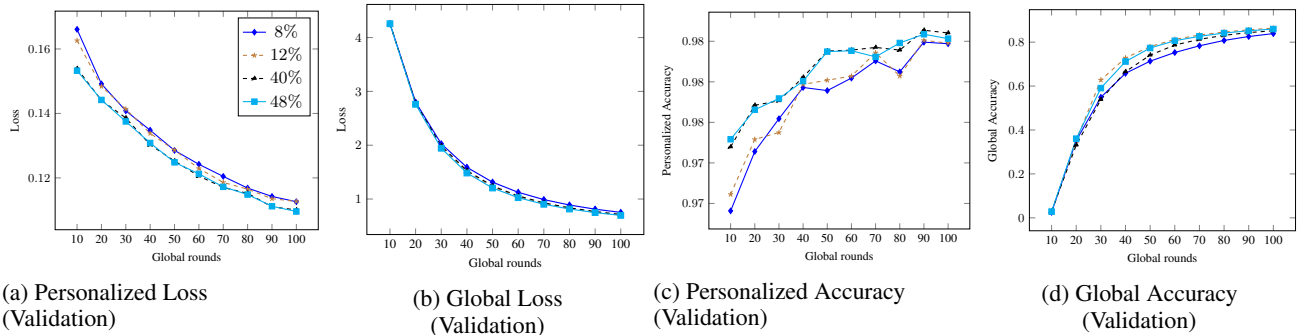


Figure 41: Full team participation (4 teams) but partial devices participation on EMNIST datasets in convex settings (MCLR)

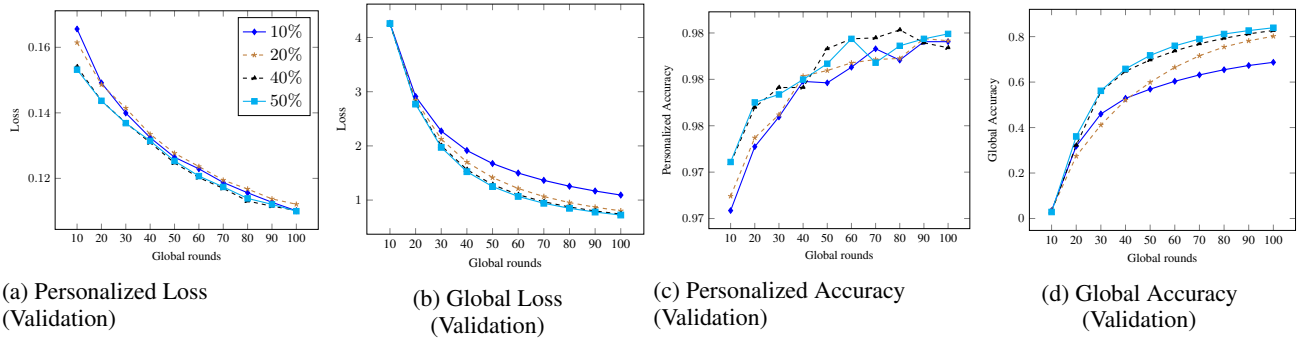


Figure 42: Full team participation (5 teams) but partial devices participation on EMNIST datasets in convex settings (MCLR)

D.5.3 Partial participation of Teams and full participation of Devices

We conducted a series of experiments in both convex (see Figure 43, Figure 45, and Figure 47) and non-convex settings (see Figure 44, Figure 46, and Figure 48) using EMNIST, MNIST, and FMNIST datasets. From there, we observed if the participation of teams is limited, then the personalized and global model both converges slowly. The same behaviour has been observed in all datasets for both convex and non-convex experiments (see Figure 43 to Figure 48).

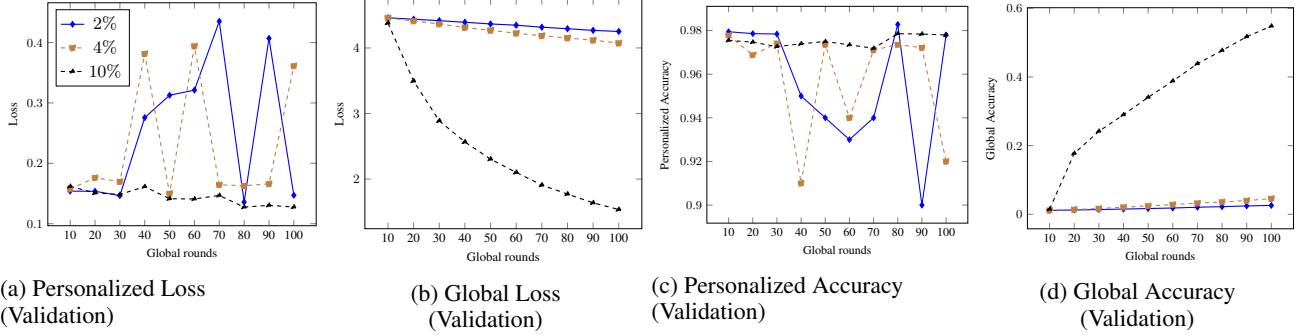


Figure 43: Partial participation of team (2%, 4%, and 10%) and full devices participation of devices on EMNIST datasets in convex settings (MCLR)

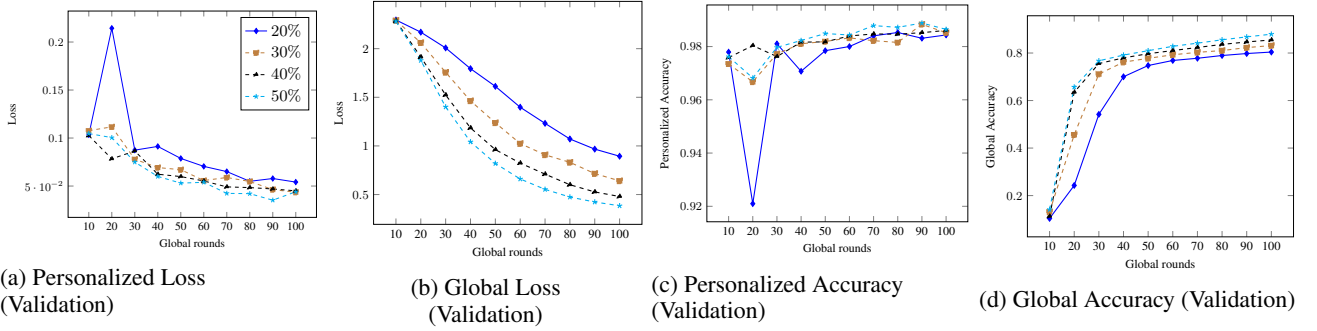


Figure 44: Partial participation of team (20%, 30%, 40%, and 50%) and full devices participation of devices on EMNIST datasets in convex settings (CNN)

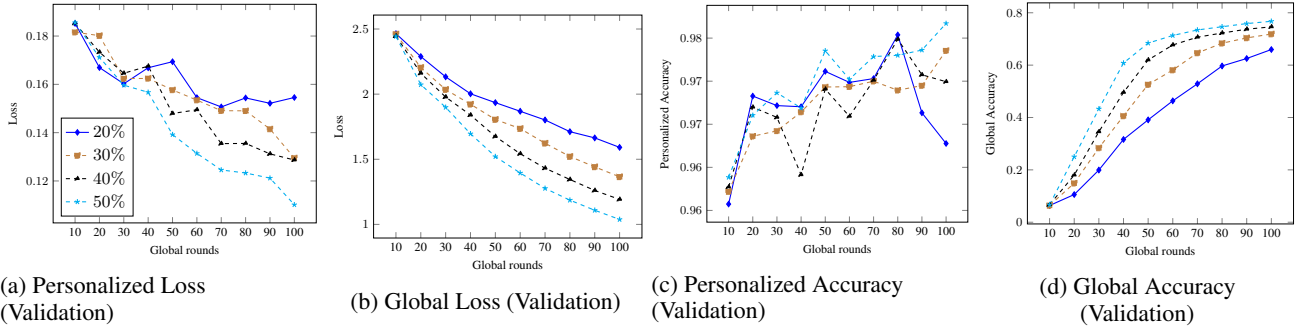


Figure 45: Partial participation of team (20%, 30%, 40%, and 50%) and full devices participation of devices on MNIST datasets in convex settings (MCLR)

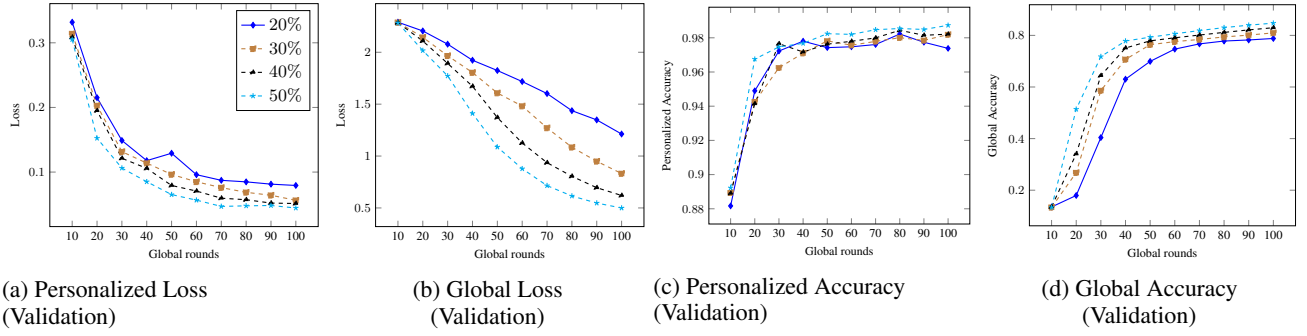


Figure 46: Partial participation of team (20%, 30%, 40%, and 50%) and full devices participation of devices on MNIST datasets in convex settings (CNN)

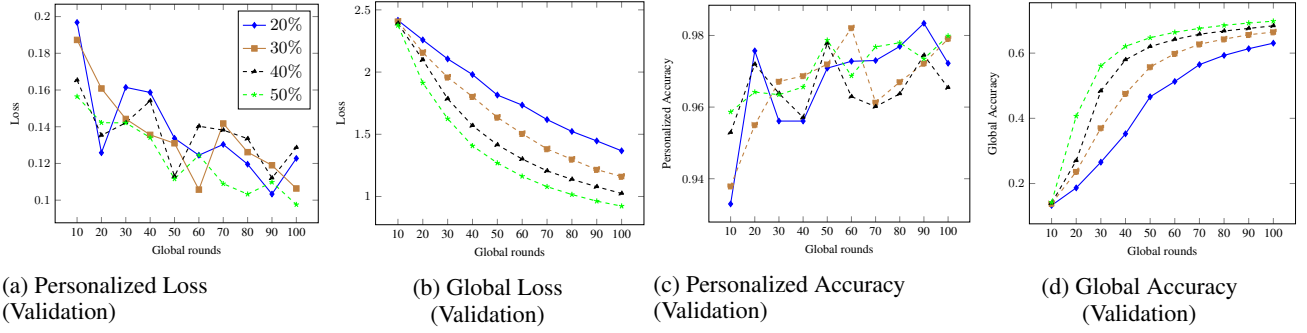


Figure 47: Partial participation of team (20%, 30%, 40%, and 50%) and full devices participation of devices on FMNIST datasets in convex settings (MCLR)

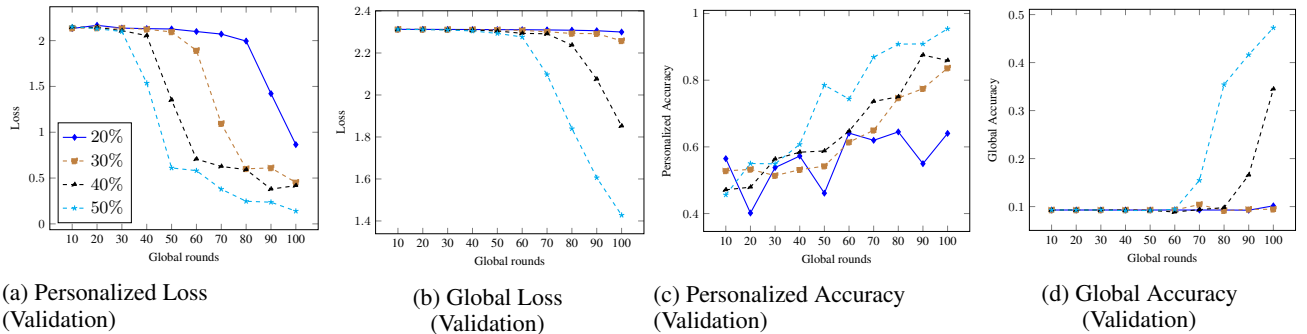


Figure 48: Partial participation of teams (20%, 30%, 40%, and 50%) and full devices participation of devices on FMNIST datasets in convex settings (CNN)

D.5.4 Partial participation of Teams and Devices

We conducted experiments for convex scenarios on EMNIST, MNIST, and FMNIST datasets (see Figure 49, Figure 50, and Figure 51). From the experiments, it was observed that when 20% of teams participated in each global round, increasing the number of devices participating in each team iteration resulted in improved convergence of both personalized and global models.

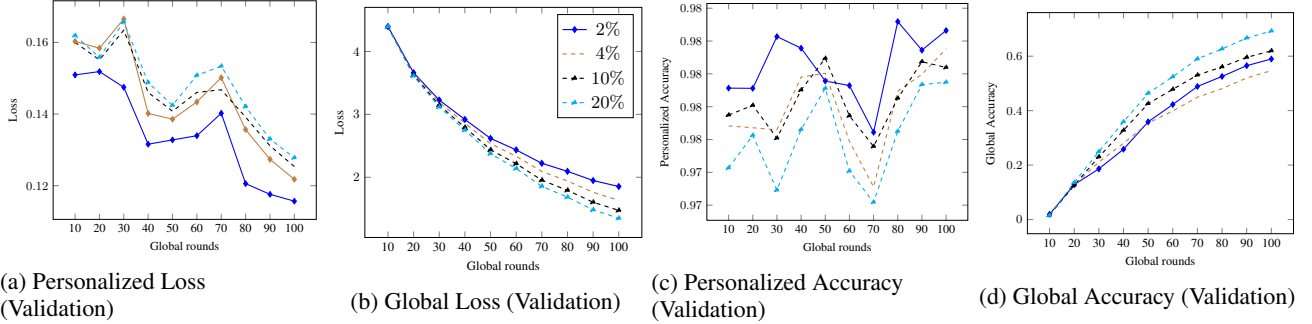


Figure 49: Partial participation of team (20%) and devices (2%, 4%, 10%, and 30%) on EMNIST datasets in convex settings (MCLR)

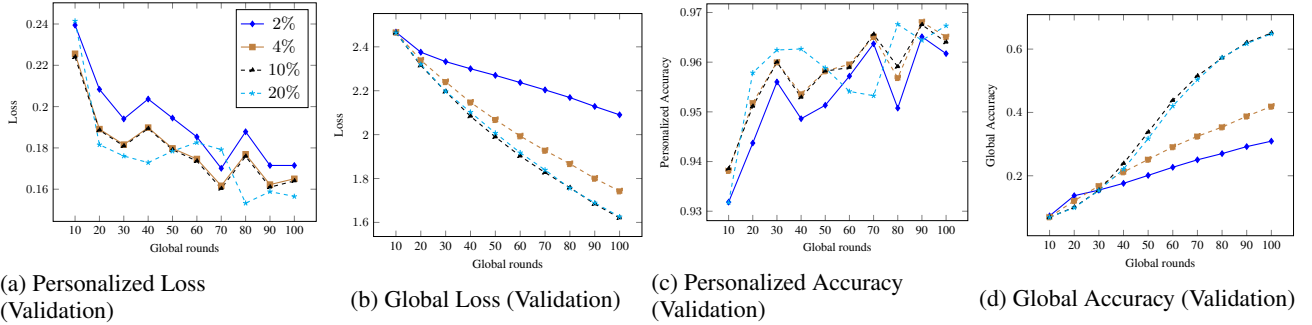


Figure 50: Partial participation of team (20%) and devices (2%, 4%, 10%, and 30%) on MNIST datasets in convex settings (MCLR)

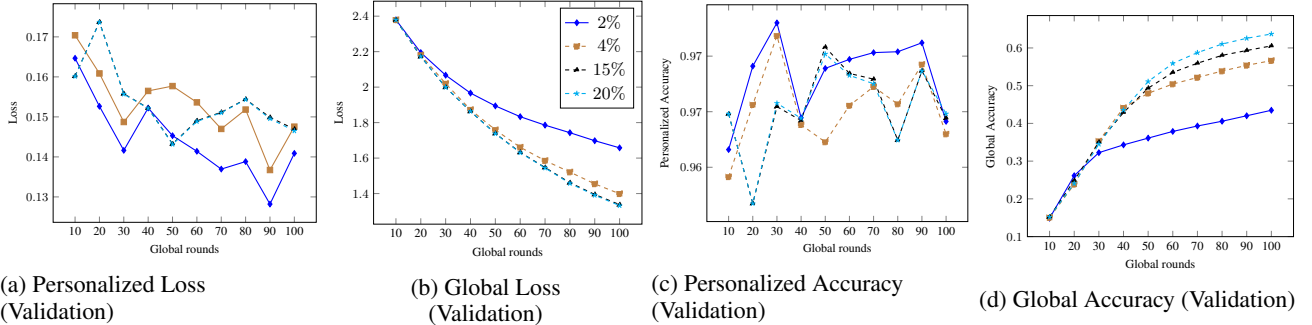


Figure 51: Partial participation of team (20%) and devices (2%, 4%, 15%, and 30%) on FMNIST datasets in convex settings (MCLR)

Discussions: Based on our empirical observations, we conclude that the convergence and performance of PerMFL are optimal when both teams and devices are fully present throughout the entire global iterations. However, PerMFL also demonstrates good performance even with variations in team and device participation. When teams fully participate but there is partial device participation, PerMFL achieves fast convergence. On the other hand, when the number of participating teams is limited, the convergence of the global model is slower, requiring a higher number of global rounds to converge. It is important to note that the convergence of PerMFL is slowest when both teams and devices have very low participation (2%) in each global rounds.

D.6 Effect of team iterations on convergence of PerMFL

In this study, experiments were conducted to investigate the impact of team iterations on the convergence of PerMFL. The objective was to gain insights into how varying the number of team iterations influences the convergence behaviour of the model. Here we studied (1) the effect of the number of team iterations on the convergence of PerMFL when teams have full involvement but devices have fractional involvement in the entire learning process. (2) Effect of team iterations on the convergence of PerMFL while teams and devices both have fractional involvement. i.e., all devices are not participating in each global rounds only a fraction of devices are participating.

D.6.1 Effect of number of team iterations on the full participation of Teams and partial participation of Devices.

In our experiments (see Figure 52, Figure 53 Figure 54, Figure 55, and Figure 56), we observed for both convex and non-convex scenarios, the convergence of PerMFL's personalized and global model improves if we increase the team iterations. This improvement occurs because when we increase the team iterations, more devices within the teams can actively contribute to the process.

D.6.2 Effect of number of team iterations on the partial participation of Teams and Devices

In our experiments, we specifically investigated the impact of low team and device participation on the convergence of the global model. The objective was to determine whether increasing the number of team iterations could expedite the convergence process. Our findings, as depicted in Figure 57 and Figure 59, indicate that when team participation is set at 20%, increasing the team iterations lead to improved convergence of the global model. However, when team participation is extremely low (2%), as shown in Figure 58 and Figure 60, simply increasing team iterations is insufficient. In such cases, a higher number of global iterations is necessary to achieve convergence for the global model.

Discussions: Based on our findings, we can infer that team iterations play a crucial role in improving the performance of both the global and personalized models. However, when there is limited participation from teams and devices in each global round, relying solely on team iterations is inadequate. In such cases, it becomes necessary to increase the number of global rounds to enable more teams to participate and, consequently, enhance the performance of PerMFL.

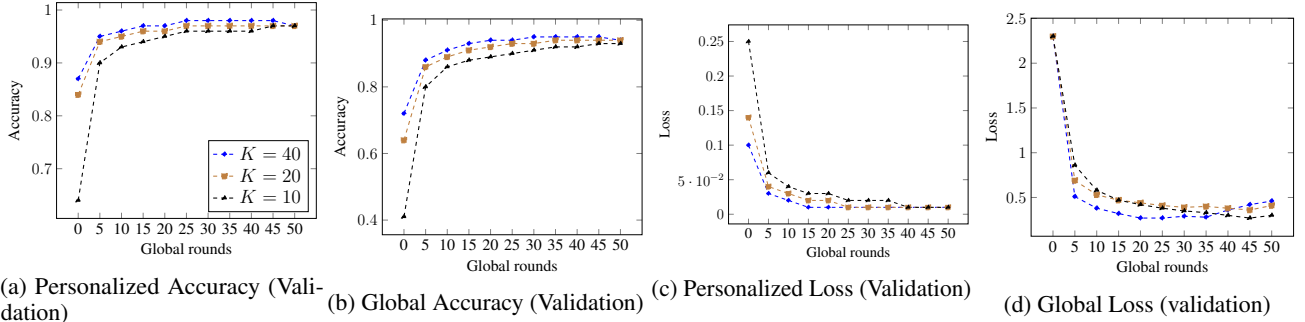


Figure 52: Effect of Team iterations on the convergence of PerMFL in non-convex settings (CNN) on MNIST while teams and devices have full participation

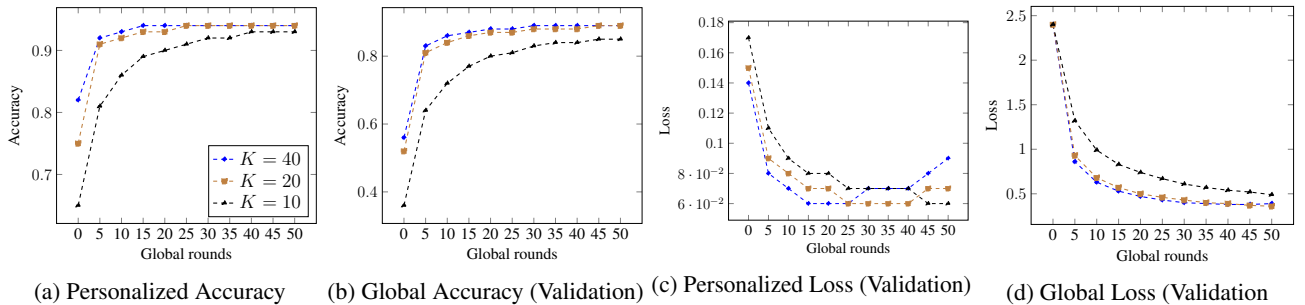


Figure 53: Effect of Team iterations on the convergence of PerMFL in strongly convex (MCLR) settings on MNIST while teams and devices have full participation

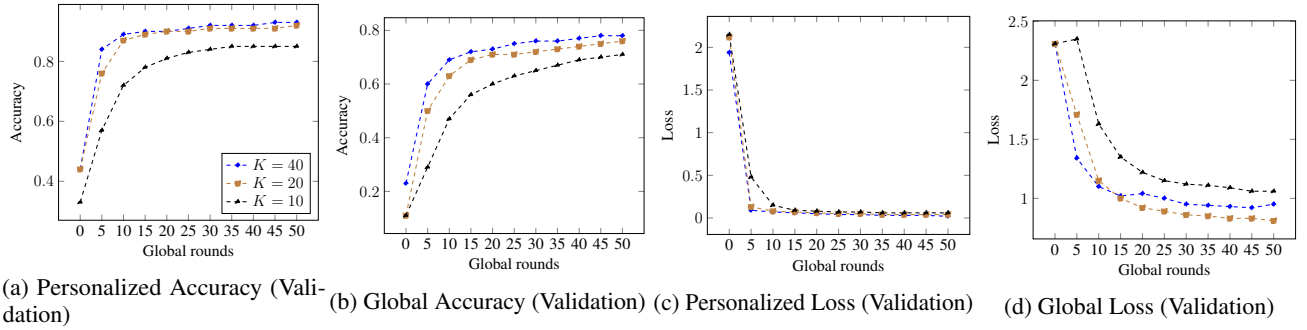


Figure 54: Effect of Team iterations on the convergence of PerMFL in non-convex settings (CNN) on FMNIST while teams and devices have full participation

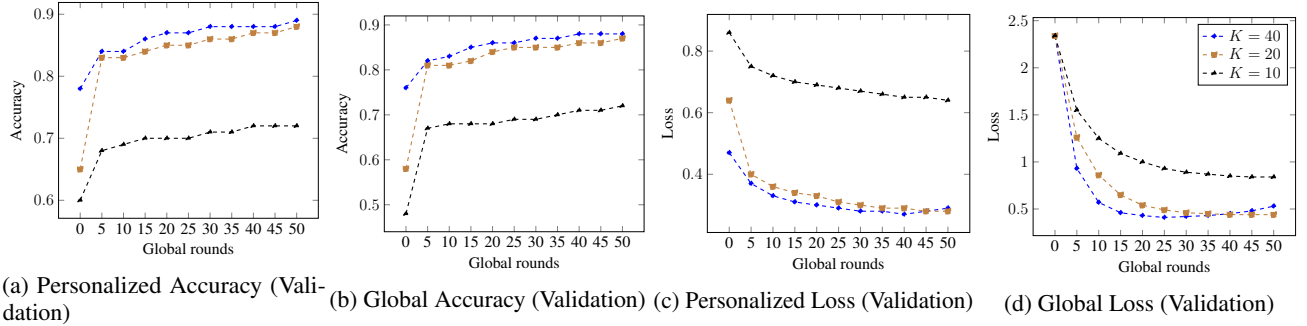


Figure 55: Effect of Team iterations on the convergence of PerMFL in non-convex settings (DNN) on Synthetic dataset while teams and devices fully participate.

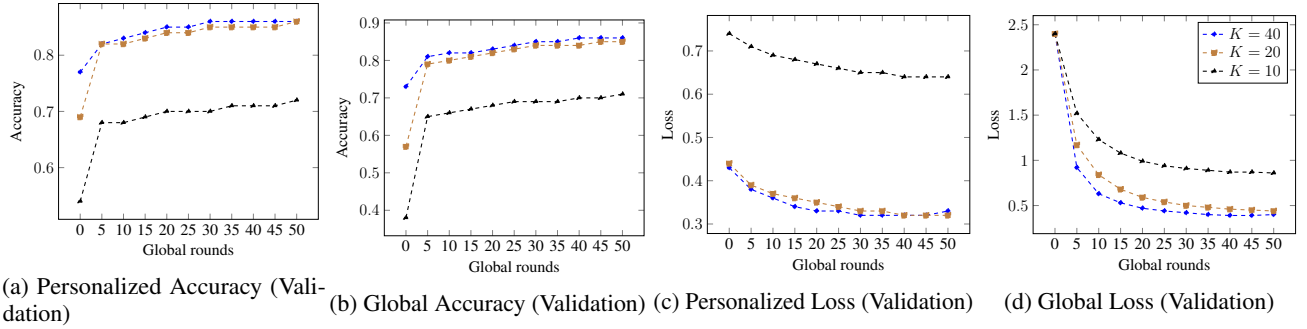


Figure 56: Effect of Team iterations on the convergence of PerMFL in strongly convex settings (MCLR) on Synthetic dataset while teams and devices fully participate.

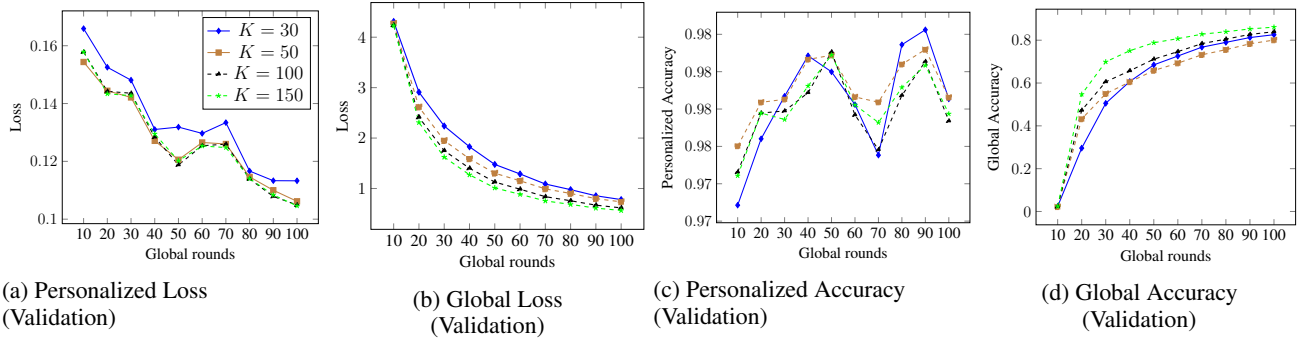


Figure 57: Effect of Team iterations $\{TE = 30, 50, 100, \text{ and } 150\}$ when team (20%) and devices (2%) are partially participated in the PerMFL using EMNIST datasets in convex settings (MCLR)

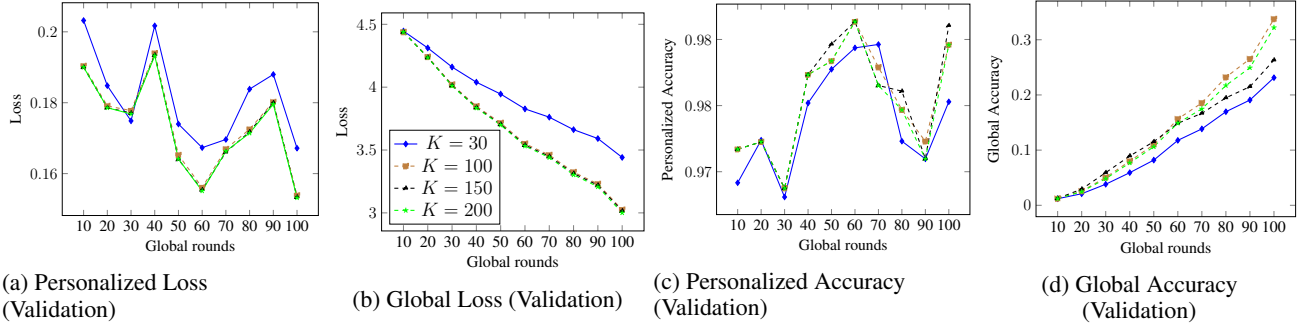


Figure 58: Effect of Team iterations $\{TE = 30, 100, 150 \text{ and } 200\}$ when team (2%) and devices (2%) are partially participated in the PerMFL using EMNIST datasets in convex settings (MCLR)

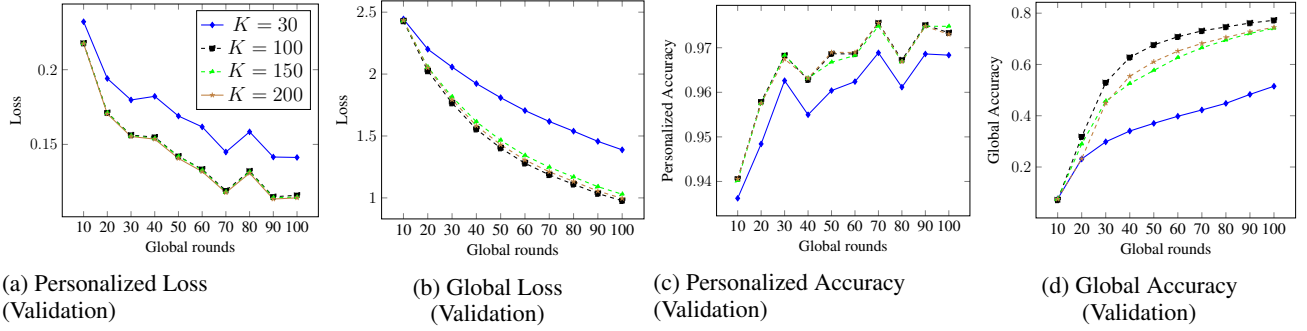


Figure 59: Effect of Team iterations $\{TE = 30, 100, 150 \text{ and } 200\}$ when team (20%) and devices (2%) are partially participated in the PerMFL using MNIST datasets in convex settings (MCLR)

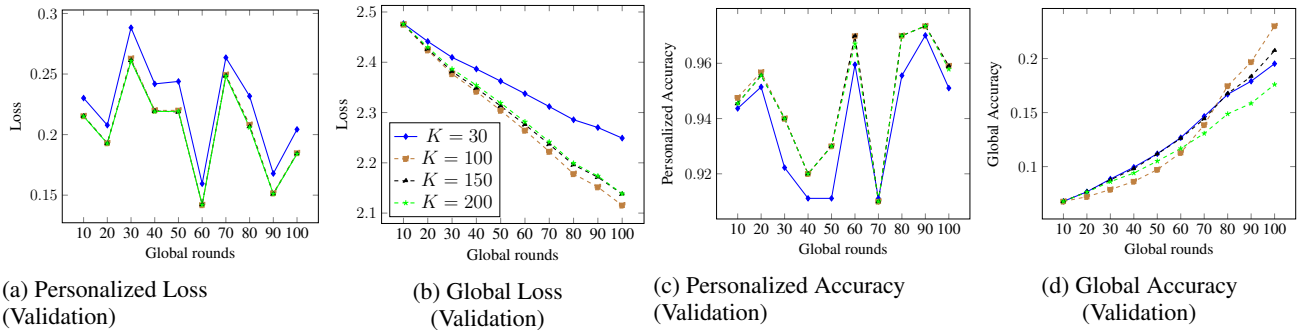


Figure 60: Effect of Team iterations $\{TE = 30, 100, 150 \text{ and } 200\}$ when team (2%) and devices (2%) are partially participated in the PerMFL using EMNIST datasets in convex settings (MCLR)

D.7 Convergence analysis

Based on the convergence results presented in Figure 62, Figure 61, and Figure 63, we observed that PerMFL(PM) achieved faster convergence compared to AL2GD. Additionally, the convergence of PerMFL(GM) and h-SGD was found to be similar for both strongly convex and non-convex scenarios.

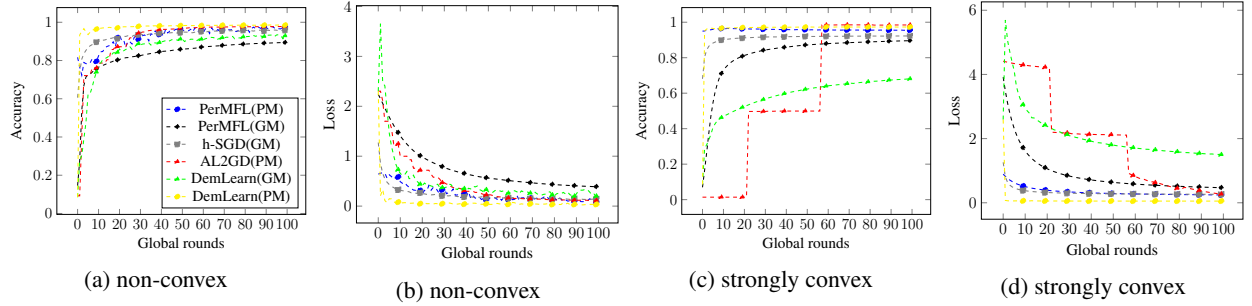


Figure 61: Convergence comparison of PerMFL with multi-tier SOTA in strongly convex and non-convex settings on EMNIST

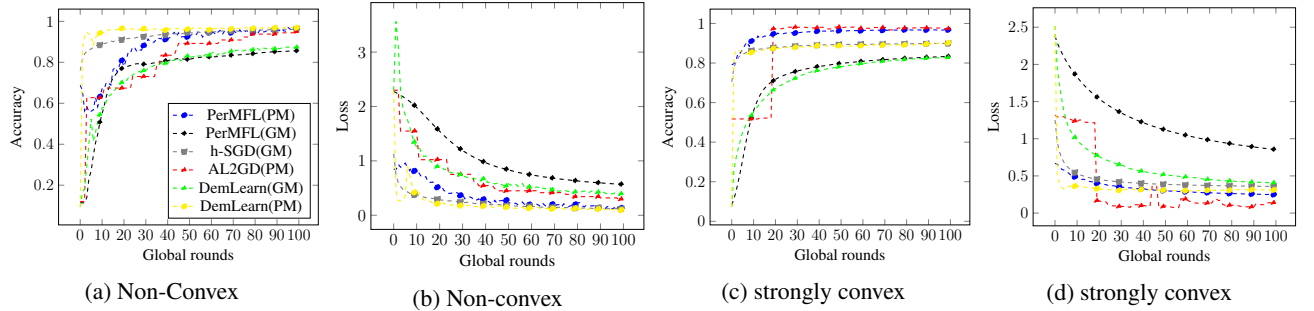


Figure 62: Convergence comparison of PerMFL with multi-tier SOTA in strongly convex and non-convex settings on MNIST

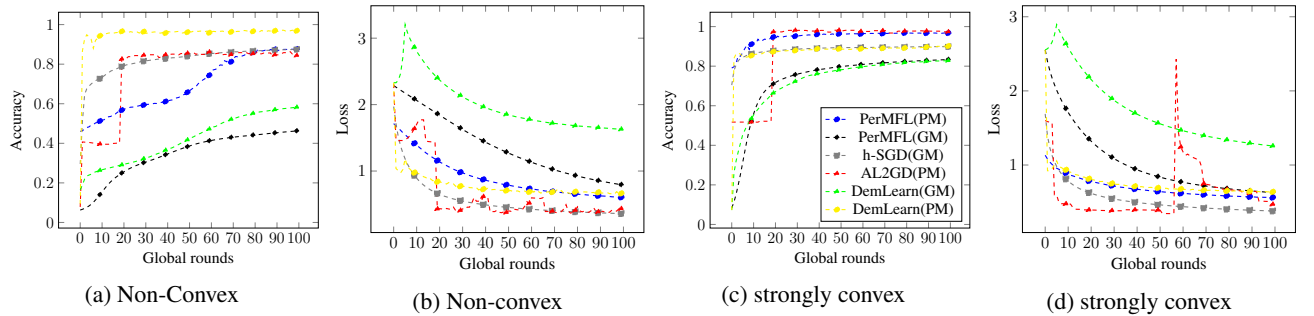


Figure 63: Convergence comparison of PerMFL with multi-tier SOTA in strongly convex and non-convex settings on Synthetic datasets

D.8 Performance analysis on FEMNIST and CIFAR100 datasets

We have experimented the performance of PerMFL with the state-of-the-art multi-tier federated learning algorithms on Federated EMNIST (FEMNIST) and CIFAR100 datasets (see Table 3) for the strongly convex setup. From there, we observed PerMFL(PM) produce better results than AL2GD. h-sgd produces a better global model than PerMFL. For the CIFAR100 dataset, AL2GD overcame the performance of PerMFL(PM). The performance of PerMFL(GM) and h-SGD both are equivalent.

Table 3: Performance comparison of PerMFL with SOTA. (Validation accuracy(mean/std))

Algorithm	MCLR (Strongly convex)	
	FEMNIST	CIFAR100
h-SGD (GM)	0.6405(± 0.005)	0.1232(0.001)
AL2GD (PM)	0.4467(± 0.01)	0.65.87(± 0.07)
PerMFL (GM)	0.5757 (± 0.0)	0.1368 (± 0.0)
PerMFL (PM)	0.8129 (± 0.0)	0.6695 (± 0.001)